CHARACTERIZATION METHODOLOGY FOR DECOMMISSIONING LOW AND INTERMEDIATE LEVEL FISSILE NUCLIDE CONTAMINATED BURIED SOILS AND PROCESS PIPING USING PHOTON COUNTING

A Dissertation

by

MEGAN LEIGH PRITCHARD

Submitted to the Office of Graduate and Professional Studies of
Texas A&M University
in partial fulfillment of the requirements for the degree of

DOCTOR OF PHILOSOPHY

Chair of Committee,	Pavel V. Tsvetkov
Committee Members,	G. Donald Allen
	Vladimir Horvat
	Craig Marianno
	Sean M. McDeavitt
Head of Department,	Yassin A. Hassan

May 2014

Major Subject: Nuclear Engineering

ABSTRACT

A new approach to- and method for characterization of fissile nuclide contaminated soils and process piping has been developed and implemented for low and intermediate level wastes, using new calibration bases for photon counting. The method has been validated by integrating the capabilities of MCNP5 and ISOCS for a LaBr scintillator detector in combination with known radioactive standards. In addition, the developed methods consider nuclear safety as the priority while retaining realistic fissile mass and enrichment estimation techniques.

The impact of a quick, portable non-destructive assay process to the decommissioning and remediation arena is extremely valuable. Traditional methods have inherent limitations in time consumption, resources, stability, and rigidity. In addition to optimizing a material blending and storage program, gaining a real-time understanding to the nature of fissile material prior to disturbance aids a nuclear safety program and culture invaluably.

In this dissertation, detailed detector-waste models were developed and utilized to create a quick uranium mass and enrichment estimation process by taking advantage of the resolution and discrimination capabilities of the LaBr equipped InSpector 1000 instrument. The analysis takes into account multiple possible scenarios that may be encountered during decommissioning and remediation of a fuel fabrication and buried nuclear waste facility, while keeping nuclear safety controls in mind.

As an inherent part of the process, the models were validated by performing a series of code-to-software and software-to-standard benchmarking procedures, which provided substantiation for use of the detector for the derived purposes, in addition to ensuring that the Monte Carlo-based calibration approach was conservative, as compared to other methods.

The scenarios analyzed for the calibration basis were selected based on historical knowledge and in-field experience at the Westinghouse Hematite Decommissioning Project.

The techniques developed in this dissertation offer a new characterization method for fissile material quantity and enrichment with a portable, passive non-destructive gamma assay system without relying on continual macroscopic system analysis. In addition, it provides early detection of large quantities of fissile material prior to exhumation or disturbance to enhance nuclear safety processes. This places the first priority on nuclear and radiological safety while preserving the time and money saving aspects of production-based projects.

ACKNOWLEDGEMENTS

I would like to offer my sincere thanks and gratitude to my advisor Dr. Pavel Tsvetkov for his support during the course of this dissertation and all graduate work I did at Texas A&M University over the years. I would also like to thank my Ph.D. committee members Craig Marianno for joining at the last minute, Sean McDeavitt, Donald Allen, and Vladimir Horvat, who was my first college physics professor as a freshman.

I also acknowledge the support of family and friends, for continuing to offer support and encouragement when the doctorate seemed to last forever. A special thanks to my husband Brian Shreckengost for offering daily help in life to allow me to complete the dissertation. And lastly to my office mates in Zachry 19A, David Ames, Tom Lewis and Deji Alajo, who made graduate school more fun that I could have ever imagined.

I also want to thank Dr. Kemble Bennett during his tenure as the Dean of the Dwight Look College of Engineering for awarding me the Dean's Endowed Excellence Fellowship in its inaugural year.

This dissertation is based upon work financially supported by Nuclear Safety Associates under contract to Westinghouse Electric Company, LLC.

NOMENCLATURE

‘	Foot (12”)
“	Inch (2.54 cm)
AEC	Atomic Energy Commission
Bq	Becquerel
CdTe	Cadmium Tellurium
CFR	Code of Federal Regulations
Ci	Curie
cm	Centimeter
cpm	Counts per Minute
CZT	Cadmium Zinc Telluride
D&D	Decontamination and Decommissioning
DU	Depleted Uranium
EAF	European Activation File
ENDF	Evaluated Nuclear Data Files
FC	Field Container: Nominal 20 gallon bucket used to contain excavated radiological Hot Spots
FENDL	Fusion Evaluated Nuclear Data Library
FOV	Field of View
FSS	Final Status Survey
FWHM	Full Width at Half Maximum

g	Gram
γ	Photon
GEANT4	GEometry ANd Tracking Monte Carlo Code
GWD	Giga-Watt Days
HDP	Hematite Decommissioning Project
HEU	Highly Enriched Uranium
IAEA	International Atomic Energy Agency
ILW	Intermediate Level Waste
ISOCs	In-Situ Object Counting System
K	Potassium
k_{eff}	Effective Multiplication Factor
keV	Kilo Electron Volt
kg	Kilogram
L	Liter
LaBr	Lanthanum Bromide ($LaBr_3$)
LED	Light Emitting Diode
LEU	Low Enriched Uranium
LLW	Low Level Waste
LWR	Light Water Reactor
μ	Micro (1.0×10^{-6})
m	Meter
M	Mega (1.0×10^{6})

MCA	Multi-Channel Analyzer
MCNP5	Monte Carlo N-Particle Version 5
MDA	Minimum Detectable Activity
MeV	Mega Electron Volt
mg	Milli-Gram
MTU	Metric Ton Uranium
NaI	Sodium Iodide
NCS	Nuclear Criticality Safety
NCS Exempt Material	Material that is safely subcritical by virtue of its low fissile nuclide concentration, and which does not warrant application of criticality safety controls.
Non-NCS Exempt Material	Material that has a fissile concentration greater than the limit established for NCS Exempt Material. These materials require criticality safety controls to ensure their safe handling, packaging, processing, and storage.
NIST	National Institute of Standards and Technology
NORM	Technologically Enhanced Naturally Occurring Radioactive Material
NPS	Nominal Pipe Size
NRC	Nuclear Regulatory Commission
ORNL	Oak Ridge National Laboratory

PDF	Probability Distribution Function
PVC	Polyvinyl Chloride
PWR	Pressurized Water Reactor
R^2	Coefficient of Determination
Ra	Radium
ROI	Region of Interest
SCALE(5)	Standard Computer Analysis for Licensing Evaluation, Version 5
SNM	Special Nuclear Material
Th	Thorium
U	Uranium
UO_2	Uranium Dioxide
USEI	U.S. Ecology Idaho
VDM	Virtual Data Manager
vol.%	Percentage by Volume
wt.%	Percentage by Weight

TABLE OF CONTENTS

Page

LIST OF FIGURES

FIGURE Page

FIGURE Page

LIST OF TABLES

TABLE Page

CHAPTER I

INTRODUCTION AND LITERATURE REVIEW

Significant cost savings and operational efficiency may be observed by performing rapid non-destructive classification of radioactive waste at or near its point of retrieval. Quickly categorizing waste enables the use of multiple waste streams and enhances appropriate safety measures.

Recent improvements in gamma spectroscopy technologies have provided the capability to perform rapid in-situ analysis using portable and handheld devices such as battery operated medium and high resolution detectors. Gamma spectroscopy is the most commonly used method for qualitative determination of gamma emitting isotopes for various samples [1, 2].

Gamma spectroscopy and portable devices instantly deliver information to the user. With appropriate calibration standards, the responses lead to information such as uranium enrichment or uranium mass in the sample. Monte Carlo methods can serve as a valuable tool to minimize the number or eliminate experimental measurements needed for a detector calibration.

The site selected for this work is discussed extensively as a case history. It is in the process of being decommissioned and remediated and has a need for both in-situ and ex-situ characterization methods. Characterization includes primarily low level waste soils containing debris waste, sludge, thorium, radium, depleted and enriched uranium, technetium, and various other contaminated items. The process of identifying a need,

pinpointing a solution, and developing a method to acquire and analyze data are the backbone of this work. Integration of conservatism and historical knowledge into the developing method aims to satisfy nuclear criticality safety during non-destructive assay (NDA) while retaining a degree of realism often lost in NCS measurements.

Nuclear fuel cycle facility decommissioning is a daunting task being undertaken by many past production facilities that had grasped some aspect of the nuclear industry, even in very small proportions. Decommissioning can have multiple facets associated with the full scope process. All decommissioning processes involving fissile material or possible fissile material require a nuclear criticality safety program in order to ensure safe handling, packing, processing, transportation, and storage of nuclear material. One aspect of the decommissioning scope common to facilities operating in the 1960s is remediation of buried process wastes and subsurface piping. The characteristics of the material buried are often unknown. Incomplete and inaccurate burial logs are commonplace in facilities of the era.

I.A. TECHNICAL STATUS OF THE QUESTION

Passive NDA was developed with the need for increased nuclear material safeguards with rapid measurement methods that would not alter the state of the material under interrogation. Gamma-ray assay is one method of passive NDA, exploiting the gamma-ray interaction with matter and resulting ionization [3]. A detailed analysis of the spectrum is used to determine the identity and quantity of gamma-ray emitters in the source. Of particular interest to NCS is fissile source material.

Since the initial development of passive NDA, multiple facets of science have taken hold and utilized the capabilities. With the increased development of smaller electronics, handheld and portable devices have recently received increased interest [4]. Portable NDA methods have been applied in the following arenas:

- Radioactive waste segregation
- Environmental soils
- Crude oil pipeline scales
- Borehole logging
- Safeguards
- Radiation protection

I.A.1 Industries with Portable NDA Methods

I.A.1.a Radioactive Waste Segregation

Significant cost savings and operational efficiency may be realized by performing rapid non-destructive classification of radioactive waste at or near its point of retrieval or generation. Disposal regulations and waste acceptance criteria drive the need to segregate waste streams into various hazard levels. Recent improvements in gamma spectroscopy technologies have provided the capability to perform rapid in-situ analysis using portable devices including lanthanum halide and high purity germanium scintillators.

Pajarito Scientific Corporation has developed the TechniCART [5] as a piece of portable non-destructive assay equipment for in-situ measurements. The device is similar to the portable ISOCS detection system from Canberra Industries [6]. The detection

equipment consists of high purity germanium detectors, detector cooling mechanism, a multi-channel analyzer, a laptop computer with suitable software for analysis, and some sort of cart. The systems are modular and capable of being transported to new areas for assay, but the portability is limited.

Early screening and segregation of the waste with portable NDA equipment does allow a site operator to efficiently sentence and repackage waste, as necessary. Pajarito claims that the throughput of containers to any downstream high sensitivity assay units can be more effectively controlled and managed. The primary drawbacks of their technique are the lack of portability, long assay times, need for stable environmental conditions, and cost. However, in many cases, the benefits will outweigh the drawbacks.

I.A.1.b Environmental

In-situ gamma-ray spectroscopy is used for environmental measurement applications such as geophysical exploration, assessment of doses to the population due to radioactive fallout, and determination of soil erosion rates [7]. Environmental radiation measurements are often taken in-situ to prevent disturbance of entire areas of intact earth or to obtain more rapid results on a larger footprint.

Fallout nuclides, such as ^{137}Cs, measurements in soil are a common environmental application. The primary shortcoming of in-situ measurements on fallout nuclides is that the depth distribution of the radionuclide in the soil is unknown. With levels sometimes on the same order of magnitude as background radiation, discrimination in environmental measurements can be cumbersome.

Fernandes, et al. studied the applicability of gamma-ray portable spectrometers for in-situ measurements of ^{137}Cs contaminated soil by deriving an efficiency curve and Minimum Detectable Activity (MDA) for two detectors: CdTe and NaI. It was concluded that the in-situ portable system was only appropriate with activities one or more orders of magnitude larger than environmental levels. Specifically, the CdTe crystal is too thin to yield a large enough efficiency for low activity radionuclides, despite its excellent energy resolution. The NaI was not able to appropriately discern the nuclides of interest in the study (^{137}Cs and ^{7}Be) [8]. Nuclide activity is another term used to describe the radioactive decay rate of a nuclide.

Gutierrez-Villanueva et al. used Monte Carlo methods to estimate ^{137}Cs inventories by considering typical depth distributions corresponding to uncultivated and cultivated soils. The efforts were intended to show that laboratory calibration can practically be replaced by Monte Carlo simulation and therefore only require a small number of experimental measurements. The research showed that MCNP properly reproduced efficiency values and peak to forward-scatter ratios for a portable HPGe detector [9].

I.A.1.c Crude Oil Pipelines

Scale accumulation in oil pipelines is a common problem in the oil industry and leads to reduced fluid flow and costly disposal issues [10]. Deposits seen in pipelines include barium and calcium carbonates and sulphates, or iron sulphide. Radium salts arise from the uranium and thorium present in oil-bearing rock formations and may replace the

calcium and barium [11]. This creates what is industry known as NORM (technologically enhanced naturally occurring radioactive material) [12].

Industry safety regulations require that samples be measured and counted in their original form within the pipe, thus creating non-homogeneous sample geometries. Habib et al. developed a technique using Monte Carlo to derive detection efficiencies based on actual sample geometries. A portable ORTEC HPGe detector was utilized for the measurements and an activity was calculated using the Monte Carlo calibration [13]. Photopeak net counts were derived from the peak search algorithm in ORTEC Gamma Vision software.

The research concluded that Monte Carlo simulation is a valuable tool to assist in detector efficiency for calculation of activity in non-homogeneous sample geometries. Researchers concluded that the results are adequate for safety purposes and to help reduce personnel exposure to radiation and facilitate NORM management plans.

I.A.1.d Borehole Logging

Natural gamma-ray borehole logging is recognized as a feasible technique for evaluating uranium deposits [14]. Uranium mine grade and reserve is evaluated through means of borehole logging. The measurement is acquired by lowering a detector probe into a hole and acquiring the response therein.

Uranium exploration in the world's main uranium producing countries including Kazakhstan and China utilize an old method called gross-count gamma-ray logging whereby the total gamma-ray intensity is measured. This includes contributions from ^{40}K,

uranium series, and thorium series. The use of natural gamma-ray spectra logs was suggested in 1970; however, gross-count gamma logs are still the primary method used today [14].

In recent years, borehole spectroscopy with a NaI scintillator has been used to eliminate the effects of ^{40}K and thorium series elements. Drawbacks within the industry are noted as follows: the cost for a spectrometer is several times greater than that for a gross-count scintillator, comprehensive performance for the NaI detector is not excellent, spectral measurements require more time than gross-count surveys, the system is difficult to maintain in the field, and frequent calibration is necessary [14, 15].

Wu and Tang developed a new method utilizing Monte-Carlo simulation models to acquire response functions for calculation of activity concentrations of ^{40}K, ^{232}Th, and ^{238}U present in rock [14]. A $LaBr_3$ crystal was selected for the measurements because of its higher resolutions and shorter integration time under synonymous physical and geometric conditions. In this work, $LaBr_3$ is referred to as LaBr for simplicity.

In their application, Monte-Carlo simulation minimizes the amount of experimental work required and can deal with the physical and geometric conditions tactfully. For a complex logging environment, the arrangement is described in a robust manner. The calculated response functions offer direction for the design of borehole detection systems, provide a technical basis and basic data for spectral analysis of natural gamma-rays, and offer a sourceless calibration in uranium quantitative interpretation.

I.A.1.e Safeguards

The International Atomic Energy Agency (IAEA) uses a variety of gamma radiation detectors to verify nuclear material. Hand-held NaI radioisotope identification devices are used to detect the presence of radioactive material where a lower resolution is sufficient, as they benefit from a generally higher sensitivity [16]. The IAEA continues to investigate the possible uses of LaBr in portable detectors. Portable enrichment measurements are typically made with a system of portable Canberra HPGe detectors, portable semiconductor CZT and portable NaI monitoring equipment. The system is more "modular" than portable [17].

Dias et al. investigated the use of LaBr scintillation detectors for enrichment estimations in Brazilian nuclear facilities under safeguards. It was concluded that the overall performance of the LaBr detector was adequate for enrichment measurements on thin containers. The temperature stability and repeatability of measurements showed promise for use of the crystal in safeguards applications in the future [18].

Mace and Smith deployed an automated system composed of NaI and LaBr detectors in a field prototype for enrichment measurements on UF_6 cylinders for the IAEA. The design, calibration and characterization was successful in proof-of-principle, and the authors are continuing work on a viability of the hybrid NDA method that combines traditional (185.7 keV) and non-traditional (high-energy neutron capture gamma rays) signatures in a single instrument [19].

I.A.1.f Radiation Protection

Following an exposure event, triage-style assessments are used to identify persons potentially exposed to high doses of radiation. Historically, simple Geiger-Mueller (G-M) probes were used for these purposes, although it is recognized that these instruments contain no information on incident photon energy. In the event of a criticality, it is impossible to differentiate between photons emitted by contamination and activation of sodium in the exposed worker's blood with a G-M counter.

Veinot et al. examined the use of a portable gamma spectrometer for assessing blood sodium activation. The portable spectrometer was successfully able to detect low levels of neutron dose and discriminate between surface contamination and blood sodium activation [20].

I.A.2 Portable Detector Options

Scintillation spectrometers play a large role in detection and spectroscopy of energetic photons as well as neutrons. They are utilized in nuclear and high-energy physics research, medical applications, diffraction, NDA, nuclear treaty verification and national security, and geologic exploration [21].

Ideal scintillators possess high detection and scintillation efficiency, good energy, time and spatial resolution, short dead-time, fast scintillation response and mechanical and chemical stability [21]. These requirements have driven considerable research and development in new inorganic scintillators with enhanced performance.

Traditional methods of locating radionuclides have relied on G-M counters and gross gamma ray counting through NaI scintillator detection methods. The NaI crystal

can be produced in large sizes, yielding a good detection efficiency [3]. The light output is bright and intrinsic efficiency high. NaI scintillator detectors are relatively small, cheap and portable. This makes NaI detectors popular and easy to use for field detection of radioisotopes in safeguards applications [16]. However, NaI detectors are sensitive to changes in the environment and can be subject to shifts in the spectrum. Additionally, the poor resolution renders them not very suitable for complicated mixtures of gamma-ray producing materials.

Cerium-doped scintillating fibers composed of lithium-silicate glass are the center of the development effort in producing a detector with sufficient sensitivity to search for undeclared materials (in this section referred to as LaBr:Ce, or LaBr shortened, and LaCl:Ce, or LaCl shortened). They are portable and sensitive to both neutron and gamma radiation; however, tests have shown that there was insufficient discrimination between gamma and neutron radiation [16].

Recent developments revealed the LaBr to be a valuable scintillator for room temperature gamma spectroscopy when compared to the NaI [16, 22]. Originally, noted limitations include the high cost and temperature instability; however, these factors have been substantially circumvented in the last few years. Experience has shown that LaBr offers better performance than LaCl:Ce in terms of resolution, especially in comparison to NaI. It is possible to obtain 2.8% relative energy resolution values at 661 keV from a large sample of LaBr:Ce [21]. This is because of the very high light output at a wavelength suited for the photocathode and very small non-proportionality with photon energy of the

scintillator (less than 5%). The properties of LaBr:Ce, LaCl:Ce and NaI(Tl) are summarized in Table I .

Table I. Comparative Properties of Scintillators

Property	LaBr:Ce (5%)	LaCl:Ce (10%)	NaI(Tl)
Density (g/cm^3)	5.29	3.79	3.67
Decay time (ns)	20	25	240
Light Output (ph/MeV)	63,000	46,000	39,000
Energy Resolution (at 662 keV)	<3% 6.4% (185.7 keV)	<4%	7-8%
Wavelength (mm)	380	350	415

LaBr crystals do have a drawback in their internal radioactivity due to naturally occurring radioisotopes ^{138}La and ^{227}Ac. ^{138}La, which makes up 0.09 percent of naturally occurring lanthanum, produces two energies: a 0.7887 MeV gamma-ray from beta decay (34%) to stable ^{138}Ce and a 1.4358 MeV gamma-ray from electron capture (66%) to stable ^{138}Ba [14, 23].

Enrichment determinations on UF_6 containers suffer from several severe limitations. In recent years, efforts were made to overcome some of the limitations. These included use of CZT detectors; however, their small size and low efficiency limit their use. LaBr detectors have a much higher efficiency than the largest CZT detectors and their energy resolution is comparable to CZT and 2-3 times better than NaI detectors. For these reasons, they are particularly attractive for applications involving enrichment measurements. The efficiency of the LaBr is measured to be about a factor of two below

a 3 in. NaI [24] and comparable to that of a coaxial germanium detector. Below 344 keV, the LaBr efficiency is higher than that of the germanium detector (around 25% more at 185.7 keV).

Factors affecting linearity of the overall detection chain can be the conversion of the photon energy into scintillation light, the electron multiplication factor in the photo-multiplier tube (PMT), or the conversion of the pulse height to a channel number. The main source of non-linearity is due to the visible light production as a function of the photon energy [24]. The LaBr has shown a maximum non-proportionality of about 5% compared to a 1 in. x 1 in. NaI(Tl) at around 20%.

High resolution gamma spectroscopy is performed with HPGe detectors. These systems require liquid nitrogen to cool down and achieve high resolution, typically in the range of 550-700 eV FWHM at 122 keV. When coupled with appropriate software, they are heavily utilized in safeguards applications for the intrinsic determination of Pu isotopic composition and U enrichment. Alternative cooling mechanisms have been developed, particularly for unattended systems [16].

Portable HPGe systems are available and typically come equipped with a cart, a laptop computer, a heavy collimator, and a detector with cooling mechanism. Although the systems are advertised as portable, they are still relatively cumbersome for continuous field measurements. Hand-held NaI detectors may be used to supplement portable HPGe systems in order to locate hot spots prior to measurement. DOE complex sites have determined that this is the most effective means to attain a quantitative assay suitable for in-situ characterizations [5].

A hand-held, light weight HPGe detector would be an ideal device for in-situ and ex-situ field characterization. Devices that are advertised as such are both very expensive (approximately 4 times that of a LaBr system) are not entirely hand-held or light weight. For purposes described herein, the capabilities of the LaBr are considered overly adequate. In this context, adequate is defined as resolution high enough to isolate uranium photons, uranium photopeak count rates at least an order of magnitude above background, and environmental operating conditions within instrument limits.

I.A.3 LaBr and InSpector 1000

For the reasons listed in the previous section, the LaBr crystal is selected for this research. The LaBr inorganic scintillator was discovered in 2001 and, as previously mentioned, has proven to be an excellent combination of high light yield and energy resolution. Operating conditions are more robust than the NaI and the higher resolutions offer better characterization potential in mixed gamma fields. This leads to better isotope classification. In general, compared to a NaI detector, the LaBr is able to obtain more peaks and need shorter integration time under the same physical and geometric conditions. The NaI has also been shown to be difficult to maintain in the field, requiring frequent calibration [15, 18].

The InSpector 1000 instrument from Canberra Industries is a hand-held MCA with a LaBr probe, designed for easy portability, decontamination and rugged conditions. It offers easy nuclide identification for less sophisticated users, or full spectral analysis capabilities for expert users. The LaBr scintillator probe is a sourceless stabilized gamma probe with energy resolution between that of a NaI scintillator and HPGe detector. The

sourceless stabilization allows performance throughout extreme temperature variations and limits energy drift that generally degrades isotope identification results. The result is a uniform response over the full temperature range. This feature is useful in site processes, which operate in year round extreme and harsh temperature environments. The specifications that are pertinent to this work are detailed in Table II [25].

Table II. InSpector 1000 Specifications

Performance		Environmental	
Energy Range	30 keV to 3 MeV	Operating Temperature	-10 to + 50 °C
Integral	0.1% over top 99% of conversion range	Humidity	up to 80%
Throughput	> 50 kcps	Shock	can withstand drop from 1 m onto concrete (not including probe)
Input Count Rate	> 500 kcps total	Protection Rating	meets IP 54 specifications
Live Time Preset	1 – 1,000,000 s		
Channel Storage	32 bits		
Spectral Data Storage	512 spectra of 1024 channels each		
Battery		**Physical**	
Type	two-cell rechargeable Li-ion	Weight	< 2.4 kg (5 lb 3 oz)
Operating Time	~ 9 hours	Size (without probe)	19.0 x 16.5 x 6.4 cm (7.5 x 6.5 x 2.5 in)

The distinct difference between the traditional NaI used in “gross gamma counting” remediation surveys and the InSpector 1000 with a LaBr probe is the qualitative distinction that can be made using the InSpector 1000 and associated MCA. This

qualitative distinction is used to maximize quantitative capabilities with the proper technical basis. Isolating the fissile nuclide contribution to a gamma signature and allocating the response correctly can greatly reduce on-site handling time and enhance safety measures. The LaBr technology combined with the calibration basis provided in this dissertation provide a means of early characterization of fissile material for proper handling and risk of the radiological material at hand.

I.B. SITE HISTORY AND OVERVIEW

In order to tailor the methods to specific needs and satisfy an implementation technique, a specific facility must be described. The specific needs of the facility allow options within the methods to be selected. Additionally, it converts a theoretical idea to an actual application. The recipient facility for the methods described herein is the Westinghouse Hematite Decommissioning Project.

I.B.1 The Hematite Decommissioning Project

The Westinghouse Hematite Decommissioning Project (HDP) is a former nuclear fuel cycle facility located near Festus, Missouri that is currently undergoing decommissioning. Decontamination and Decommissioning (D&D) of the equipment and surfaces within the process buildings, in addition to the buildings themselves, was accomplished in the first phase of the project. The current phase of the site-wide remediation operations includes clean-up of facility process wastes that were consigned to unlined burial pits, and removal and disposition of building slabs and subsurface piping [26]. These tasks require categorization and characterization of fissile and non-fissile

radionuclides and hazardous materials before on-site handling and finally shipment to a permanent resting place. Because fissile nuclides are included in the process, a nuclear criticality safety program was implemented. The work in this dissertation is intended to provide a novel methodology to aid in optimization of the processes described. Additional benefits lie in understanding the radiological health risk and industrial hygiene risk (unrelated to nuclear criticality safety) of the material under investigation.

I.B.2 Nuclear Criticality Safety (NCS) and the InSpector 1000

Traditionally, remediation surveys for classification of and decision making for fissile material are performed with a windowed 2 x 2 sodium iodide (NaI) detector set to detect ^{235}U gammas (> 75 keV). The HDP has implemented an NCS program based on a gross gamma screening response from a NaI detector. HDP burial pits contain an abundance of depleted uranium ($\leq$ 0.96 wt. % ^{235}U in UO_2), thorium, and radium. These nuclides emit gammas and produce high count rates in a windowed NaI. Detection of these nuclides is pertinent for waste management and radiological exposure purposes, but can cause unnecessary criticality safety controls on material free or in low concentration of ^{235}U, but in high concentration of another nuclide.

Criticality safety controls traditionally impose volume, mass, spacing, and concentration restraints which result in administrative and engineered controls on processes. Stringent, but required, these controls are resource intensive. When the controls are not necessary, valuable resources are wasted. As an effort to eliminate many of the unnecessary criticality safety controls, in addition to gaining a real-time understanding of the nature of the material under interrogation, a program designed around

the discrimination capabilities of a portable multi-channel analyzer (MCA) was developed. The equipment selected is an MCA coupled to a lanthanum bromide (LaBr) scintillator probe which is known for its excellent energy resolution for immediate material categorization. This allows qualitative discrimination between ^{235}U and other nuclides not of concern from an NCS standpoint. Utilizing these properties of the detector, NCS is able to exercise exemption from criticality control on items or areas. This proves especially pertinent in the case of locating an in-situ Stop Work point (a potential subcritical mass limit) based on NaI detector response.

Specific to HDP operations, the limits above which materials encountered during remediation activities are designated as Non-NCS Exempt Material are based upon the concentration of fissile nuclides in the material, or the total fissile nuclide mass content of the material. Non-NCS Exempt Material is the classification given to the material that has a fissile nuclide concentration greater than the limit established for NCS and requires criticality safety controls to ensure its safe handling, packing, processing, and storage [27]. Specifically, materials determined to satisfy either of the following limits are designated as NCS Exempt Material and require no controls to ensure they remain safely subcritical:

- A fissile nuclide concentration ≤ 0.1 g ^{235}U/L; or
- A total fissile nuclide mass content ≤ 15 g ^{235}U/L and occupying a volume of at least 5 L; or
- A ^{235}U/total U enrichment ≤ 0.96 wt. %

I.C. RESEARCH OBJECTIVES

The objective of this dissertation is to develop a methodology and validate it via practical implementation for identification and quantification of low and intermediate level fissile nuclide contaminated waste, particularly pertaining to decommissioning of fuel cycle facilities but can be extrapolated to many applications. The contribution of this work is a method to quickly characterize ^{235}U in common, heterogeneous configurations using Monte Carlo methods and show that this method is easily implemented for a decommissioning site. The objective is accomplished utilizing Canberra's InSpector 1000 with LaBr probe portable gamma spectroscopy instrument. The research consists of the following components:

- Development of a high fidelity model of the detector and its response functions;
- Scoping studies of the non-destructive assay process input parameters;
- Development of methods for estimating fissile material mass and enrichment based on detector responses;
- Parametric studies to determine optimal implementation (e.g., detector field of view) of developed methods;
- Validation via benchmark and practical implementation scenarios for developed methods.

During remediation of unknown buried material and enclosed pipes, most physical parameters of the sample for the assay are also unknown. This research investigates how to apply conservative assumptions to unknown parameters in order to obtain a bounding

estimate on fissile material in low (LLW) and intermediate level waste (ILW) matrices. Development of the conservative assumptions and an appropriate assay process are key milestones to reach the final objective. In this context, conservative assumptions are defined as modeling assumptions that are intended to over-predict the actual value by some, but not exhorbent amounts. Likely no more than 20% overage. For example, the highest value from a set of values was selected and used for each described case.

The developed methods offer many advantages to NCS and field operations over traditional means of in-field material assay. Foremost is the application of appropriate safety measures. Characterizing fissile material upon discovery and/or before visualization and disturbance can add a drastic measure of safety to any fissile material handling operation. Quick quantification of the radionuclides present ensures an even further level of radiological safety. Further, time and financial resources can be drastically reduced when nuclear material is correctly identified and adequately characterized, eliminating unnecessary controls. Adequately characterized, in this context, is defined as a material characterization that satisfies the site regulatory requirements for material control and accountability.

I.D. PROCEDURE AND METHODS

The goal of many gamma-ray spectroscopy applications is to compute a corrected count rate for the gamma-ray of interest based on the raw rate of data acquisition, rate-related loss and an attenuation correction factor. When correction and attenuation factors are properly defined, the corrected count rate is often directly proportional to the desired quantity, such as mass of ^{235}U or enrichment. Obtaining proper correction and attenuation

factors is not a simple task and depends on a multitude of modeling assumptions and empirical relationships.

Because the size and shape of nuclear material samples vary widely, it is difficult to construct appropriate calibration standards. In principle, calibration standards are not needed if the detector efficiency is accurately known as a function of source position and energy, if the counting geometry and the sample size and shape are accurately known, and if the gamma-ray emission rates are accurately known. The use of calibration standards reduces or eliminates the need to accurately know the detector efficiency, the counting geometry, and the specific activities.

In decommissioning and environmental remediation of LLW from former fuel processing facilities, little is known about the sample. The source term may be the best known material characteristic based on facility records, but form and geometry vary significantly.

The MCNP physics modeling code is used extensively in this research as a calibration basis. The code simulates detector responses to gamma-ray sources by mimicking the inherently random behavior of real physical events. The source region, which is both point-like and distributed, is selected, and each gamma-ray is tracked and tallied as it undergoes collisions within the detector volume. The final tally distribution represents the energy spectrum "seen" by the detector and can thus be used to obtain the overall efficiency for the source/detector/universe geometry [28].

The question is posed as to how well the base modeling assumptions represent the actual configuration and which factors render the model invalid. As configurations and

heterogeneity become more and more complex, the attempts to match reality to a base model become more distant. For nuclear criticality safety applications, it is important to provide bounding scenarios in the base model assumptions. However, maintaining a degree of realism is also desired. The model and underlying assumptions must be understood to a degree of reliability for the realistic applications. Experimental testing, validation, and parametric studies serve as the basis for this understanding.

Using various three dimensional physics models, a calibration basis and validation methodology is developed for Canberra's InSpector 1000 with LaBr probe instrument. The methods are implemented into an NCS program for low and intermediate level waste characterization both in-situ and ex-situ at Westinghouse HDP. In addition, methods to characterize low and intermediate level fissile material holdup in subsurface piping is also developed. Using parametric studies and experimental validation, these methods are intended to serve as a basis for bounding fissile material loading in an array of scenarios encountered at LLW/ILW remediation sites.

CHAPTER II

HEMATITE DECOMMISSIONING PROJECT DESCRIPTION

The Hematite facility of Westinghouse Electric Company LLC is located on a site in Jefferson County, Missouri, approximately ¾ mile northeast of the unincorporated town of Hematite, Missouri and 35 miles south of the city of St. Louis, Missouri. The site is a former nuclear fuel cycle facility that is currently undergoing decommissioning. The Hematite site consists of approximately 228 acres, although operations at the site were confined to the "central tract" area which spans approximately 19 acres. The remaining 209 acres, which is not believed to be radiologically contaminated, is predominately pasture or woodland.

The central tract area includes former process building slabs, subsurface piping, facility administrative buildings, a documented 10 CFR 20.304 burial area, two evaporation ponds, a site pond, storm drains, sewage lines with a corresponding drain field and several locations comprising contaminated limestone fill [26].

II.A. SITE HISTORY

From its inception in 1956 through 1974, the Hematite facility was used primarily in support of government contracts that required production of high enriched uranium (HEU) products. From 1974 through the plant closure in 2001, the focus changed from government contracts to commercial fuel production. Specifically, operations included the conversion of uranium hexafluoride (UF_6) gas of various ^{235}U enrichments to uranium oxide, uranium carbide, uranium dioxide pellets, and uranium metal. These products were

manufactured for use by the federal government and government contractors and by commercial and research reactors regulated by the AEC and its successor, the NRC. Research and development was conducted at the plant, as were uranium scrap recovery processes. Since its inception, seven owners have overseen the plant. Mallinckrodt Chemical Works, Mallinckrodt Nuclear Corporation, United Nuclear Corporation, Gulf United Nuclear Fuels Corporation, and General Atomic Company owned the plant for the government-focused phase of operations. Combustion Engineering Inc. (CE) and Westinghouse Electric Company LLC owned the plant during the commercial phase of operations [29].

Much of the work on behalf of the government was classified, and therefore, specific details regarding the exact nature of the process are not known. Hematite also contracted directly with the Oak Ridge AEC office and other government contractors for the recovery of uranium from scrap materials. Scrap recovery projects at Hematite included the recovery of uranium from scrap generated by a variety of U.S. Navy projects.

The Hematite facility was used for the manufacture of low enriched (i.e., $\leq$ 5.0 wt.% ^{235}U/U), intermediate enriched (i.e., > 5 wt.% and up to 20 wt.% ^{235}U/U) and high enriched (i.e., > 20 wt.% ^{235}U/U) materials during the period 1956 through 1974. In 1974 production of intermediate and high enriched material was discontinued and all associated materials and equipment were removed from the facility. From 1974 to the cessation of manufacturing operations in 2001, the Hematite facility produced nuclear fuel assemblies for commercial nuclear power plants.

On September 11, 2001, Westinghouse notified the NRC that all principal activities, specifically those related to the manufacture of nuclear reactor fuel utilizing LEU, at the Hematite site had ceased. Westinghouse received an amended license in April 2002 to change the scope of activities to those associated with decommissioning and reduce the possession limits for sources and Special Nuclear Material (SNM).

Accountable uranium inventory was removed and D&D of equipment and surfaces within the process buildings was undertaken. This effort resulted in the removal of the majority of process piping and equipment from the buildings. At the conclusion of that project phase, the accessible surfaces of the remaining equipment and surfaces of the buildings were sprayed with fixative in preparation for building demolition. More recently, the former process buildings have undergone demolition, with the majority of the building demolition debris shipped off-site. The building slabs remain, and are part of the scope of current decommissioning activities.

The Hematite site is known to contain the following radionuclides as contaminants: ^{99}Tc, ^{232}Th, ^{234}U, ^{235}U, and ^{238}U. Trace amounts of ^{241}Am, ^{237}Np, ^{239}Pu, and ^{240}Pu are expected to be present in trace concentrations [26].

II.A.1 Decommissioning Areas

II.A.1.a Burial Pits

Historic operations at the Hematite site resulted in the generation of a large volume of process wastes contaminated with uranium of varying enrichment. Records indicate that as early as 1958, facility process wastes were consigned to on-site unlined burial pits.

Historic documentation [29] indicates that 40 unlined pits were excavated and used for the disposal of contaminated materials generated by fuel fabrication processes between 1965 and 1970.

Consignment of the waste to the burial pits was reported to be in compliance with AEC regulation 10 CFR 20.304 [30]. Facility operating procedures described the size and spacing requirement for the burial pits, in addition to the required thickness of overlying soil cover (4-ft), and the quantity of radioactive material that could be buried in each pit. It is possible that burial procedures were not followed, and over time the overburden soil thickness may have changed.

United Nuclear Corporation (UNC) and Gulf United Nuclear Fuels Corporation (GUNFC) maintained detailed logs of burials for the period of July 1965 through November 1970. The Burial Pit Log Books contain approximately 15,000 data entries listing the date of burial, pit number, a description of the particular waste consignment, the uranium mass associated with the subject waste, and miscellaneous logging codes. Some log books also list a percent enrichment for the uranium [31].

The information recorded in the Burial Pit Log Books indicates that the waste consignments comprised a wide variety of waste types. This is further supported by interviews with past employees [32]. A listing of the types of waste materials that may be present in the burial pits is provided in Table III. The primary waste types expected to be encountered are trash, empty bottles, floor tile, rags, drums, bottles, glass wool, lab glassware, acid insoluble, and filters. Buried chemical wastes include hydrochloric acid,

hydrofluoric acid, potassium hydroxide, trichloroethylene (TCE), perchloroethylene (PCE), alcohols, oils, and waste water.

Table III. Buried Waste Characteristics

Process Metals and Metal Wastes	
• High enriched uranium (93-98%)	• UO_2 samarium oxide
• Depleted and natural uranium	• UO_2 gadolinium
• Beryllia UO_2	• Molybdenum
• Beryllium plates	• Uranium dicarbide
• uranium-aluminum • uranium-zirconium	• Cuno filter scrap that included beryllium oxide
• Thorium UO_2	• Niobium pentachloride
Chemical Wastes	
• chlorinated solvents, cleaners, and residues (PCE, TCE)	• ammonium bichloride • liquid organics
• acids and acid residues	• sulfuric acid
• potassium hydroxide (KOH) insoluables	• uranyl sulfate
• ammonium nitrate	• acetone
• oxidyne	• methyl-alcohol
• ethylene glycol	• chlorafine
	• pickling solution
Other Wastes	
• floor tiles	• contaminated limestone
• process equipment waste oils	• UO_2 ThO_2 paper towels
• oily rags	• pentachloride from vaporizer
• TCE/PCE rags	• used magnorite
• used sample bottles	• $NbCl_5$ vaporizer cleanout
• Green salt (UF_4)	• Item 51 Poison Equipment
• calcium metal	• Asbestos and Asbestos Containing Material

The recorded [31] total uranium mass associated with the waste consignments range from 178 g ^{235}U to 802 g ^{235}U per burial pit with a maximum amount associated

with any single waste consignment (i.e., burial item) of 44 g ^{235}U. The uranium enrichment of waste items consigned to the burial pits ranged from 1.65 to 97.0 wt.% ^{235}U/U. The waste consignments representing the highest recorded ^{235}U content included:

- Wood filters (4 entries ranging from 22 to 44 g ^{235}U);
- Metal shavings (one entry at 41 g ^{235}U);
- Leco crucibles (4 entries ranging from 29-31.6 g ^{235}U); and
- Reactor tray (one entry at 40.4 g ^{235}U).

After over one year of remediation operations, it is well understood that many more items and larger quantities of ^{235}U were consigned to the burial pits. Additionally, based on interviews with former site employees [32], it is possible that on-site burials other than those conducted under 10 CFR 20.304 [30] may have occurred as early as 1958 or 1959. Burial logs for undocumented pits do not exist and it is not known where they are located or what they may contain.

II.A.1.b Subterranean Structures

Several former process buildings and facility administration buildings are situated on the Hematite Site. The former process buildings were built on a foundation of concrete. Each of the former process buildings required a combination of storm water drains and lines, sanitation drains and lines and process drains and lines. The storm water lines are interconnected with the process drain lines from the former process buildings. The process drain lines (when in use) were intended to collect condensate from evaporation processes, overflow of water from various systems, and provide a route for free-release solutions

from laboratory sinks. Both the storm water lines and the process drain lines are interconnected and tie into a large main trunk that extends to the nearby local creek. The sanitation lines are completely independent from the other lines and lead to septic tanks which filter into a sand and gravel drain field [26, 37].

The process piping is composed of cast iron while some of the sanitation lines could comprise PVC.

II.B. NUCLEAR SAFETY PROCESS

II.B.1 Burial Pits

NCS governs the requirements for appropriate fissile material characterization thus driving the pursuance of better characterization methods. This section provides an overview of the main process employed for buried waste and contaminated soil remediation activities as they pertain to nuclear safety. From a NCS perspective, the general aim of the buried waste and contaminated soil remediation activities is to:

- Identify, carefully extract, and segregate any item(s) or region(s) of soil/waste that contain, or could potentially contain, fissile material in quantities that would warrant NCS controls. These items are referred to as Non-NCS Exempt Materials in this process.
- Evaluate and characterize the segregated Non-NCS Exempt Materials for fissile nuclide content, to ensure safe handling, packing, processing, storage, and proper disposition.

Prior to removal of soil/waste from a remediation area of the Hematite site, comprehensive in-situ radiological survey and visual inspection of a clearly defined survey area (i.e., area to be exhumed) is undertaken to identify Non-NCS Exempt Materials.

The objective of in-situ radiological surveys is to identify hot spots. From an NCS perspective, Hot Spots are defined as a distinct in-situ location where detector radiation measurements indicate the presence of an elevated quantity of ^{235}U (whether one object, a group of objects, or a cluster of material) when compared to the quantity of ^{235}U in the surrounding area. The in-situ radiological survey typically uses NaI scintillator probes to provide gross gamma ray measurements of the surface area of interest. The NaI is set to detect ^{235}U gammas (> 75 keV).

Any item or region of soil/waste with an average fissile nuclide concentration exceeding 0.1 g ^{235}U/L is defined as a Hot Spot. The 0.1 g ^{235}U/L threshold provides a high degree of assurance that any items with elevated levels of ^{235}U contamination would be identified. The NCS program is also used as a vehicle to drive compliance in waste management for alternate disposal at U.S. Ecology Idaho [27].

HDP burial pits contain an abundance of depleted uranium ($\leq$ 0.96 wt. % ^{235}U/U in UO_2), thorium, and radium. These nuclides have a high gamma emission rate and produce high count rates in windowed NaI detectors. Detection of these nuclides is pertinent for waste management and radiological exposure purposes, but can cause unnecessary criticality safety controls on material free or in low concentration of fissile nuclides.

Criticality safety controls traditionally impose volume, mass, spacing, and concentration restraints which result in administrative and engineered control on processes. Stringent, but required, these controls can be resource intensive. When controls are not necessary, valuable resources are wasted and the integrity of an NCS program is undermined. Any effort to eliminate or reduce unnecessary criticality safety controls, in addition to gaining a real-time understanding of the nature of the material, is greatly appreciated by an NCS program.

Field characterization serves an important role in the NCS process in order to better understand if it falls into any of the above categories prior to handling, packaging, transport, or storage. Potentially, the material could even be characterized prior to exhumation or disturbance.

II.B.2 Concrete Slabs and Subterranean Structures

Typically concrete structures such as foundations and slabs are exempt from criticality safety during decommissioning operations due to the small potential to contain significant quantities of fissile material. However, spills of process materials during manufacturing operations at HDP have been documented [29]. It is possible that these incidents, especially those involving solutions, may involve significant quantities of fissile material.

To address the potential for encountering significant quantities of fissile material associated with contaminated concrete during decommissioning operations, all concrete excavation is controlled. This control consists of a thorough assay of the concrete prior to

excavation. The assay methods used are a combination of destructive core sampling and NDA.

There are several hundred feet of subterranean piping located within the Hematite Site. Typically, this type of decommissioning debris does not necessitate concern regarding NCS. However, the legacy processing plant was designed such that the process piping used for evaporator overflows, process water runoff, and laboratory sinks were directly conjoined with this underground system. Therefore, excavation of the storm water piping extending to the nearby creek is handled as if it were process piping. In addition, the legacy processing plant was designed in a manner that tied the laboratory sinks and industrial washing machines used to clean personal protective equipment to the sanitation lines. Therefore, excavation of the sanitation lines is treated as if it were process piping. The remaining portion of the subterranean piping consists of the processing lines used for evaporator overflows, process water runoff, and laboratory sinks that were formerly used during fuel manufacturing operations.

Prior to excavating any section of piping, the pipe section is first assayed using NDA equipment to assign fissile mass quantities to each foot of pipe. This information is used to determine whether the pipe section must be extracted intact from the ground or whether it can be crushed in place and exhumed as debris.

If the intact pipe assay determines the material meets NCS Exempt Material criteria, the pipe may be crushed in place. Prior to exhumation of the debris, the material undergoes an additional surface assay and remediation process mirroring the process for the burial pits. If the decision is made to excavate the pipe intact, it must first be

determined via assay whether the section of pipe falls into the NCS Exempt Material or Non-NCS Exempt Material limits.

II.C. CURRENT DECOMMISSIONING STATUS

D&D of the equipment and surfaces within the process buildings, in addition to the buildings themselves, was accomplished in the first phase of the project. The current phase of the site wide remediation operations includes clean-up of the burial pits, removal and disposition of building slabs and subsurface piping, removal of contaminated limestone, removal of an on-site storage barn, and removal of a buried contaminated roof.

II.C.1 Site Remediation Objectives

HDP remediation areas are excavated to a depth where historical knowledge, and/or visible and radiological evidence indicate that buried wastes, radiological contaminants, and chemical contaminants of concern have been removed. Once these objectives are met, Final Status Survey (FSS) and hazardous material remediation goals can be verified. Verification of FSS goals is accomplished by a combination of in-situ radiological surveys and sample extraction analysis. Verification of hazardous material remediation goals is accomplished by a combination of direct measurements and sample extraction and analysis [26].

Following verification that FSS and hazardous material remediation goals have been achieved, the subject HDP remediation areas may be declared “remediated”, allowing initiation of site restoration activities such as backfilling and grading.

II.C.2 Burial Pits

The burial pits have been undergoing remediation since March 19, 2012 and have been subjected to disturbances in the past and characterization sampling initiatives. An extensive site sampling and survey program was implemented in 2008. In total, 146 sample cores were exhumed across the site, 73 of which were exhumed from the area of land occupied by the documented burial pits. Analysis of all the sample cores exhumed from the burial areas of the site revealed a maximum ^{235}U concentration of 153 pCi/g, equivalent to 0.11 g $^{235}U/L$[1] [27].

Excavation in the burial pits is a cumbersome process occurring both by hand shoveling into 20 L buckets and in 6-inch excavator lifts, when applicable. A combined effort between environmental engineers, nuclear engineers, civil engineers and construction engineers allows each 6" vertical excavation of waste to occur. Some of the excavated material will be used as re-use soil, and the remainder is considered waste.

As of August 2013, the documented burial pits sit at excavation depths between 8 and 20 feet deep, depending on the grid location. Suspected undocumented burial pit areas have not officially begun remediation, although burial pits have been identified in other

---

[1] Conversion of pCi/g to g $^{235}U/L$ concentration:

Specific activity of ^{235}U = 2.16107x10^{-6} Ci/g ^{235}U = 2.16107x10^{6} pCi/g ^{235}U,

$$\frac{153\frac{pCi}{g}(sample)}{2.16107\times10^{6}\frac{pCi}{g}235U} = 7.08 \times 10^{-5} g\ U235(sample),$$

$$7.08\ x\ 10^{-5}\ g\frac{U235}{g}(sample)\times 1.6\ g\frac{sample}{cc} = 0.11\ g\frac{U235}{L}$$

undocumented areas. A few grid locations are believed to be fully remediated and are currently subject to final remediation objectives to ensure completion.

II.C.3 Subterranean Structures

The former process buildings and other structures were demolished and reduced to grade level prior to decommissioning concrete slabs, foundations, subterranean process piping, and other subterranean structures.

In order to excavate the subterranean structures such as piping, surrounding soil, and septic systems, it is necessary to first remove any concrete slabs that are located on the surface of the ground above the piping. Once the concrete slabs are removed, soil is exhumed to expose the structure. Exposed piping is either crushed in place or lifted intact dependent on the appropriate excavation method.

As of August 2013, approximately 75% of the concrete slabs have been removed, and decommissioning of the subterranean piping is on-going.

CHAPTER III

METHODOLOGY AND NON-DESTRUCTIVE ASSAY APPLICATION

The calibration methods proposed herein were developed for a LaBr detector coupled to an MCA for NCS applications in decommissioning. With slight modifications to assumptions and geometrical modeling, this dissertation's methodology and framework can be applied for other purposes, to other detectors, and additional scenarios. The methodology is centered on the InSpector 1000 instrument from Canberra Industries with the LaBr IPROL-1 detector probe, for use at the Westinghouse Hematite Decommissioning Project, but the method application area is greater. The calibrations methods described could potentially be applied to currently operating facilities not in decommissioning status, or any soil area with fissile material contamination. Alterations in underlying assumptions easily convert the NCS premise to others, including material control and accountability or shipment characterization.

An attempt is made to achieve appropriate and quick ^{235}U characterization in anticipated application environments while preserving assurance of conservative (over predicted) values for nuclear safety. This is implemented through gamma spectroscopy. By utilizing the visibility of the ^{235}U photon at 185.7 keV in the given environments, conservative estimations to ^{235}U quantity and enrichment were developed without traditional reliance on attenuation coefficients. The decommissioning arena offers multiple characterization scenarios, each with a different set of built in conservatisms.

Conservatism in this context describes assumptions used in the modeling process that are likely above the actual value, but still within the realm of reason. For example, a conservative assumption may be a density that was seen in only one sample, but was the highest. It was then be applied to all cases as the conservative approach.

The areas of applicability are dependent on site-specific conditions; however, the same general approach can be utilized. The comprehensive set of fissile material estimation methods are developed for multiple general HDP scenarios:

- Dispersed ^{235}U in low-Z medium (i.e., soil) within a cylindrical container;
- Dispersed ^{235}U in low-Z medium slabs (i.e., in-situ and ex-situ ground material);
- Lumped ^{235}U in low-Z infinite medium;
- ^{235}U held up as UO_2 within piping.

A visual representation of the methodology is presented in Figure 1. The operational domains and design features of the selected site and detector (HDP and InSpector 1000 with LaBr probe) were used in the methodology development process to formulate assumptions and constraints for the process development. NCS limitations offer an additional design parameter in that the most conservative (bounding) application of any scenario is most desired. There are near countless encountered modeling geometries at a decommissioning site, but a selection process based on nuclear safety narrows the possibilities to a few conservative scenarios. An example is material composition for a "typical pail": stainless steel, plastic, tin, or glass—all materials seen in operations. The material with the highest attenuation was selected as conservative. Scoping calculations

offer a parametric study of the effects of each input component to the final result. This allows selection of the most conservative approach to apply the calibration basis. The calibration basis is then implemented as part of the overall process.

In this methodology, the LaBr detector and associated calibration basis is an integral component of the larger site nuclear safety program. Consequently, conservatism is interlaced with the desire to produce accurate assay results. Balancing the safety and accurate uranium assay aspects influences the overall derived methodology.

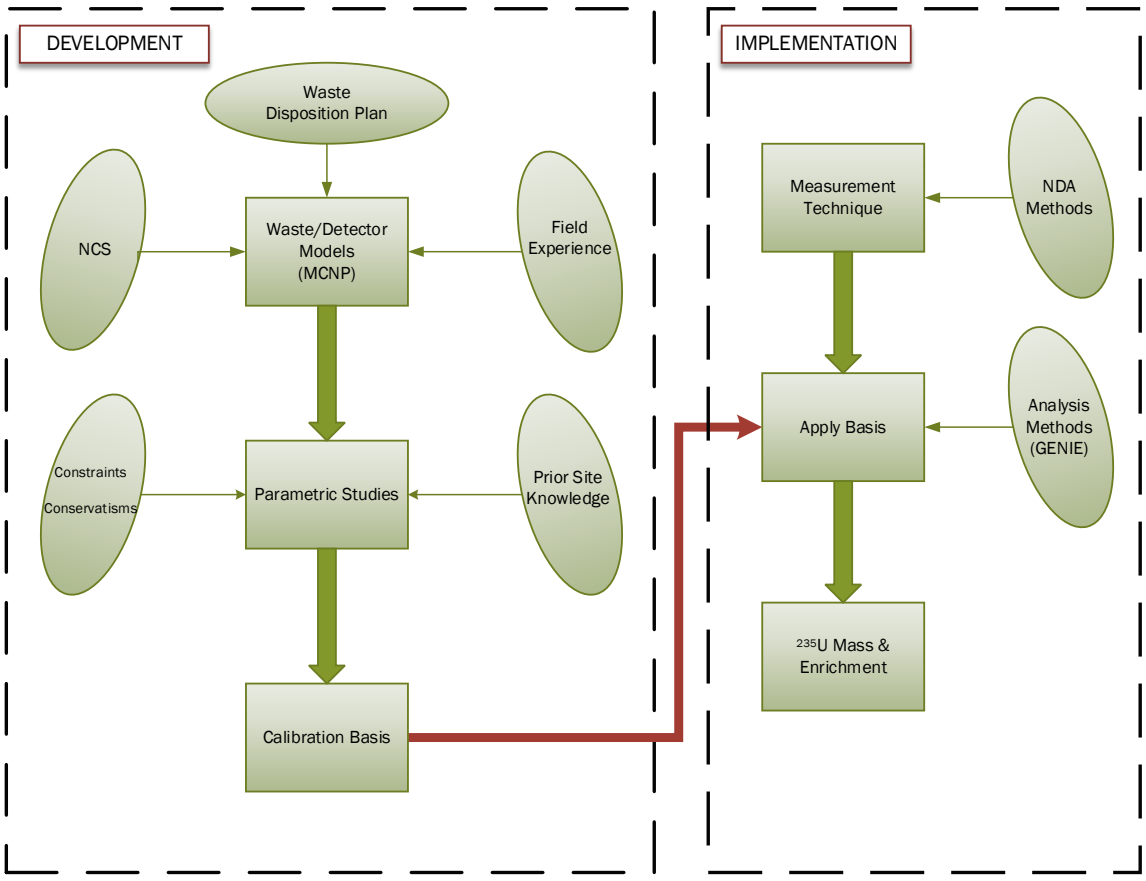

Figure 1. Methodology Scheme for Integrating Components.

For the left hand side (Development), two milestones are achieved in order to feed into the final developed product, a calibration basis. There are three components that feed into the Waste/Detector Models. Examples of each are given below:

- NCS- drives conservatism modeling assumptions such as full theoretical density of UO_2,
- Waste Disposition Plan- drives geometrical configurations such as 1' pipe sections for characterization and maximum fissile concentration limit of 0.1 g ^{235}U/L,
- Field Experience- drives modeling assumptions such as saturated soil as the contents of excavated drums to be loaded into Field Containers.

Once the basic Waste/Detector Models are developed, they are put through a series of parametric studies in order to determine which produces the most conservative results and remain within the adequate performance of the detector. Examples of each are given below:

- Constraints/Conservatism- drives geometric modeling assumptions for the parametric studies such as enrichment,
- Prior Site Knowledge- drives modeling assumptions for the parametric studies such as pipe sizes used, which are based on the site plans and drawings.

After the Waste/Detector Models are developed and put through a series of parametric studies, the most conservative calibration for each geometric scenario is selected taking into account what can easily be implemented in the field. These final

calibration bases are applied during the operational process, which leads to the right hand side (Implementation).

Before the calibration basis is applied, the measurement technique must be dictated. This takes into account traditional methods of NDA such as placement of the scintillator probe and count time. In addition, if the facility has measurement methods in place already, it may be best to keep those in mind.

Once the measurement is collected, the developed basis can be applied. The acquisition software is not related the quantification method, but they work together. The acquisition software (GENIE 2000) collects and analyzes the spectrum and photopeaks prior to the application of the calibration basis. At this point, the final result is achieved, that being ^{235}U mass and in some cases, enrichment.

The core of the methodology relies on a non-traditional calibration basis derived from Monte Carlo methods. Implementing a Monte Carlo based method requires development on both the measurement side and modeling side. Marrying the two components in the world of safety and conservatism is the subject of this dissertation. Specifics of the developed methodology are detailed in the following sections.

III.A. NON-DESTRUCTIVE ASSAY OVERVIEW

Non-destructive testing describes a wide group of analysis techniques used in science to evaluate the properties of a material, component or system without causing damage. The methods do not permanently alter the article being inspected, and therefore serve as a highly valuable technique that can save time and money in product evaluation and research. Gamma spectroscopy is one type of NDA.

Gamma spectroscopy is a quantitative study of the energy spectra of gamma-ray producing sources. A detailed analysis of the spectrum is used to determine the identity and quantity of gamma-ray emitters within the source. Of particular interest to NCS is fissile material.

The goal of many gamma-ray spectroscopy applications is to compute a corrected count rate for the gamma-ray of interest based on the raw rate of data acquisition, rate-related loss and an attenuation correction factor. When correction and attenuation factors are properly defined, the corrected count rate is often directly proportional to the desired quantity, such as mass of ^{235}U or enrichment. Obtaining proper correction and attenuation factors is not a simple task and depends on a multitude of modeling assumptions and empirical relationships.

Because the size and shape of nuclear material samples vary widely, it is difficult to construct appropriate calibration standards. In principle, calibration standards are not needed if the detector efficiency is accurately known as a function of source position and energy, if the counting geometry and the sample size and shape are accurately known, and if the gamma-ray emission rates are accurately known. The use of calibration standards reduces or eliminates the need to accurately know the detector efficiency, the counting geometry, and the specific activities [3].

In decommissioning and environmental remediation of low level waste from former fuel processing facilities, little is known about the sample. The source term may be the best known material characteristic based on facility records, but form and geometry vary significantly.

III.B. INSPECTOR 1000 WITH LABR PROBE

The InSpector 1000 instrument from Canberra Industries is a hand held, portable MCA with a LaBr probe. The LaBr probe is a sourceless, stabilized gamma probe with energy resolution superior to that of the NaI scintillator. Sourceless stabilization allows performance in extreme temperature variations and limits energy drift that can degrade isotope identification results. This results in a uniform response over the full energy range. This is useful in HDP operations which operate in year round extreme and harsh temperature environments (see Table II) [25].

The distinct difference between the lower cost Ludlum 2" x 2" NaI originally used in HDP remediation surveys and the InSpector 1000 with a LaBr probe is the qualitative distinction that can be made using the InSpector 1000 and associated MCA. The Ludlum 2" x 2" NaI utilizes a gross gamma counting system with no qualitative information. This qualitative distinction capability with an MCA is used to maximize quantitative capabilities with the proper technical basis.

Although NDA typically relies on energy spectra, methods of locating a radioactive source vary. As mentioned above, common methods of locating radionuclides have relied on NaI scintillator detectors and gross gamma-ray counting. The NaI crystal can be produced in large sizes, yielding a good detection efficiency. The light output is bright and intrinsic efficiency is high. NaI scintillator detectors are small, cheap, and portable. This makes NaI detectors popular and easy to use for field detection of radioisotopes. However, NaI detectors are sensitive to changes in the environment and can be subject to shifts in the spectrum.

Temperature dependence of the NaI scintillator has been studied for many years [33]. It has showed a maximum light output at about 20-30°C and then a reduced light output to about 70% at -40°C and to about 95% at 60°C. The decay time constant of the NaI light pulse exhibits a strong dependence at low temperatures [34]. According to Saint-Gobain, the thermal stability of the new LaCl and LaBr crystals is much better [35, 36]. The temperature performance of the LaBr crystal is much better than the LaCl, which is stable within ± 5% for the temperature range of -50 to 100°C. Again, according to Saint-Gobain, the light output of the LaBr is stable within ± 2% in the temperature range of -50 to 100°C, independent of the shaping time constant [35]. Based on temperature stability measurements performed by Moszynski et. al, the LaBr scintillator crystal offers superior performance for portable environmental measurements (border monitoring) [34].

Additionally, the poor resolution renders NaI not very suitable for complicated mixtures of gamma-ray producing materials. HDP presents harsh environmental conditions and mixtures of materials that require at least a medium resolution spectrum in order to isolate ^{235}U photopeaks. The presence of thorium poses interference problems because of both the number of photopeaks and the proximity to uranium photopeaks. In addition, the positive identification of uranium may depend on the 143 keV photopeak. This is because the radium contamination produces a 185.7 keV photon and qualifying the positive presence of uranium will depend on the presence of a 143 keV photopeak. For these reasons, the LaBr crystal is selected for this research.

The LaBr inorganic scintillator was discovered in 2001 and has proven to be an excellent combination of high light yield and energy resolution. Operating conditions are

more robust than the NaI and the higher resolutions offer better characterization potential [24]. This leads to better isotope classification. Methods of quantification and how those methods are applied to real scenarios are a subject of this dissertation.

III.B.1 Integration of InSpector 1000 and MCNP

Total efficiency incorporates two general components: intrinsic efficiency of the scintillator crystal and the absorption efficiency of the geometry and surroundings. It relates the number of photons emitted by the source to the number of pulses counted in the spectrum. A value reported by MCNP as the 'F8 tally' in the 186 keV energy bin is the number of 185.7 keV photons that deposit their entire energy in the sensitive volume of the crystal, divided by the number of 185.7 keV photons emitted from the source material. Theoretically, this takes into account the intrinsic efficiency of the detector and the absorption efficiency of the geometry and surroundings. This equates to overall (total) efficiency [28]. Adding an asterisk in front of the 'F8' (i.e. *F8) changes the unit from deposition of pulses to energy deposition in MeV.

The measured MCA spectrum must be processed in order to determine the number of detected photons in the 185.7 keV photopeak above the Compton continuum and the background. This number is then divided by the efficiency predicted by MNCP based on the given model to obtain the ^{235}U decay rate and then the mass of ^{235}U present in the sample.

When the InSpector 1000 with LaBr detector collects a spectrum, the raw number of counts in each photopeak is displayed. This displayed value is used in a mathematical

relationship (calibration function) obtained from an array of Monte Carlo calculations for the given geometry to obtain an estimate of ^{235}U grams.

Figure 2 is an overlay of the computational MCNP spectrum for 100 wt.% ^{235}U/U to an LaBr detector 60-second field measurement of what could be considered HEU. The MCNP spectrum is not broadened and serves as merely a hypothetical scenario of homogeneous ^{235}U and soil. Using the methods described within, the counts from the MCNP 186 keV energy bin, shown in blue, are used to quantify the ^{235}U based on the same photopeak, shown in red.

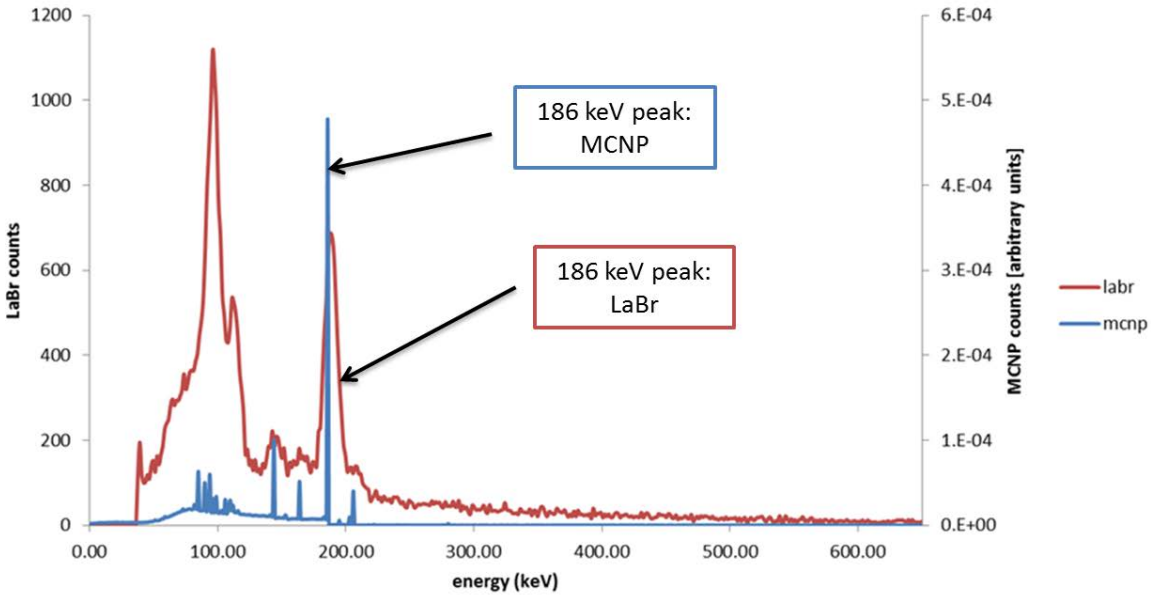

Figure 2. Field Measured LaBr Spectrum Overlayed on MCNP Spectrum for HEU.

The large peak visible in the measured spectrum around 100 keV is due primarily to uranium x-rays and their ionization by higher energy photons and other decay products.

^{235}U produces several x-rays in the 90-100 keV range, which are visible in both the simulated and measured spectrum. ^{238}U (^{234Th}) has a photopeak at 92 keV which may also contribute to this large peak. In addition, other heavy decay products in the sample may contribute x-rays to this energy region. Since the simulation contains nothing other than ^{235}U, above ~250 keV, no characteristic gamma rays exist. For this reason, the plot flattens. The measured spectrum is showing background radiation contributions from higher energy photons and external sources.

A limitation of modeling the LaBr detector in MCNP (model shown in Figure 5) is that MCNP does not simulate any of the light properties of scintillators. Uncertainties can thus stem from the creation, transport, and collection of light in the detector system. The light response of a LaBr crystal is known to be a function of energy (referred to as "non-linearity") and crystal temperature. Light transport in the detector is influenced by a reflective coating and the possible existence of slight imperfections in the crystal. Additionally, the behavior of the PMT in converting light into signal can vary depending on several factors including temperature [3].

III.C. DETECTOR CALIBRATION

Performance of a detector is characterized, in part, by efficiency. A gamma spectrum is interpreted in two ways: energy (identify radionuclides) and activity (quantify radionuclides). The energy interpretation is gained through an energy calibration, whereas, the activity interpretation is gained through an efficiency calibration.

III.C.1 Energy Calibration

The pulse height analyzer on the InSpector 1000 divides the range of all possible voltages into bins, or channels, and keeps a running count of how many pulses arrive in each bin, thus producing a histogram of the number of counts versus PMT output voltage. The PMT voltage varies directly with photon energy; however, that variation is not a simple proportion and it may not be linear [3]. For this reason, the scintillation detector must be calibrated with photons of a number of known energies before it is used to acquire the energy spectrum of an unknown sample. The calibration results in a relationship that allows an association of a given channel number with its appropriate energy. The final result is an identified radionuclide.

III.C.2 Efficiency Calibration

The efficiency calibration is used to quantify activities of radionuclides from a gamma spectrum. The detection efficiency depends on the energy of the incident photon, the detector material, the materials surrounding the crystal, the source/sample geometry, and the attenuation in the source matrix. Generally, it is determined experimentally by measuring calibration standards with known activity. The known standards are used to interpolate (through empirical relationships) an absolute efficiency calibration curve for a measurement. However, there are many ways to develop an efficiency calibration for a detector system.

Daily quality control calibrations were performed to verify the energy calibration and pulse height before shift, after shift and following each measurement to ensure the obtained results are valid. The source check between measurements was required because

one instrument was being used and instrument error was a potential problem. Valid results for a known check source at these three points ensured that the instrument was performing as expected.

III.D. HIGH PURITY GERMANIUM (HPGE) DETECTOR AND ISOCS

A common method of material assay at decommissioning sites includes use of Canberra's In Situ Object Counting System (ISOCS) software coupled with an HPGe detector. The HPGe detectors offer excellent energy resolution but require cryogenic cooling and are subject to variations in temperature and humidity [16]. They are also very expensive-the most expensive of the three detectors discussed here (NaI, LaBr and HPGe). However, their use in material assay, coupled with the ISOCS software, is valued as the "final" estimate for fissile gram quantities.

The ISOCS mathematical calibration software is a simple tool that allows the user to describe the geometry and couple a detector characterization and material attenuation factors to determine an overall efficiency curve. The overall efficiency is then applied to the spectrum obtained on the assay sample during the "analysis" process. In order to obtain an appropriate efficiency curve, each detector must be characterized [37].

III.D.1 Characterization

The HPGe and LaBr detectors used at HDP for this work have been characterized by Canberra's in-house program. The process uses NIST-traceable sources and the MCNP code to develop a radiation response profile of each individual detector in free space. The

free space encompasses a 1000 meter diameter sphere around the detector covering an energy range of 10 keV through 7 MeV [37, 39].

There are three steps in the characterization process. The first is the development and validation of an MCNP model for the LaBr/HPGe detector. The second step is the generation of a large number of efficiency data sets with the validated MCNP detector model in response to point-like sources at many locations about the detector. The final step is the generation of a detector characterization file, which contains the relationship of the detector to this point-efficiency data, and the validation of the resulting characterization file.

The MCNP calculations yield efficiencies at each point source location on the grid at 14 different energies. Using interpolation of the MCNP data, the efficiencies at a large number of nodal points are generated. The efficiency grids at the 14 energies are then combined to produce the detector characterization. Efficiency at any arbitrary spatial point between the grid nodes is obtained by linear interpolation. At a given spatial location, efficiency at any arbitrary energy between 45 keV and 3000 keV is obtained by parabolic interpolation.

The end result, the characterization file, representing the detector response to a point source in vacuum at any location and any energy, can be used in conjunction with the ISOCS software [40]. The ISOCS software calculates the efficiency for macroscopic sources by integrating the response over the active volume of a given geometry, taking into account the attenuation through the materials in the geometry.

This approach is directly comparable to efficiencies generated through the F8 tally in MCNP for a given geometry. A more detailed discussion of these comparisons in relation to method validation is in Section VI.B.

III.E. ENRICHMENT ESTIMATION METHODS

The objective of uranium enrichment measurement methods is to determine the $^{235}U/U$ isotopic ratio which, for most samples, is the determination of the ratio $^{235}U/(^{234}U+^{235}U+^{238}U)$. Among the various methods to determine the ratio, the oldest and most widely employed method uses the 185.7 keV full energy peak [41, 17].

In passive gamma counting, the ^{235}U enrichment is correlated with the count rate of the 185.7 keV photon emitted by ^{235}U during alpha decay. This gamma-ray occurs in 55% of the alpha decays of this isotope. Weaker gamma-rays at 143, 163, and 205 keV are also characteristic of ^{235}U; however, the 185.7 keV is commonly used for enrichment estimation, especially in environmental samples [42]. ^{238}U does not possess a primary decay gamma-ray; however, the ^{234m}Pa and ^{234}Pa daughters are used to identify ^{238}U. The characteristic photons used to identify ^{238}U are 766 keV and 1001 keV from ^{234m}Pa.

For the purposes described herein, the enrichment estimation was obtained by measuring the activity ratio of $^{235}U/^{238}U$ based on the gamma-rays associated with the decay of ^{235}U at 185.7 keV and the 1001.0 keV ^{234m}Pa photon from the decay of ^{238}U using gamma spectroscopy.

The purpose of enrichment estimation in this work was two-fold: to properly assign the ^{235}U mass calibration, and to clear items (i.e., pellets) from NCS control through declaration as depleted uranium (≤ 0.96 wt.% $^{235}U/U$).

CHAPTER IV

APPLIED SOFTWARE AND CODE SYSTEMS

Modeling and simulation play a critical role in modern scientific and technical endeavors, to the extent that scientific advances are dependent on their effective use. Modeling and simulation practices are also used as a basis for safety, operations, and well-being of field personnel in today's commercial day-to-day operations. Simulation can enhance our understanding of known systems, provide qualitative and quantitative insights into experimental work, especially those experiments deemed risky, provide quantitative results to replace experiments, and extend limited experimental data into new domains of parameter space [43]. Given the difficulties of dealing with radioactive, and specifically fissile, materials, modeling and simulation will play a critical role in advancing nuclear research programs and commercial applications.

Most of the available, well-established code systems and software for NDA compute a corrected count rate for the gamma-ray of interest based on the raw rate of data acquisition, rate-related loss and an attenuation correction factor. When correction and attenuation factors are properly defined, the corrected count rate is often directly proportional to the desired quantity, such as mass of ^{235}U or enrichment. Obtaining proper correction and attenuation factors is not a simple task and depends on a multitude of modeling assumptions and empirical relationships.

Coupling measurements, software, and instrumentation has traditionally been a daunting task. State of the art measurement instrumentation is underutilized without the

correlated software to appropriately process the information. Likewise, sophisticated data processing is unnecessary s without adequate field measurement tools. Software capable of interacting with instrumentation and providing feedback and customization for individual scenarios allow more efficient and accurate interrogation of known or unknown materials. Field instrumentation is considered adequate when its intended purposes fall within the area of applicability described by both the manufacturer and literature. An accurate interrogation of materials is going to develop as the material model and assay approaches the real value.

IV.A. CODE SYSTEMS AND SOFTWARE

A collection of code systems and software were selected based on their ability to meet the outlined research objectives and capabilities and limitations of the utilized equipment. Since comparison of the computational tools is intended, the code systems must be able to produce comparable results.

The Monte Carlo based code MCNP was heavily utilized for creating the 3D system models representing the theoretical scenario for each geometrical configuration. MCNP requires an externally calculated radiation source term as input. The source term was calculated using the ORIGEN-S module of the SCALE code system. The mathematical calibration software, ISOCS, was used to develop 3D geometries for detector efficiency calibration using empirical relationships. MCNP and ISOCS perform similar geometry modeling tasks with some limitations to the ISCOS geometry software. Matching geometries were created in both in order to make comparisons of the mathematical calculations housed within each code. GENIE 2000 was used for processing

gamma spectra, developing analysis sequences, and to produce NDA measurement results. Each code or software with its associated purpose is summarized in Figure 3.

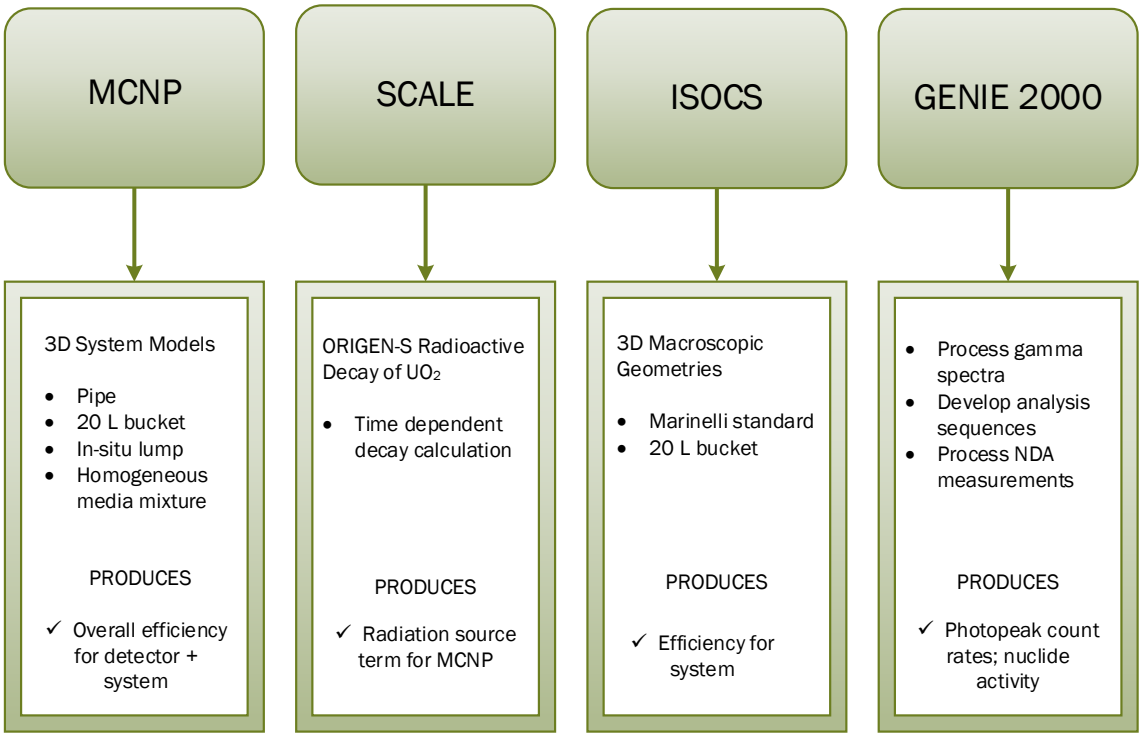

Figure 3. Code System and Software Summary.

IV.A.1 MCNP5

MCNP (Monte Carlo N-Particle) is a general purpose code that can be used for neutron, photon, electron, or couple neutron/photon/electron transport. MCNP is the internationally recognized code for analyzing the transport of neutrons and gamma rays, and is developed and maintained by Los Alamos National Laboratory.

Pointwise cross section data are used and each case was run for a total of six hours computer time. For photons, the code accounts for incoherent and coherent scattering, the

possibility of fluorescent emission after photoelectric absorption, absorption in pair production with local emission of annihilation radiation, and bremsstrahlung. The ENDF/B-VI nuclear data library was used in these cases.

MCNP is a code that is continuously undergoing development at Los Alamos National Laboratory and has periodic releases. The distinction of the number 5 in MCNP5 is for identifying the version of MCNP. The current release (2013) is version MCNP5 (1.60); however, for validation and license purposes, MCNP5 (1.40) is used for this work. MCNP5 is very versatile with its inherent standard features such as: multiple source description options, flexible tally structure, an extensive collection of cross section data, a large collection of variance reduction techniques, and geometry and output tally plotters [28].

The code is applicable in two modes: criticality and external source modes. The source mode is primarily for shielding evaluations. Monte Carlo is used to calculate the system multiplication factors (k_{eff}), the energy spectrum for neutrons and photons, and the reaction rate distribution.

MCNP simulates detector responses to gamma ray sources by mimicking the inherently random behavior of real physical events. The source region, which is both point-like and distributed, is selected, and each gamma-ray is tracked as it undergoes collisions within the detector volume. The final tally distribution represents the energy spectrum "seen" by the detector and can thus be used to obtain the overall efficiency for the source/detector/universe geometry.

IV.A.1.a Verification and Validation

Because the code is used to develop a real safety basis, a verification was performed by running test problems included with the code, and comparing the results to those provided with the code. Additionally, a validation compares the computational method with documented experiments to determine any bias that might exist between the calculated reactivity of a given system and actual conditions. It is a process that determines and establishes computational method applicability, adequacy, and uncertainty. The validation is conducted using the ENDF/B-VI continuous energy group cross section library.

ANSI/ANS-8.1 [44] requires that calculation methods used for NCS (e.g., determining k_{eff} of a system or deriving subcritical limits) be validated to determine the appropriate biases and uncertainties for the areas of applicability. The bias and uncertainty represent the numerical difference between the results of modeling experiments with a computer code and the experimental response.

The verification and validation is outlined in Reference 45 and based on guidance through the Nuclear Regulatory Commission's Software Quality Assurance Program and Guidelines [46].

IV.A.1.b Light Production

MCNP5 terminates the scintillation process at the point the photon interacts within the scintillator volume and does not simulate the transport of light. In other Monte Carlo codes, such as GEANT4 (GEometry ANd Tracking), scintillation light photons are

transported until they reach the photocathode of the PMT [47]. Pozzi et. al have coupled MCNP-PoliMi, with post-processing scripts to convert energy deposited in the detector to scintillation light output [48]. Depending on the task to be addressed, each code offers advantages and disadvantages. In the case of detector time response studies on nonlinear scintillators, the lack of scintillation photon transport and detection within the code is a disadvantage.

Other simulation tools for this purpose exist, such as PHOTOTRAK, which models the transport and detection of scintillation photons and has been successfully coupled to MCNPX [49]. However, recent research in this has shown that GEANT4 is a better tool overall to simulate the light production of a scintillator [50].

Simulating the light response of the scintillator may be necessary in applications utilizing nonlinear scintillators with studies needing the time-resolved detection of photons at the light readout device. Because the LaBr is considered a linear scintillator and the simulations described herein are not time-dependent response functions, the simulation accuracy resulting from modeling the light response is not necessary. In addition, in the evaluation by Ghal-Eh et. al of NaI scintillator response in two Monte Carlo codes: one tracking light behavior and one not, the discrepancies were less than 5% from each other and experimental results [47].

IV.A.2 SCALE

The SCALE (Standardized Computer Analysis for Licensing Evaluation) code system serves in conjunction with MCNP by calculating and supplying a source term. SCALE is developed and maintained by Oak Ridge National Laboratory (ORNL) and is

widely accepted around the world for criticality safety analysis, radiation source term and shielding, problem dependent resonance self-shielding of cross section data, sensitivity and uncertainty, and reactor physics analysis [51].

ORIGEN-S is a depletion and decay module within the SCALE code system, and it can be called from a control module or run as a stand-alone program. ORIGEN-S computes time-dependent concentrations and radiation source terms which are simultaneously generated or depleted through neutronic transmutation, fission, and radioactive decay [52]. In relation to this dissertation, ORIGEN-S was used in stand-alone mode for calculating a radiation source term as a function of time for UO_2.

IV.A.3 ISOCS

The ISOCS software serves as a tool for calibrating the detector efficiency as a function of energy for a wide variety of source geometries and activity distributions. The ISOCS method consists of characterization of the detector, user input of source geometry data, and the ISOCS software, which uses these to produce the overall efficiency calibration.

The ISOCS software is a complex ensemble of computer codes that use mathematical techniques to compute detector efficiencies [6]. It contains a series of mathematical models that can simulate a variety of common sample shapes (boxes, cylinders, spheres, pipes, stacked boxes, stacked discs, Marinelli beakers, etc.). The ISOCS software as well as its validation and verification is developed and maintained by Canberra Industries.

IV.A.3.a Characterization Implemented in ISOCS

Prior to use of the software for calibration purposes, the specific LaBr scintillation detector was characterized. This initial characterization was performed by Canberra Industries on each individual detector. First, an MCNP model of the detector was developed. The model was then independently validated using measurements with a NIST traceable source. Given the validated model, the response characteristics of the detector were generated to cover any location inside a sphere of radius 500 meters, centered on the detector, and over a photon energy range of 45 keV through 7 MeV [39]. This characterization produced intrinsic efficiencies for input into ISOCS.

IV.A.4 GENIE 2000

GENIE 2000 is a comprehensive set of capabilities for acquiring and analyzing spectra from MCAs. Its functions include MCA control, spectral display and manipulation, basic spectrum analysis and reporting. Operational capabilities include comprehensive spectrum analysis for alpha and gamma spectroscopy, quality assurance, system automation and turnkey packages for specific applications [53].

The core of the GENIE 2000 software is a module known as Virtual Data Manager (VDM), which manages all information flow within the system. The VDM is responsible for communications within the layers of the software including the compute modules. The modules are small modular programs that perform basic functions—start/stop of acquisition, transfer of spectrum from MCA to disk, peak search, etc. This modular nature makes possible the flexibility of operating individual modules or together in sequence.

Sample information and calculations from ISOCS are used in GENIE 2000 analyses to directly correlate geometry and efficiency with spectral algorithms and measurement results. This allows modification of parameters in a geometry template during analysis in order to optimize measurement geometries by experimentation and feedback. A single spectrum may be manipulated over and over again while never acquiring an additional measurement.

Each spectrum is analyzed with a customized analysis sequence file. The sequences used include: Peak Locate, Peak Area, Efficiency Correction and Nuclide Identification.

IV.A.4.a Peak Locate

Peak locate is used to pinpoint photopeaks in a spectrum for later quantification and identification. This sequence utilizes a 2^{nd} differential peak locate algorithm to identify inflection points and isolate the peak. The centroid of the peak is selected at the minimized function. An unchanged sign of the 2^{nd} derivative over many channels in a spectrum is classified as a Compton Edge or Continuum. A significance threshold set at 3 results in a peak confidence at or below 95% for most cases.

Another method is a user specified peak locate. This technique is analogous to a "forced ROI" or "forced locate" and no peak search or peak tests are performed. The ROI centroid is calculated as the geometric center of the ROI channel contents. This method is limited in repeated applications for scenarios where the spectrum is subject to energy drift.

IV.A.4.b Peak Area

The peak area algorithm is one of the more robust and difficult sequences in the scheme. Simple summation was used for identified singlet photopeaks. The summation/non-linear least squares fit method was utilized for peak area calculation of multiplets. This method first determines a ROI and compares the centroids of neighboring peaks for separation criteria. Then, the background (continuum) is calculated using the expected FWHM for the detector and subtracted. The resulting net peak areas serve as the basis for activity calculations.

IV.A.4.c Efficiency Correction

The efficiency correction algorithm is used to translate counts per second into source gamma-rays per second in order to calculate activity. This calculation uses the defined geometry and associated calibration standards to apply attenuation factors to materials and the macroscopic configuration. The efficiency is calculated for multiple photopeak energies and applied to collected spectra and peak areas. Knowing the efficiency of the system is the key to understanding the source activity.

IV.A.4.d Nuclide Identification

Nuclide libraries include information on all potential nuclides that may be encountered and their associated gamma-ray energy and relative intensity. The nuclide library is compared to the identified photopeaks. This algorithm ties a nuclide name to a photopeak and uses the combined information to assign an activity to that nuclide. Nuclide mass for the sample is easily deduced from nuclide activity.

CHAPTER V

REPRESENTATIVE MODELS

The set of geometric models must represent an array of scenarios encountered for Non-NCS Exempt Material at HDP. The hundreds of actual geometric arrangements have to be summarized in a bounding form in a few modeling configurations. Often, multiple modeling scenarios are tested, and when feasible, all modeling options are allowed to be matched to the real configuration for an accurate assay. However, in some cases, the bounding scenario is the only option supplied for field implementation, in order to maintain conservatism.

V.A. DESIGN INPUTS

Each model is only as good its inputs and assumptions. The known materials were modeled as accurately as possible, with manufacturer's descriptions and dimensions, when available. When those were not available, a conservative substitute was applied. In this context, a conservative substitute would be around 20% higher than an actual value, in order to account for outliers and uncertainty.

V.A.1 Canberra Industries Model IPROL-1 Intelligent LaBr Probe

A schematic diagram of Canberra's IPROL-1 LaBr probe was supplied by the manufacturer with all details described and illustrated. An illustration based on that description is shown in Figure 4. The probe contains the LaBr crystal, the housing, and the PMT.

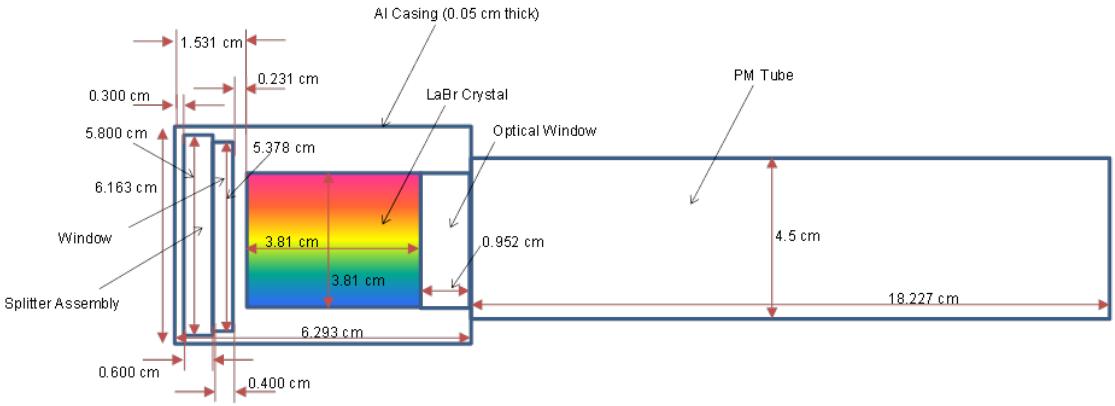

Figure 4. Dimensions of the Canberra Industries Model IPROL-1 Intelligent LaBr Probe.

V.A.2 Detector Geometry

The IPROL-1 probe was modeled using the dimensions in Table IV. The model was simplified for input into MCNP, keeping only those attributes that are pertinent to photon attenuation. The simplified representation is shown in Figure 5.

Table IV. LaBr Detector Dimensions

Parameter	Dimension	
	[in]	[cm]
Crystal height	1.5	3.81
Crystal diameter	1.5	3.81
Detector OD	2.426	6.263
Detector length	2.478	6.393
Crystal position from window	0.603	1.531

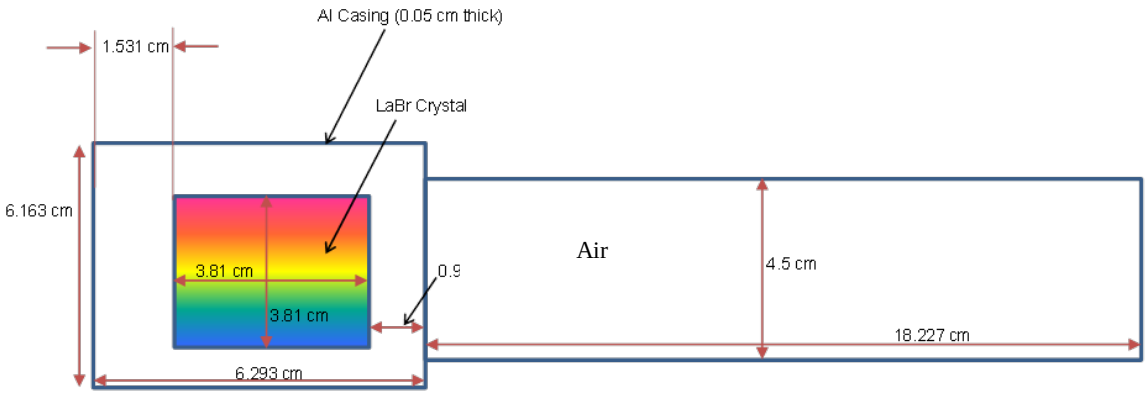

Figure 5. MCNP Representation of the Canberra Industries LaBr Probe.

The potassium glass window and beam splitter assembly were neglected and modeled as air in the probe the following reasons:

- The potassium glass window is 0.231 cm thick and designed with the intention of transmitting photons. Per recommendation from Canberra Industries, the potassium window could be neglected [54]. A sample test was performed at the start of the work to test a pure potassium window with a similar density. The effect on 75 – 2000 keV detector response was less than 2%.
- The splitter assembly allows the LED output to be measured, which allows for correction of fluctuations in LED output (temperature effects, voltage). The only effect on detector response would be light attenuation through the board, but it was made to be minimal such that negligence could be assumed [54].

V.A.3 Tungsten Silicone T-Flex Ribbon Wrap Collimator

The T-Flex Ribbon Wrap is a flexible ribbon wrap material produced by Nuclear Power Outfitters (NPO), a brand of Eichrom Technologies. It is ideal for small or irregular sized components at any desired thickness, width and length. The attenuation properties of the tungsten silicone materials are similar to those of traditional lead, but the density is less than that of lead [55]. For field implementation and detector cable integrity, less weight is advantageous.

Selection of a collimator depends on the scenario and desired results. The original use of the collimator was for performing measurements on 1-foot segments of pipe to assign ^{235}U grams. Photon contribution from neighboring 1-foot segments needed to be reduced.

A series of calculations was performed in order to determine what size collimator would be used for these purposes. In order to select a collimator thickness, a design goal had to be selected. The goal was to reduce 185.7 keV photon counts from outside the desired detector field of view by at least 25%. Reduction of higher energy photons was an added advantage but not intended to be reduced by 25%. This value was selected in hopes that it would allow some background photon reduction without forcing a cumbersome material weight added to a detector probe, which ended up being the case. The value of 25% was selected as a design constraint which could have been tweaked, depending on the results. The added weight (and material cost) versus reduction in surrounding photon contribution was the balance under evaluation.

Table V gives results for each potential design parameter change. These efficiencies were calculated using a simple, fixed ISOCS geometry and varying the collimator dimensions. The probe was fixed at 6-in from the pipe and, for this study, the collimator was recessed at 1-in below the LaBr crystal, leaving 3-in to cover the crystal surrounds. The ISOCS reported uncertainty for each value is 8%.

Table V. Potential Collimator Design Efficiencies

Probe height [cm]	Recess (from end cap) [cm]	Thickness [cm]	Width [cm]	185.7 keV efficiency	1001 keV efficiency
15.24	no collimator			3.01670E-04	1.48283E-04
15.24	1.531	0.3175	10.16	2.57163E-04	1.42546E-04
15.24	1.531	0.635	10.16	2.55927E-04	1.39629E-04
15.24	1.531	0.9525	10.16	2.55882E-04	1.38133E-04
15.24	1.531	1.27	10.16	2.55880E-04	1.37366E-04
15.24	1.531	1.5875	10.16	2.55880E-04	1.36996E-04
15.24	1.531	1.905	10.16	2.55880E-04	1.36827E-04
15.24	1.531	2.2225	10.16	2.55880E-04	1.36756E-04
15.24	1.531	2.54	10.16	2.55880E-04	1.36730E-04

These results are also shown graphically in Figure 6. The initial drop in efficiency for the 185.7 keV photon, from no collimator to 0.3175 cm (1/8-in) thick collimator was about 15% . The design goal of 25% attenuation was not quite reached; however, the trade-off between added weight (also cost) and benefit was maximized. The 1001 keV photon continues to be attenuated slightly, up to approximately 1.27 cm (½-in) thick collimator material because it is more penetrating than the 185.7 keV photon. This is clear by looking at the efficiency with no collimator. The 1001 keV photon has an efficiency twice that of the 185.7 keV photon.

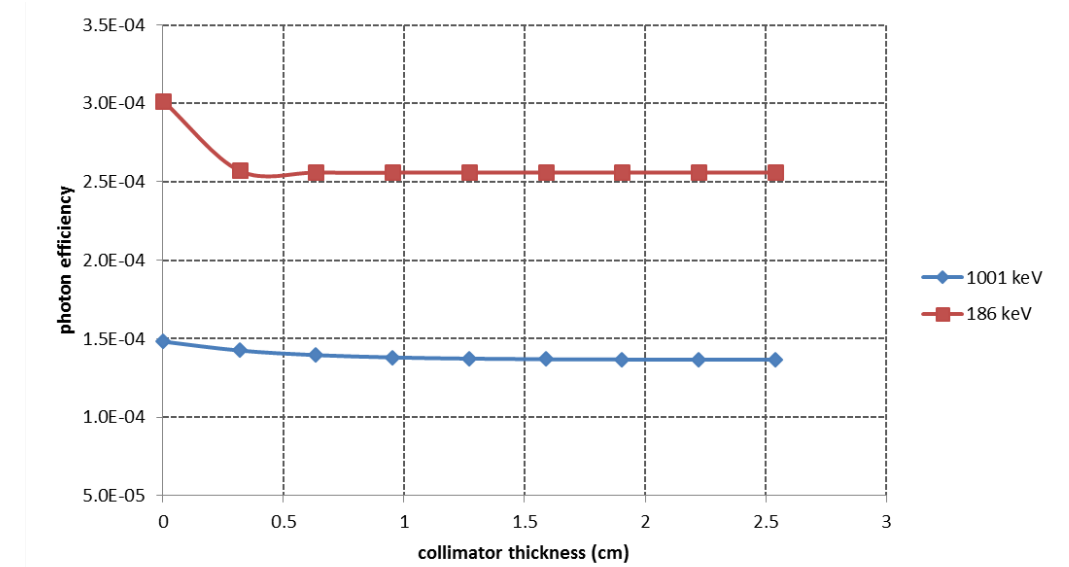

Figure 6. Calculated Efficiencies for Uranium Photons in ISOCS.

The final manufactured design was 0.3175 cm (1/8-in) thick tungsten silicone at a 4-in width and enough to wrap the ribbon four times around. This equated to a final ½-in thick collimator on each side of the detector and added approximately two pounds to the probe. A picture of the ribbon is shown in Figure 7.

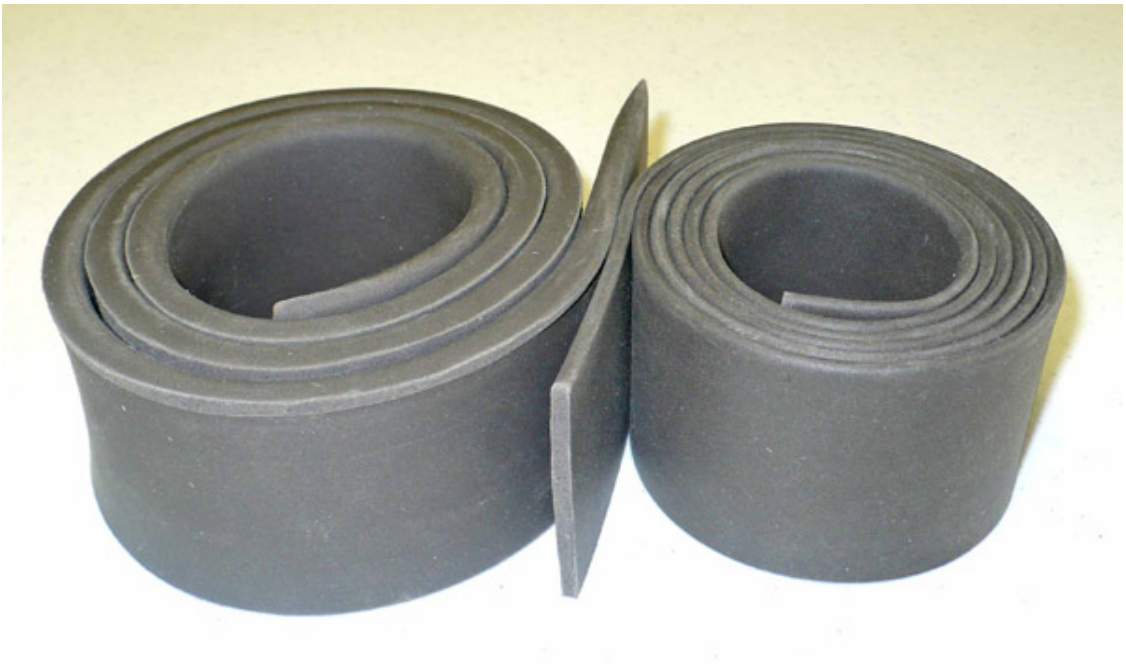

Figure 7. NPO T-Flex Ribbon.

V.A.4 Field Container

The 5 gallon drum used for isolation of radiological hot spots has the dimensions shown in Table VI. The walls of the container are assumed in the simulation to be stainless steel in order to stay consistent with previous calculations performed for HDP and for more conservative results than would have been produced using plastic.

Table VI. HDP Field Container Dimensions

Volume [cm^3]	Container Type	Outer Radius [cm]	Inner Radius [cm]	Outer Height [cm]	Inner Height [cm]
18,925	Drum	11	10.955	50.179	50.133

V.A.5 Waste Medium Configuration

The waste medium is composed of some mixture of a source material and a benign waste. Specifications for dry soil are taken from Reference 56. The benign waste is always a variation of clean soil. The source material is specified as a concentration or mass of a uranium compound. The waste medium configurations evaluated include:

- A uniform distribution of 0.1 g ^{235}U/L in dry soil with a density of 1.73 g/cm^3 for cut depths of 2-, 4-, 6-, and 8-inches; fixed at 6-inch depth for the Field of View (FOV) study [Soil Remediation Models].
- Multiple mass lumps of UO_2 in dry soil with a density of 1.73 g/cm^3 for cut depths of 2-, 4-, 6-, and 8-inches [Soil Remediation Models].
- A homogeneous mixture of UO_2 and wet soil with a density of 2.03 g/cm^3 for fill fractions of 25, 50, 75, and 95 percent at 5 wt.% and 100 wt.% ^{235}U/U [Soil Remediation Models].
- A distribution of various mass quantities of UO_2 at 5 wt.% and 100 wt.% ^{235}U/U in 1-ft sections in segmented and annular (360°) configurations [Subterranean Piping Models].

V.A.6 Material Specification

V.A.6.a Uranium Material Specification

The uranium was modeled as UO_2 particulate at its full theoretical density of 10.96 g/cm^3. However, due to the manner in which the uranium is intermixed with the waste,

the actual density of the uranium within the waste was lower and dependent on the concentration under consideration (see Table XIII).

The calibration analysis considers two uranium enrichments of 5 wt.% and 100 wt.% $^{235}U/U$. These are selected for two purposes. 100% was considered bounding for NCS purposes, meaning that it requires the smallest amount of fissile material for criticality. 5% was considered bounding, yet realistic, for photon detection purposes, meaning that is accounts for a significant amount of self-attenuation. The UO_2 material composition for each enrichment case is shown in Table VII and Table VIII.

Table VII. UO_2 Composition (100 wt.% $^{235}U/U$ Enrichment) used in MCNP Model

Nuclide	MCNP Nuclide ID	Mol. Wgt	Atom Density [a/b-cm]	Density [g/cm^3]	Weight %
^{235}U	92235	235.0439219	2.4717E-02	9.6470	88.02%
^{238}U	92238	238.0507813	0.0000E+00	0.0000	0.00%
^{16}O	8016	15.9949145	4.9434E-02	1.3130	11.98%
Total			7.4151E-02	10.960	100.00%

Table VIII. UO_2 Composition (5 wt.% $^{235}U/U$ Enrichment) used in MCNP Model

Nuclide	MCNP Nuclide ID	Mol. Wgt	Atom Density [a/b-cm]	Density [g/cm^3]	Weight %
^{235}U	92235	^{235}.0439219	1.2376E-03	0.4830	4.41%
^{238}U	92238	238.0507813	2.3218E-02	9.1779	83.74%
^{16}O	8016	15.9949145	4.8911E-02	1.2991	11.85%
Total			7.3367E-02	10.9600	100.00%
Wt. frac U in UO_2	0.8814710				

V.A.6.b Waste Material Types

The calibration analyses used the following waste material types to represent the in-situ, containerized, and pipe hold-up waste materials under investigation:

- Dry soil at a density of 1.73 g/cm^3.
- Saturated soil at a density of 2.03 g/cm^3.
- UO_2 tap density[2] of 3.5 g/cm^3.
- Overall lump density of 2.78 g/cm^3 for dry soil.

When appropriate, the waste material type was uniformly mixed with the uranium under evaluation. This was the case for modeling in-situ waste (trash) comingled with uranium. The UO_2 subterranean pipe hold up was not mixed with any other waste material.

Dry Soil

The dry soil was based on the 30% void fraction soil composition provided in ARH-600 [56] and adjusted to a density of 1.73 g/cm^3 as shown in Table IX. The MCNP nuclide ID is in the form ZZZAAA, where ZZZ is atomic number and AAA is the mass number (000 for elemental composition in natural abundance).

[2] Tap density is also known as tapped density. It is defined as the density at which a powder is packed into a formed shape. As the void fraction decreases, the tapped density increases.

Table IX. Dry Soil Composition (30% by Volume Void) used in MCNP Model

Nuclide	MCNP Nuclide ID	Mol. Weight	Atom Density [a/b-cm]	Density [g/cm^3]	Weight %
^{16}O	8016	15.994915	3.2835E-02	0.8721	50.41%
Si	14000	28.085508	1.4059E-02	0.6557	37.90%
Al	13000	26.981538	1.2411E-03	0.0556	3.21%
Ca	20000	40.078023	9.6526E-04	0.0642	3.71%
Fe	26000	55.846818	5.5158E-04	0.0512	2.96%
Mg	12000	24.305052	5.1561E-04	0.0208	1.20%
Na	11000	22.989770	2.7279E-04	0.0104	0.60%
		Total	5.0440E-02	1.7300	100%

Table X gives the dry soil material composition when uniformly mixed with UO_2 at a fixed enrichment of 100 wt.% ^{235}U/U and a fixed concentration of 0.1 g ^{235}U/L.

Table X. Dry Soil Composition (30% by Volume Void) when Intermixed with 100 wt.% ^{235}U/U in UO_2 at a Concentration of 0.1 g/L used in MCNP Model

Nuclide	MCNP Nuclide ID	Mol. Weight	Density [g/cm^3]	Weight %
Si	14000	28.085508	0.6557	37.90%
Al	13000	26.981538	0.0556	3.21%
Ca	20000	40.078023	0.0642	3.71%
Fe	26000	55.846818	0.0512	2.96%
Mg	12000	24.305052	0.0208	1.20%
Na	11000	22.989770	0.0104	0.60%
^{16}O	8016	15.994915	0.8721	50.41%
^{235}U	92235	235.043922	0.0001	0.01%
		Total	1.7301	100%

Saturated Soil

The dry soil compositions, as shown in Table IX and Table X, were utilized in the lump model and in-situ models. The water saturated soil compositions were utilized in

the loaded field container and in-situ models. This was selected based on process knowledge and observed conditions within burial pits.

A water saturated soil composition, as shown in Table XI and Table XII, was based on the dry soil composition with some fraction of the 30% void assumed to be filled with water. The fraction of the void space containing water is referred to as the *saturation*. For fully saturated conditions, the saturation value is 100%. Cases with saturation exceeding 100% (effectively slurries of mud and water) were not considered since the maximum density occurs for saturated soil conditions. The fully saturated soil composition is shown in Table XI.

Table XI. Fully Saturated Soil Composition used in MCNP Model

Nuclide	MCNP Nuclide ID	Mol. Weight	Atom Density [a/b-cm]	Density [g/cm^3]	Weight %
Si	14000	28.08551	1.41E-02	0.6560	32.30%
Al	13000	26.98154	1.24E-03	0.0556	2.74%
Ca	20000	40.07802	9.66E-04	0.0643	3.16%
Fe	26000	55.84682	5.52E-04	0.0512	2.52%
Mg	12000	24.30505	5.16E-04	0.0208	1.03%
Na	11000	22.98977	2.73E-04	0.1040	0.51%
^{16}O	8016	15.99492	4.29E-02	1.1385	56.08%
H	1000	1.007976	2.01E-02	0.0336	1.65%
		Total	8.06E-02	2.0300	100%

Table XII. Fully Saturated Soil Composition when Intermixed with 100 wt.% $^{235}U/U$ in UO_2 at a Concentration of 0.1 g/L used in MNCP Model

Nuclide	MCNP Nuclide ID	Mol. Weight	Density [g/cm^3]	Weight %
Si	14000	28.085508	0.6557	32.30%
Al	13000	26.981538	0.0556	2.74%
Ca	20000	40.078023	0.0642	3.16%
Fe	26000	55.846818	0.0512	2.52%
Mg	12000	24.305052	0.0208	1.03%
Na	11000	22.989770	0.0104	0.51%
^{16}O	8016	15.994915	1.1385	56.08%
^{235}U	92235	235.043922	0.0001	0.00%
^{238}U	92238	238.050781	0.0000	0.00%
H	1000	1.007976	0.0336	1.65%
		Total	2.0301	100%

The composition for water saturated soil intermixed with UO_2 with 5 wt.% $^{235}U/U$ is similar to that shown in Table XII with an increased density of ^{238}U.

Lumped UO_2 and Soil

The in-situ lumped model creates a fictitious lump of 100 wt.% $^{235}U/U$ in UO_2 at 3.5 g/cm^3 intermixed with dry soil. The composition and lump density calculation are provided in Table XIII.

Table XIII. Material Characteristics of Dry Soil with 3.5 g/cm^3 UO_2 Lump used in MCNP Model

Nuclide	MCNP Nuclide ID	Mol. Weight	Density [g/cm^3]	Weight %
Si	14000	28.085508	0.6557	23.59%
Al	13000	26.981538	0.0556	2.00%
Ca	20000	40.078023	0.0642	2.31%
Fe	26000	55.846818	0.0512	1.84%
Mg	12000	24.305052	0.0208	0.75%
Na	11000	22.989770	0.0104	0.37%
^{16}O	8016	15.994915	0.9979	35.90%
^{235}U	92235	235.043922	0.9242	33.25%
^{238}U	92238	238.050781	0.0000	0.00%
		Total	2.7800	100%

Detector Materials

The 1.5”×1.5” LaBr crystal of the LaBr detector was modeled at a density of 5.30 g/cm^3 and was represented as a combination of lanthanum (MCNP ID 57000) and bromine (MCNP ID 35000), with a lanthanum-bromine atom ratio of 1:3. Aluminum at a density of 2.69 g/cm^3 was used to model the LaBr body casing. The MCNP cross-section library 13000 was used for Al. Air was modeled at a density of 0.0012929 g/cm^3 and as a combination of nitrogen (MCNP ID 7014), oxygen (MCNP ID 8016), and argon (MCNP ID 18000) at weight fractions of 0.755, 0.232, and 0.013, respectively. The tungsten silicone collimator composition was taken, in part, from the collimator manufacturer’s recommendation. The chemical formula for silicone used in this calculation is $(CH_2)_3SiO$. The collimator material is 89% tungsten and 11% silicone by weight. The material composition is detailed in Table XIV.

Table XIV. Tungsten Silicone Collimator Composition used in MCNP Model

Weight Fraction	Element	Chemical formula	Atom % (of silicone)	Atom% * atomic mass	wt. % of compound (silicone)	wt.% of total (W-Si)
11%	C	2	0.2	2.4021	0.3239	3.56%
	H	6	0.6	0.6048	0.0816	0.90%
	Si	1	0.1	2.8086	0.3787	4.17%
	O	1	0.1	1.5999	0.2158	2.37%
89%	W	1	N/A	N/A	N/A	89.0%

Structural Materials

The stainless steel 304 composition was taken from the SCALE Standard Composition Library [57] as shown in Table XV, and is used herein to conservatively represent the structural material of the containers considered in the calibration analysis.

Table XV. Stainless Steel 304 Composition

Nuclide	MCNP Nuclide ID	Mol. Weight	Atom Density [a/b-cm]	Density, g/cm^3	Weight %
C	6000	12.01104	3.19E-04	6.35E-03	0.08%
Si	14000	28.08551	1.70E-03	7.94E-02	1.00%
P	15000	30.97376	6.95E-05	3.57E-03	0.05%
Cr	24000	51.99614	1.75E-02	1.51E+00	19.00%
Mn	25000	54.93805	1.74E-03	1.59E-01	2.00%
Fe	26000	55.84682	5.85E-02	5.43E+00	68.38%
Ni	28000	58.69336	7.74E-03	7.54E-01	9.50%
		Total	8.76E-02	7.94	100%

PVC was used at a density of 1.65 g/cm^3 and was defined as a combination of hydrogen (MCNP ID 1001), carbon (MCNP ID 6000), and chlorine (MCNP ID 17000) at atom fractions of 50.0%, 33.333%, and 16.667%, respectively. Cast iron was used at a density of 7.80 g/cm^3 and was defined as a combination of Iron (MCNP ID 26000), carbon

(MCNP ID 6000), and silicon (MCNP ID 14000) at weight fractions of 94.3%, 3.4%, and 4.3%, respectively.

V.B. MCNP SOIL REMEDIATION MODELS

V.B.1 Assumptions

Because the purpose of the analysis was to provide Monte Carlo based calibration factors to predict an upper bound of ^{235}U concentration, a number of conservative assumptions were employed. These are chosen in order to coincide with the high end of an expected value and/or slightly beyond an expected condition in order to cause over prediction in the final calculated result. These assumptions also serve to simplify the analysis by reducing the number of variables that are examined as part of the sensitivity studies described in subsequent sections.

The conservative assumptions employed in this analysis are as follows:

- For HEU cases (enrichment calculated > 10 wt. %), the analysis used a fixed uranium enrichment of 100 wt. % $^{235}U/U$.
- For LEU cases (enrichment calculated $\geq$ 0.96 wt. % and $\leq$ 10 wt. %), the analysis used a fixed uranium enrichment of 5 wt. % $^{235}U/U$.
- The container (FC) was modeled as stainless steel composition.

- The uranium particulate within the in-situ waste materials was modeled as UO_2 at its full theoretical density of 10.96 g/cm^3, which is considered appropriate since this chemical form is most likely[3].
- The calibration analysis used a tap density for UO_2 of 3.5 g/cm^3. This was considered conservative and bounding of any realistic tap density for UO_2.
- As described in Section V.F, the reported results of the calibration analysis are at the 97.7% confidence level to account for statistical uncertainty.

Other assumptions employed in the calibration analysis are defined below.

- The axial sponge layer in the end cap of the LaBr detector was modeled as air. Also, the components in the detector housing above the LaBr crystal (e.g., the PMT) were neglected with insignificant effect on the results.
- The potassium window and splitter assembly within the detector was neglected with insignificant effect on the results. These components are designed to be invisible to photon interaction both in thickness and material.

V.B.2 Field Container Geometry

The 5 gallon drum used in this calibration analysis had the dimensions as shown in Table VI. The walls of the container were assumed to be stainless steel in order to stay

[3] Note that uranium metal particulate or fragments would tend to oxidize within a disposal systems such as the site burial pits. However, because of the manner in which the uranium is intermixed with the waste materials in the calculations, the actual density of the uranium within the waste is lower and dependent on the mass or concentration under considerations.

consistent with previous analyses and for conservative results. While stainless steel container walls were not considered a normal field condition, they were possible and within the realm of reason. A stainless steel wall provided more photon attenuation thereby causing a lower detected photon count rate outside the container and was thus considered conservative. This drum is further referred to as a Field Container.

V.B.3 Waste-Detector Models

V.B.3.a Lump Model

The LaBr detector was modeled centralized above the centerline of the in-situ waste materials, at a fixed height above the surface of the waste. The waste-detector configurations employed in the calibration calculations are illustrated in Figure 8 and Figure 9 for the lumped configuration model with the LaBr detector.

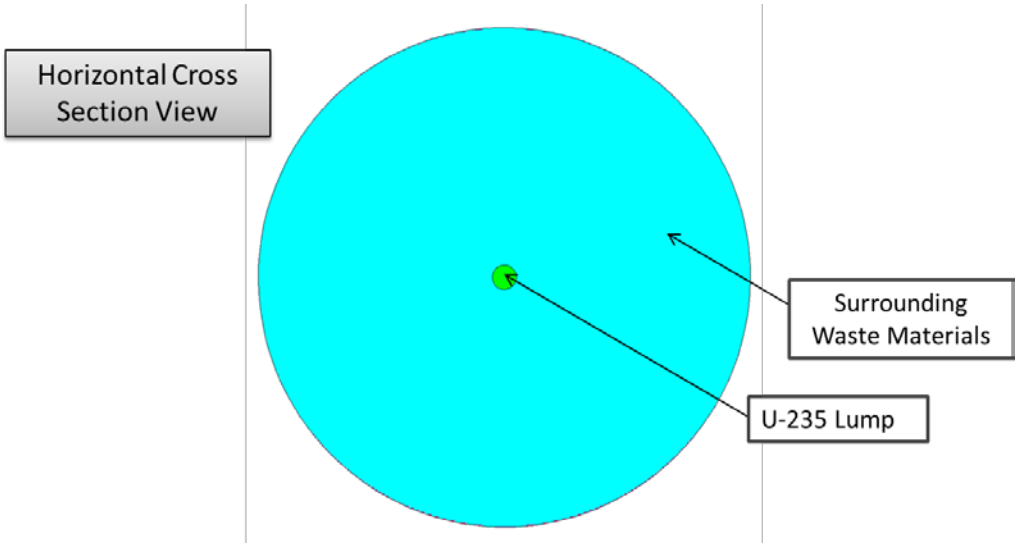

Figure 8. MCNP Schematic of Lumped Contamination Model in Horizontal Cross Section.

.

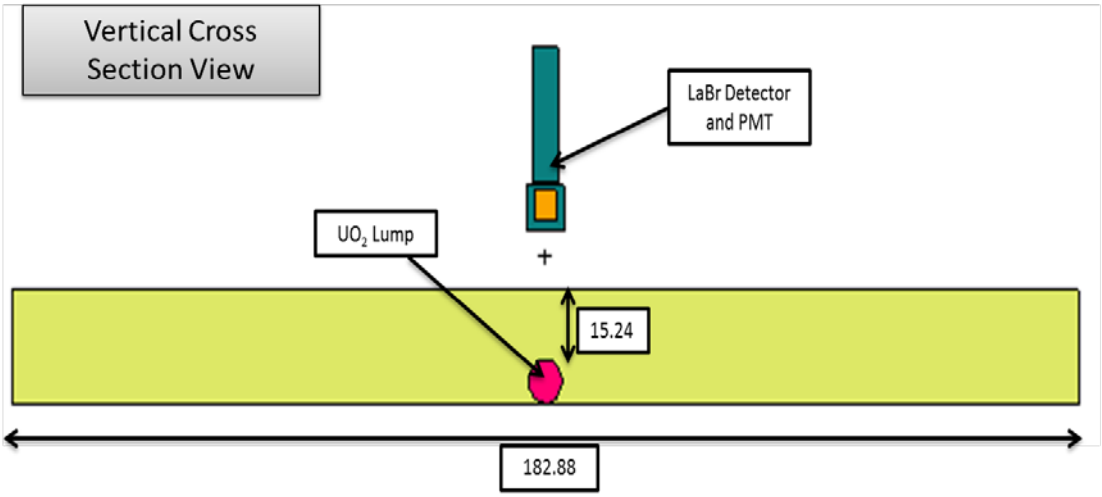

Figure 9. MCNP Schematic of Lumped Contamination Model in Vertical Cross Section (all dimensions in cm).

The lump of comingled UO_2 and soil was positioned at the base of 6-in. As the ^{235}U mass of the lump increase, the dimensions of the lump increase and it continues to approach the surface.

V.B.3.b Field Container Model

The LaBr detector was modeled on contact to the FC in the bottom position as shown in Figure 10. The fill height of the material was calculated from a specified percentage of volumetric fill for the FC. The fissile material source was homogeneously mixed in the soil and loaded into the FC to the calculated height.

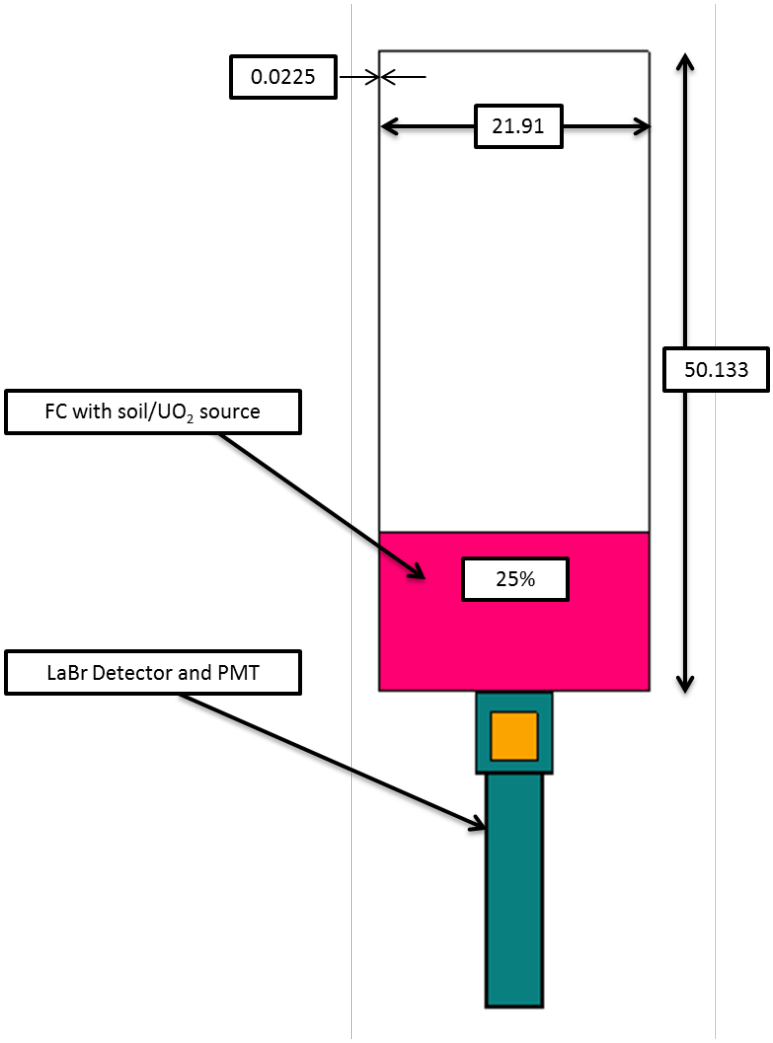

Figure 10. Vertical Cross Section Schematic of MCNP FC Model (all dimensions in cm).

V.B.3.c Homogeneous Waste Model

The homogeneous waste model was used in part for a detector field of view study, in addition to obtaining detection limits for a specified concentration of ^{235}U in the volume. Uniform UO_2 contamination was distributed throughout the soil volume to equate to a concentration of 0.1 g $^{235}U/L$. The detector probe, with and without a collimator, was

placed at 3 and 6-in from the top of the soil. The radius of the contaminated soil was varied to establish the field of view for the LaBr detector for each waste volume. Figure 11 gives a schematic diagram of an example geometry for the parametric study.

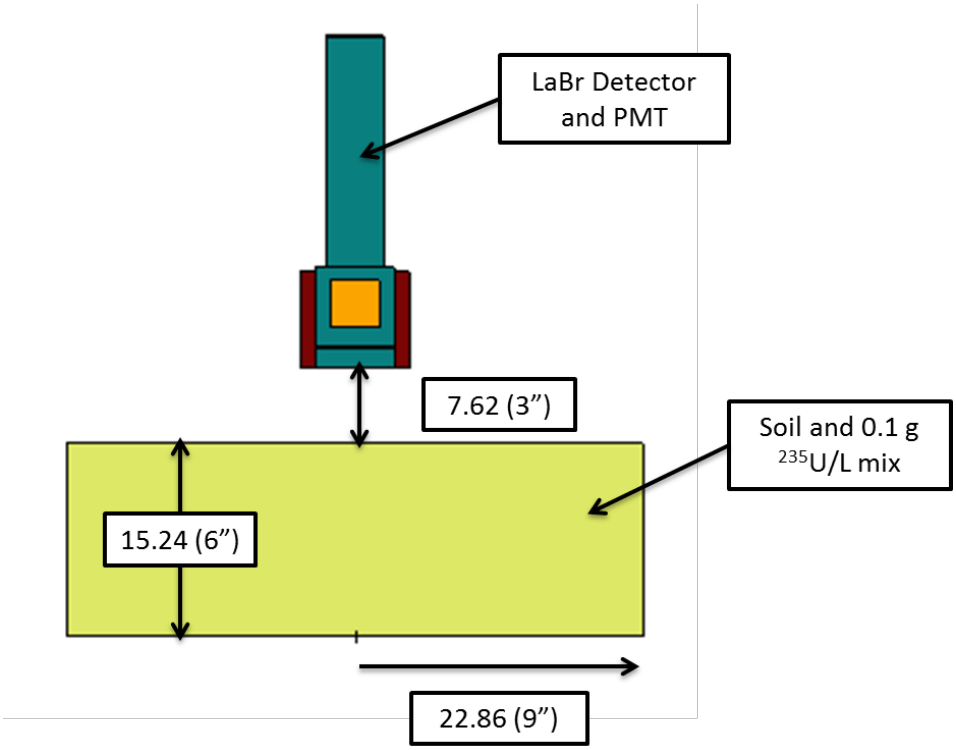

Figure 11. Vertical Cross Section Schematic of MCNP In-Situ Calibration Model.

V.B.4 Model Parameters

The waste medium model parameters and ranges examined for the model described in Section V.B.3.a is detailed in Table XVI.

Table XVI. Model Input Parameters and Ranges Investigated for the LaBr Lump Model

Model Parameter	Parameter Units	Parameter Range Examined
UO_2 Lump Mass	g	3, 6, 10, 15, 25, 50, 75, 100, 125, 200, 300, 350
Enrichment	wt.%	100
Waste Depth Above Lump	in	2, 4, 6, 8
UO_2 Lump Tap Density	g/cm^3	3.5
Soil Density	g/cm^3	1.73, 2.03
Detector-Waste Distance	in	3

In the lump model, UO_2 lumps of various masses were located at the bottom of a cut depth of soil and covered with a specified thickness of clean soil. The radius of the UO_2 lump was regulated by the supplied mass of UO_2. Clean soil was then added on top of and around the calculated radius in increments. The analysis repeated up to 350 g ^{235}U, which represents approximately half of a theoretical subcritical mass.

Based on current field knowledge, dry soil composition was selected for all in-situ measurements. Due to geometrical constraints, not all cases detailed in Table XVI are physically possible.

In the container model detailed in Section V.B.3.b, the Field Container was loaded to various fill heights with a homogenous mix of UO_2 and wet soil. The LaBr detector was placed on contact at the bottom of the container for response measurements to be applied to the developed ^{235}U mass relationship. Because self-shielding may become significant at large quantities of uranium, these cases were repeated for both 5 and 100 wt.% $^{235}U/U$. Based on field knowledge, saturated soil was utilized. This was because the majority of material placed inside the FC originates from inside a drum housing liquid.

The design input parameters for the loaded FC model are presented in Table XVII.

Table XVII. Model Input Parameters and Ranges Investigated for LaBr FC Model.

Model Parameter	Parameter Units	Parameter Range Examined
Source	N/A	Homogeneous mix
Enrichment	wt.%	5, 100
UO_2 Mass	g	3, 6, 10, 15, 25, 50, 75, 100, 125, 200, 300, 350, 700[4], 1000[3], 1500[3]
Fill Percentages	%	25, 50, 75, 95
Clean Soil Density	g/cm^3	2.03

Because the fill height fraction inside the FC was known, providing a calibration for the detector in the bottom position provides the most accurate approach for predicting the amount of ^{235}U that may be present inside the assayed container. Previous scoping studies have shown this location to be the best position for conservative (most restrictive, lowest detected count rate) measurements. Therefore, restricting the assay location to the bottom of the container and selecting a conservative fill height fraction provided a more appropriate assessment of the ^{235}U loading in the FC. In order to select a conservative fill height fraction, the estimated fill height based on visual inspection was rounded up to the nearest 25% in order to assume more media attenuation. For example, if a container was filled to 60% full, a model utilizing 75% was selected.

[4] UO_2 mass value is only used for 5 wt.% enrichment cases.

In the homogeneous waste model detailed in Section V.B.3.c, the distribution of UO_2 within the soil was varied by radius in order to obtain a limit on the detector field of view. In addition, the height of the probe was also raised to 6-in to analyze the larger viewing angle. For these cases, the enrichment was fixed at 100 wt.% ^{235}U/U because self-shielding is not a significant effect for distributed low concentrations. These cases were repeated for dry and saturated conditions.

The detailed input parameters and ranges examined in the homogenous waste model are shown in Table XVIII.

Table XVIII. Model Input Parameters and Ranges Investigated for LaBr Homogeneous Waste Model

Model Parameter	Parameter Units	Parameter Range Examined
Concentration	g^{235}U/L	0.1
Source	N/A	Homogeneous mix
Enrichment	wt.%	100
Soil Density	g/cm3	1.73, 2.03
Detector-Waste Distance	in	3, 6
Waste Radius	in	4.5, 9, 12, 18, 36

V.C. MCNP SUBTERRANEAN PIPING MODELS

V.C.1 Assumptions

Because the purpose of the analysis was to provide calibration factors to predict an upper bound of ^{235}U mass, a number of conservative assumptions on modeling parameters and configurations were employed. These are chosen in order to coincide with

the high end of an expected value and/or slightly beyond an expected condition in order to cause over prediction in the final calculated result. These assumptions also serve to simplify the analysis by reducing the number of variables that are examined as part of the sensitivity studies described in subsequent sections.

Assumptions and modeling parameters employed in this analysis beyond those described in Section V.B.1 are as follows:

- Ground material beneath the pipe was modeled as dry soil.
- Piping structural material included both PVC and cast iron.
- Detector was packaged with and without a collimator.
- The source was distributed within the pipe in annular and segmented debris configurations.
- Source material consisted of solely UO_2 at both enrichments in its' full theoretical density.
- The LaBr detector was positioned 6-in from the pipe outer surface.

Ground material can be conservatively modeled as compacted dry soil without excessively overestimating the amount of ^{235}U that may be present within the assayed pipe. Doing so produced the least detected photon count rates among all other material types that were expected to represent the ground material beneath the assayed piping, i.e., sand, water-saturated soil, dry soil, and concrete. Note that although modeling the ground material as void was conservative, doing so may result in over-predicting the amount of

^{235}U present in the pipe by as much as ~20% (and potentially greater for pipes that are larger than 4.5-in NPS).

V.C.2 Piping Description

Modeled pipe wall thicknesses represent the thicknesses of schedule 40 pipes, and examined pipe sizes ranged from 4-in to 18-in Nominal Pipe Sizes (NPS). Selected pipe sizes were collected from References 58-60. These dimensions are shown in Table XIX.

Table XIX. Schedule 40 NPS Examined in MCNP Calibration

Nominal Pipe Size (NPS)	Outer Diameter, OD		Wall Thickness, T_W	
	(inches)	(mm)	(inches)	(mm)
4.0	4.500	114.30	0.237	6.020
4.5	5.000	127.00	0.247	6.274
5.0	5.563	141.30	0.258	6.553
6.0	6.625	168.27	0.280	7.112
8.0	8.625	219.08	0.322	8.179
10.0	10.75	273.05	0.365	9.271
12.0	12.75	323.85	0.406	10.312
15.0	16.00	406.40	0.500	12.700
18.0	18.00	457.20	0.500	12.700

Among the various piping materials (structural material of the pipe) that were expected to be present at HDP [60], these pipes can be categorized as two types of piping materials:

1. Pipes constructed from light elements which consist of PVC, concrete, and clay; and
2. Pipes constructed from highly attenuating media which consist of pipes constructed from various steel alloys, e.g., cast iron.

The pipe modeled was constructed of PVC and cast iron (carbon steel) with material specifications as described in Section V.A.6 in order to correctly represent the two categories.

V.C.3 Waste Detector Model

The LaBr detector was positioned above the centerline of the intact pipe segment at a fixed height of 6-in above the surface of the outer wall. The example of the waste-detector configuration employed in the calibration analysis calculations is illustrated in Figure 12.

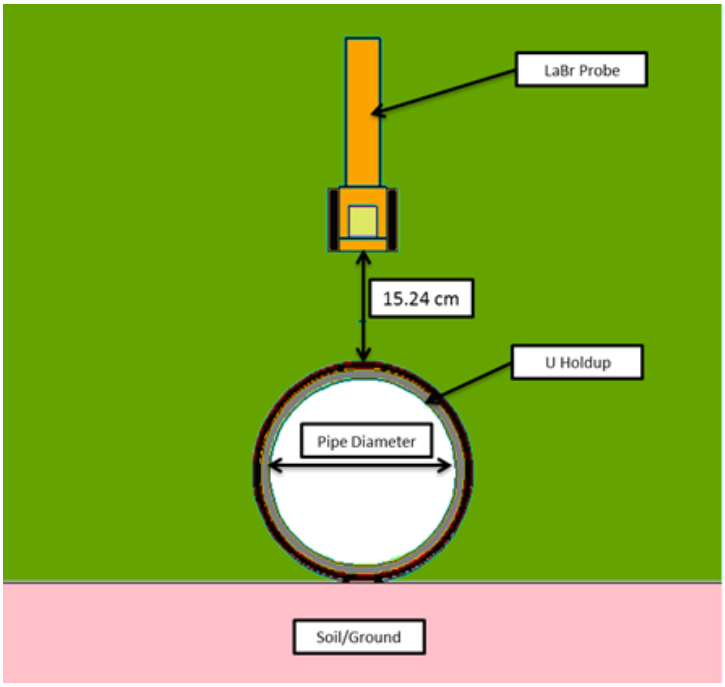

Figure 12. MCNP Schematic Diagram of the Pipe-Detector Configuration.

V.C.4 Pipe Debris Specification

The debris material was residual UO_2 that was homogeneously and uniformly deposited inside the pipe. The debris materials used consist of solely UO_2 in two debris profiles. Using supplied information from Table XIX, input parameters for the MCNP geometry were calculated.

V.C.4.a Annular Model

As shown in Figure 13, the pipe was situated on ground material consisting of clean soil. The UO_2 was deposited in 1-ft lengths with continued pipe material beyond the boundary of the UO_2. The annular distribution of debris hugs the internal edge of the pipe and a void was assumed in the center. The radius of the UO_2 varies with supplied ^{235}U mass.

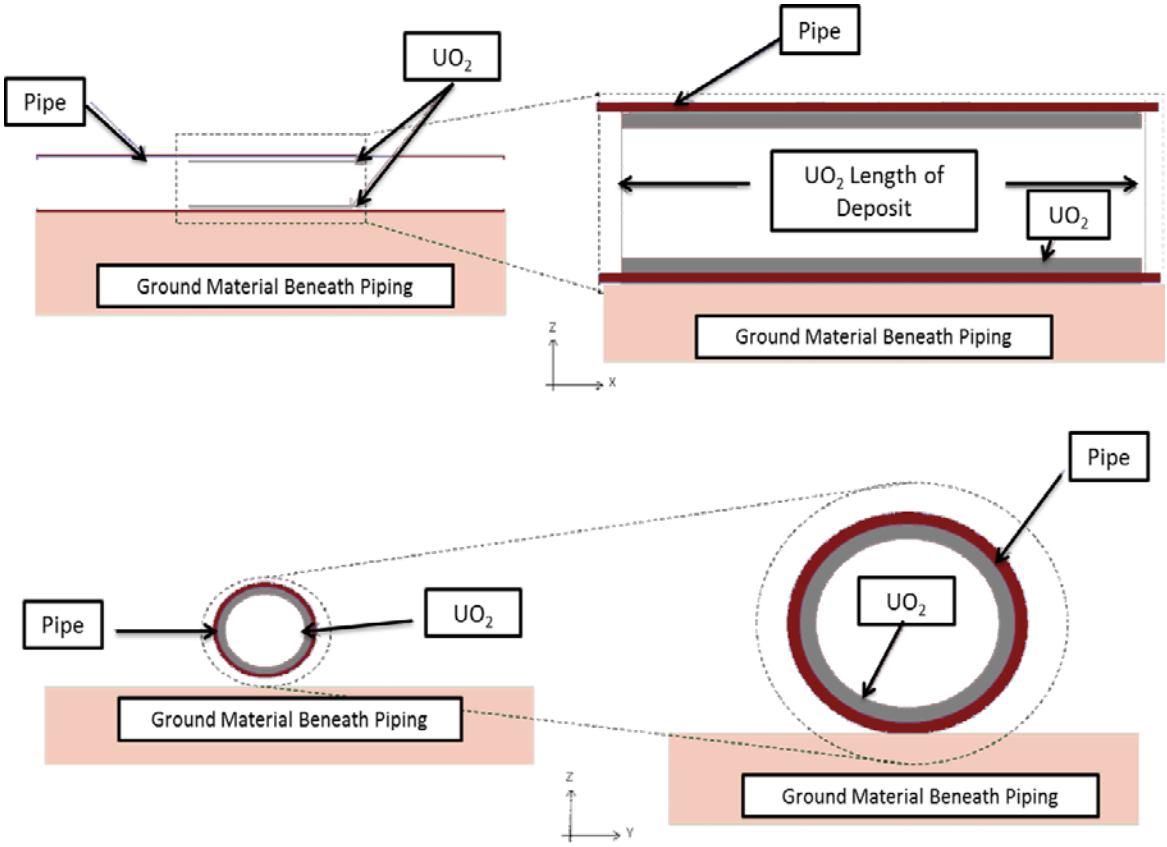

Figure 13. Illustration of the Annular UO_2 Distribution inside the Pipe Used for the MCNP Model.

With reference to the Figure 14 horizontal cross sectional view inside a pipe with the annular distribution, the volume and thickness of the source material were calculated as follows:

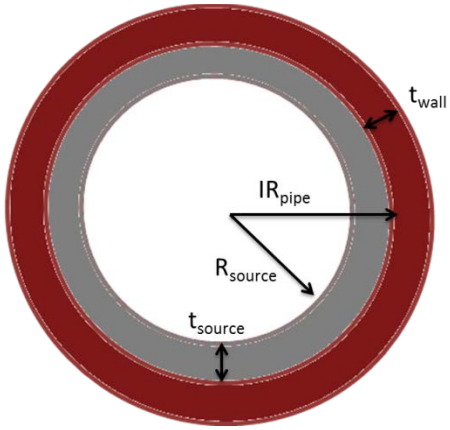

Figure 14. Illustration of Salient Parameters for the Annular UO_2 Deposit.

$$R_{source} = \sqrt{IR_{pipe}^2 - \frac{V_{source}}{\pi \cdot L_{debris}}} \quad (1)$$

$$t_{source} = IR_{pipe} - R_{source} \quad (2)$$

where: R_{source}: is the inner radius of the source region,

IR_{pipe}: is the radius to the inner wall of the pipe,

V_{source}: is the volume of the source material,

L_{debris}: is the length of the debris in the pipe,

t_{source}: is the thickness of the source region.

V.C.4.b Segmented Model

Similar to the annular distribution, the pipe in the segmented model was also seated on clean soil with a debris deposit length of 1-ft. The UO_2 was assumed to be situated at the bottom of the pipe to a height dependent on the supplied ^{235}U mass. A cross sectional view is shown in Figure 15.

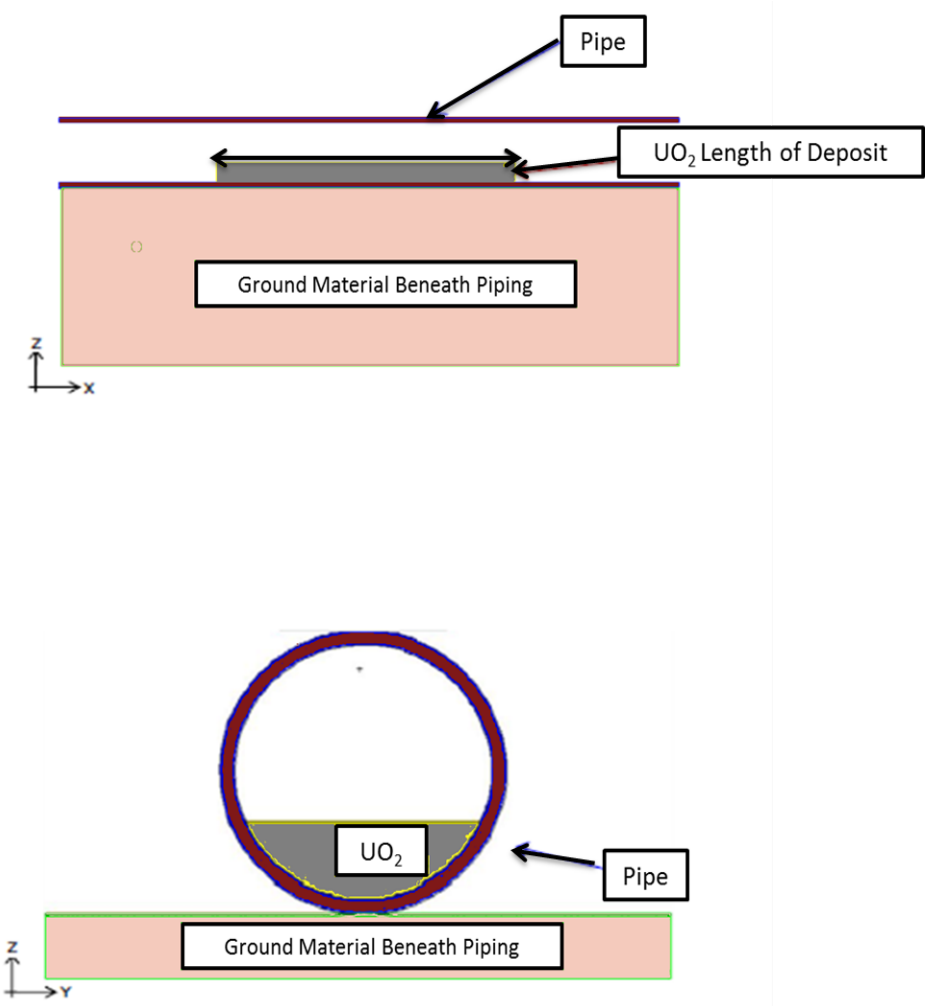

Figure 15. Illustration of the Segmented UO_2 Distribution inside the Pipe Used for the MCNP Model.

With reference to Figure 16 displaying the segmented distribution of the material inside the pipe, the geometric parameters for input into MCNP were calculated as follows:

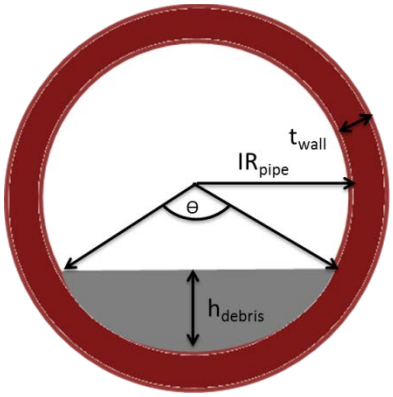

Figure 16. Illustration of Salient Parameters for the Segmented UO_2 Deposit.

The internal radius of the pipe and volume of the pipe wall was calculated based on the supplied pipe wall thickness from Table XIX and using the following relationships:

$$IR_{pipe} = OR_{pipe} - t_{wall} \quad (3)$$

$$V_{pipe}^{wall} = \pi \cdot (OR_{pipe} - IR_{pipe})^2 \cdot L_{debris} \quad (4)$$

where: IR_{pipe}: is the radius to the inner wall of the pipe,

OR_{pipe}: is the outer radius of the pipe,

t_{wall}: is the thickness of the pipe wall,

$V_{pipe,wall}$: is the volume of the wall of the pipe,

L_{debris}: is the length of the debris.

The subsequent volumes for each entity (void space, UO_2 deposit, and total debris) were calculated as follows:

$$V_{pipe}^{void} = \pi \cdot IR_{pipe} \cdot L_{debris} \quad (5)$$

$$V_{source} = \frac{M_{source}}{\rho_{source}} \quad (6)$$

$$V_{total\ debris} = V_{pipe}^{void} + V_{source} \quad (7)$$

where: $V_{pipe,void:}$ is the void space within the pipe,

M_{source}: is the mass of the source material,

IR_{pipe}: is the radius to the inner wall of the pipe,

L_{debris}: is the length of the debris,

ρ_{source}: is the density of the source material,

$V_{total,debris}$:is the total volume of debris,

V_{source}: is the volume of the source material in the pipe.

The debris encompassed both the pipe wall and the source material inside. This is because once the pipe is crushed and disposed of, all of the debris must remain within a specific concentration. To create the MCNP input geometry, further dimensions were required as follows:

$$A_{source} = \frac{V_{source}}{L_{debris}} \quad (8)$$

$$\theta - sin\theta = \frac{2 \cdot A_{source}}{IR_{pipe}^{\ 2}} \quad (9)$$

$$h_{source} = IR_{pipe} \cdot \left(1 - \cos\left(\frac{\theta}{2}\right)\right) \quad (10)$$

where: A_{source}: is the area of the source material,

V_{source}: is the volume of the source material,

L_{debris}: is the length of the debris,

IR_{pipe}: is the radius to the inner pipe wall,

h_{source}: is the height of the source material,

θ: is the angle the source material is dispersed.

V.C.5 Model Parameters

The parameters and ranges examined for the subterranean piping models described in Section V.C.4 are detailed in Table XX.

Table XX. Model Input Parameters and Ranges Examined for the MCNP Piping Model

Model Parameter	Parameter Units	Parameter Range Examined
^{235}U Mass	g	0.1, 1, 5, 7.5, 10, 15, 20, 25, 350, 700
Pipe Sizes	N/A	Table XIX
Enrichment	wt.%	5, 100
Length of Deposit	in	12
Debris Geometry	N/A	annular, segmented
UO_2 Tap Density	g/cm^3	3.5
Detector-Pipe Distance	in	6

V.D. SOURCE TERM FOR THE URANIUM MATERIAL

The source term employed for the calibration basis was determined by decaying UO_2 with a fixed ^{235}U mass content of 1 g (activity 2.161×10^{-6} Ci) for 50 years using the SCALE ORIGEN-S depletion code [52] with UO_2 bremsstrahlung photon data libraries. For decay scheme of ^{235}U and ^{238}U, see Appendix C.

A discrete line source was determined for each isotope with a significant activity, using the gamma lines and intensities reported in the ENDF/B-VI.8 decay data library. ^{231}Th is a decay product of ^{235}U that builds up within a few days. The decayed ^{235}U activity model therefore includes ^{231}Th in secular equilibrium with ^{235}U. Secular equilibrium is achieved when the half-life of the parent nuclide far exceeds the half-life of the daughter product. This causes the parent nuclide and daughter nuclide to have the same decay rate.

^{234}U was not considered in the source term because the ^{234}U photons occur at energies below 50 keV and make an insignificant contribution to the detector response, but the relatively large activity of ^{234}U in the source sample causes MCNP to spend an inordinate amount of time tracking these particles.

V.D.1 Library Specification

The ORIGEN-S depletion was performed using the PWR33GWD multi-burnup binary working library produced from data using a neutron flux spectrum from mid-cycle LWR fuel (33 Gwd/MTU). Cross sections are collapsed from ENDF/B-VI, EAF-99, and FENDL2.0 data using the neutron flux spectrum. There are many advantages to using the binary working library in relation to burn-up calculations; however, this analysis only performs nuclide decay. For this reason, this discussion only focuses on aspects relating to the nuclide decay application.

The LWR ORIGEN-S binary working library is made from card-image ORIGEN-S libraries of SCALE 5 from data of light elements, actinides, and fission products [51]. A binary data library is subdivided into three kinds of libraries: Library 1 for light elements, Library 2 for actinides, and Library 3 for fission products. There was a total of

1,946 nuclides in the library: 698 light elements, 129 actinides, and 1,119 fission products. There are no light elements and no fission products in the result of the decay of UO_2.

V.D.2 5 wt. % ^{235}U/U

The UO_2 and daughter product isotopic activities for 5 wt.% ^{235}U/U are presented in Table XXI as a function of decay time.

Table XXI. UO_2 and Daughter Product Isotopic Activities for a Uranium Enrichment of 5 wt.% ^{235}U/U from ORIGEN Calculation

Nuclide	Nuclide Activity (Ci) as a Function of Decay Time							Fraction after 50 y
	Initial	1 y	5 y	10 y	15 y	50 y	100 y	
tl207	0.000E+00	7.184E-13	1.725E-11	6.558E-11	1.405E-10	1.140E-09	3.186E-09	0.005%
pb211	0.000E+00	7.204E-13	1.730E-11	6.576E-11	1.408E-10	1.143E-09	3.195E-09	0.005%
pb214	0.000E+00	1.082E-20	1.460E-18	1.179E-17	3.994E-17	1.483E-15	1.181E-14	0.000%
bi211	0.000E+00	7.204E-13	1.730E-11	6.576E-11	1.408E-10	1.143E-09	3.195E-09	0.005%
bi214	0.000E+00	1.082E-20	1.460E-18	1.179E-17	3.994E-17	1.483E-15	1.181E-14	0.000%
po211	0.000E+00	1.981E-15	4.756E-14	1.808E-13	3.873E-13	3.143E-12	8.786E-12	0.000%
po214	0.000E+00	1.082E-20	1.460E-18	1.179E-17	3.993E-17	1.483E-15	1.181E-14	0.000%
po215	0.000E+00	7.204E-13	1.730E-11	6.576E-11	1.408E-10	1.143E-09	3.195E-09	0.005%
po218	0.000E+00	1.082E-20	1.460E-18	1.180E-17	3.995E-17	1.484E-15	1.182E-14	0.000%
rn219	0.000E+00	7.204E-13	1.730E-11	6.576E-11	1.408E-10	1.143E-09	3.195E-09	0.005%
rn222	0.000E+00	1.082E-20	1.460E-18	1.180E-17	3.995E-17	1.484E-15	1.182E-14	0.000%
fr223	0.000E+00	9.941E-15	2.387E-13	9.070E-13	1.942E-12	1.577E-11	4.408E-11	0.000%
ra223	0.000E+00	7.204E-13	1.730E-11	6.576E-11	1.408E-10	1.143E-09	3.195E-09	0.005%
ra226	0.000E+00	1.082E-20	1.460E-18	1.180E-17	3.995E-17	1.484E-15	1.182E-14	0.000%
ac227	0.000E+00	7.204E-13	1.729E-11	6.573E-11	1.407E-10	1.143E-09	3.194E-09	0.005%
th227	0.000E+00	7.104E-13	1.706E-11	6.485E-11	1.389E-10	1.127E-09	3.151E-09	0.005%
th230	0.000E+00	7.495E-17	2.030E-15	8.201E-15	1.851E-14	2.066E-13	8.272E-13	0.000%
th231	0.000E+00	2.161E-06	2.161E-06	2.161E-06	2.161E-06	2.161E-06	2.161E-06	9.196%
th234	0.000E+00	6.386E-06	6.386E-06	6.386E-06	6.386E-06	6.386E-06	6.386E-06	27.174%
pa231	0.000E+00	4.573E-11	2.288E-10	4.576E-10	6.864E-10	2.286E-09	4.569E-09	0.010%
pa234m	0.000E+00	6.386E-06	6.386E-06	6.386E-06	6.386E-06	6.386E-06	6.386E-06	27.174%
pa234	0.000E+00	8.302E-09	8.302E-09	8.302E-09	8.302E-09	8.302E-09	8.302E-09	0.035%
u234	0.000E+00	1.630E-11	8.837E-11	1.785E-10	2.685E-10	8.991E-10	1.800E-09	0.004%
u^{235}	2.161E-06	2.161E-06	2.161E-06	2.161E-06	2.161E-06	2.161E-06	2.161E-06	9.196%
^{238}U	6.386E-06	6.386E-06	6.386E-06	6.386E-06	6.386E-06	6.386E-06	6.386E-06	27.174%
Total	8.548E-06	2.349E-05	2.349E-05	2.349E-05	2.349E-05	2.350E-05	2.352E-05	100.0%

V.D.3 100 wt. % ^{235}U/U

The UO_2 and daughter product isotopic activities for 100 wt.% ^{235}U/U are presented in Table XXII as a function of decay time. Photon source activities are in Table XXIII.

Table XXII. UO_2 and Daughter Product Isotopic Activities for a Uranium Enrichment of 100 wt.% ^{235}U/U from ORIGEN Calculation

Nuclide	Nuclide Activity (Ci) as a Function of Decay Time							Fraction after 50 y
	Initial	1 y	5 y	10 y	15 y	50 y	100 y	
tl207	0.000E+00	7.184E-13	1.725E-11	6.558E-11	1.405E-10	1.140E-09	3.186E-09	0.026%
pb211	0.000E+00	7.204E-13	1.730E-11	6.576E-11	1.408E-10	1.143E-09	3.195E-09	0.026%
bi211	0.000E+00	7.204E-13	1.730E-11	6.576E-11	1.408E-10	1.143E-09	3.195E-09	0.026%
po211	0.000E+00	1.981E-15	4.756E-14	1.808E-13	3.873E-13	3.143E-12	8.786E-12	0.000%
po215	0.000E+00	7.204E-13	1.730E-11	6.576E-11	1.408E-10	1.143E-09	3.195E-09	0.026%
rn219	0.000E+00	7.204E-13	1.730E-11	6.576E-11	1.408E-10	1.143E-09	3.195E-09	0.026%
fr223	0.000E+00	9.941E-15	2.387E-13	9.070E-13	1.942E-12	1.577E-11	4.408E-11	0.000%
ra223	0.000E+00	7.204E-13	1.730E-11	6.576E-11	1.408E-10	1.143E-09	3.195E-09	0.026%
ac227	0.000E+00	7.204E-13	1.729E-11	6.573E-11	1.407E-10	1.143E-09	3.194E-09	0.026%
th227	0.000E+00	7.104E-13	1.706E-11	6.485E-11	1.389E-10	1.127E-09	3.151E-09	0.026%
th231	0.000E+00	2.161E-06	2.161E-06	2.161E-06	2.161E-06	2.161E-06	2.161E-06	49.862%
pa231	0.000E+00	4.573E-11	2.288E-10	4.576E-10	6.864E-10	2.286E-09	4.569E-09	0.053%
u^{235}	2.161E-06	2.161E-06	2.161E-06	2.161E-06	2.161E-06	2.161E-06	2.161E-06	49.862%
Total	2.161E-06	4.323E-06	4.323E-06	4.324E-06	4.325E-06	4.334E-06	4.353E-06	100.0%

Table XXIII. Photon Source Yields for Decayed ^{235}U

Isotope	Decayed ^{235}U [Bq/g ^{235}U]
u-234	0.0000E+00
u-235	7.9957E+04
u-236	0.0000E+00
u-238	0.0000E+00
th-231	7.9957E+04
pa-234m	0.0000E+00
Total	1.5991E+05

V.E. TALLY SPECIFICATION

The MCNP pulse height tally "F8" was used in this analysis with an energy mesh of 1 keV per bin with an energy range of 0 to 2,000 keV.

V.F. MCNP OUTPUT

The MCNP output file results provided the mean (average) calculated count rates in units of counts per source particle, and the statistical uncertainty in the calculated count rates as a fraction of the mean. The results were equivalent to the traditional term used to describe overall efficiency for the macroscopic system. To account for the statistical uncertainty, the MCNP calculated detector response was reduced by twice the reported uncertainty, as follows:

$$D_{97.7\%} = D_{mean} \times (1 - 2\sigma_{mean}) \quad (11)$$

where: $D_{97.7\%}$: is the minimum count rate at the 97.7% confidence level (cpm);

D_{mean}: is the mean value for the count rate as calculated by the MCNP (cpm); and

σ_{mean}: is standard deviation in D_{mean}, and is also calculated by MCNP.

MCNP produces a wealth of information about a simulation to allow the user to assess the precision of the result. The initial focus should be on the ten statistical indices calculated by MCNP in order to assess the reliability of the result. The ten statistical tests include

- Tally Mean (1)
- Relative Error (3)
- Figure of Merit (2)
- Variance of the Variance (3)
- The Empirical PDF for the Tally (1)
- Confidence Intervals

If any of these tests fails, a warning is printed in the output and the code produces additional output to aid the user in interpreting the seriousness of the failed test(s). While these ten statistical tests provide an excellent indication of the reliability of the result, they are not foolproof.

In the case of the simulations described herein, all statistical tests were passed with the exception of the cases with very low fissile material in a large geometry (i.e., 0.1 g ^{235}U in an 18" NPS). In these cases, the sampling medium was not significant to produce

enough histories for good statistics. These cases were rejected and not included in the final results.

CHAPTER VI

DETECTOR PERFORMANCE

VI.A. FIELD OF VIEW

The optimal viewing angle of a scintillator detector is at a downward 45 degree angle from the center of the crystal. The probability of a photon reaching the crystal for interaction decreases steeply outside of this viewing angle.

As a part of an effort to perform in-situ waste interrogation on a 6-in thick layer, a capable detector viewing angle was established via parametric study on waste radius and probe height. The model shown in Figure 11 is an example of one configuration utilized. Table XXIV displays the results for dry and saturated soils with various ^{235}U loadings dispersed homogeneously to equate to a concentration of 0.1 g $^{235}U/L$.

Since the 185.7 keV photopeak was utilized for uranium quantification, this was the sole photopeak investigated for the detector FOV. The FOV varies for different gamma energies.

Table XXIV. LaBr FOV Scoping Results for 0.1 g $^{235}U/L$ (100 wt.% $^{235}U/U$) from MCNP

Soil	Probe Height (cm)	Waste Radius (in)	Mass (g ^{235}U)	Detector Count Rate [/min] 185.7 keV
dry	7.62	4.5	0.6255	1819
dry	7.62	9	2.502	4162
dry	7.62	12	4.448	5156
dry	7.62	18	10.008	6345
dry	7.62	36	40.032	7260
dry	15.24	4.5	0.6255	867
dry	15.24	9	2.502	2562

Table XXIV. Continued.

Soil	Probe Height (cm)	Waste Radius (in)	Mass (g ^{235}U)	Detector Count Rate [/min] 185.7 keV
dry	15.24	12	4.448	3544
dry	15.24	18	10.008	4985
dry	15.24	36	40.032	6626
wet	7.62	4.5	0.6255	1606
wet	7.62	9	2.502	3591
wet	7.62	12	4.448	4418
wet	7.62	18	10.008	5377
wet	7.62	36	40.032	6120
wet	15.24	4.5	0.6255	761
wet	15.24	9	2.502	2225
wet	15.24	12	4.448	3047
wet	15.24	18	10.008	4190
wet	15.24	36	40.032	5623

The results are plotted graphically in Figure 17. The response from the detector is expected to be almost linear while viewing an area at 45 degree downward angle. As this area is expanded, while holding the photon source distribution constant, the detector response is expected to lose linearity. The FOV of the detector was considered appropriate for detection of uranium as long as it retained a linear response function for the 185.7 keV photon. The LaBr continues to respond linearly as follows:

- Up to approximately 12-in radius for dry waste with the detector positioned 3-in above the waste surface;
- Up to approximately 15-in radius for wet waste with the detector positioned 3-in above the waste surface; and
- Up to approximately 18-in radius for dry and wet waste with the detector positioned 6-in above the waste surface.

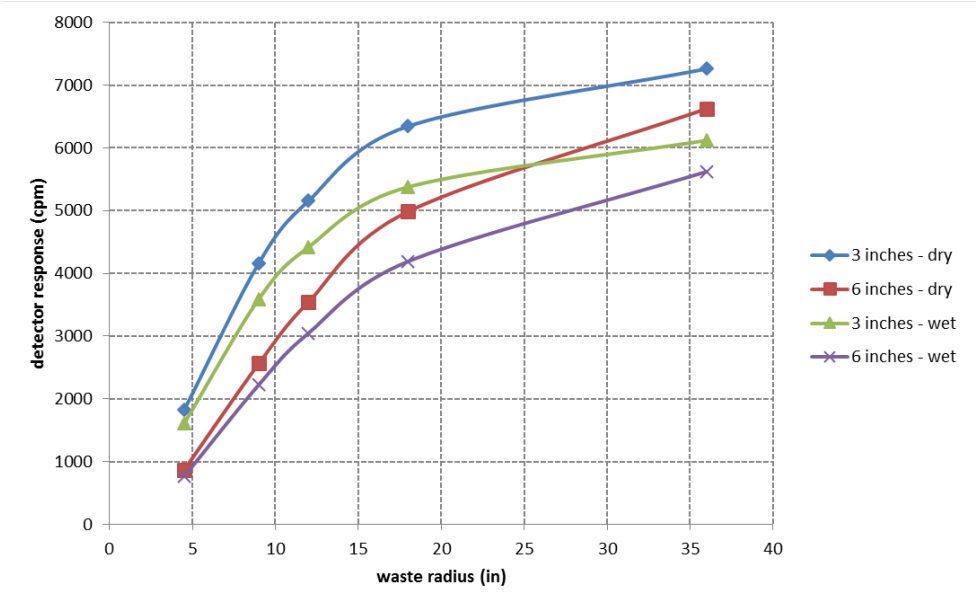

Figure 17. LaBr 185.7 keV Detector Response from MCNP for Various Probe Heights at a Fixed 6-in Waste Depth.

These results established a dimension for what was described as an "immediate surrounding area" for a hot spot (FOV). The extent of the immediate surrounding area in this context was equivalent to a disc with a radius of 18-in from the measurement location with the LaBr crystal positioned at least 6-in from the surface of the waste.

VI.B. MCNP AND ISOCS EFFICIENCIES

Typical methods of waste material characterization involve the use of Canberra's coupled software, ISOCS, with an HPGe detector as described in Section IV.A.3. This detector requires cryogenic cooling and is subject to variation in temperature and humidity, in addition to being very expensive. The ISOCS software is a simple tool that allows the user to describe the geometry and couples a detector characterization and

material attenuation factors to determine an overall efficiency. The overall efficiency is then applied to the spectrum obtained for the assay sample.

VI.B.1 Efficiency Comparison

The F8 tally obtained from MCNP directly correlates to the overall efficiency for the system, taking into account intrinsic efficiency of the detector (crystal) and the absolute efficiency of the geometry and surroundings. Table XXV compares the overall efficiencies of an ISOCS setup and the equivalent MCNP result for the two primary ^{235}U photopeaks. The primary purpose of this comparison was to isolate the discrepancies between the two methods, Monte Carlo and mathematical techniques.

The model had a fixed uranium mass at 100 grams. As the fill height increases, the percent of uranium in the source decreases. The geometry and material description utilized in this comparison was equivalent to that described in the MCNP models. The "fill" parameter is the percent fill height of the 20 L container.

Table XXV. Efficiencies for Uranium Photopeaks at Various Container Fill Heights

Parameter			ISOCS			MCNP		Comparison	
Fill	Energy	U Mass (g)	% U	Efficiency	σ (%)	Efficiency	σ (%)	% Variation	Ratio
25%	185.7	100	1.00	1.22E-03	0.08	1.36E-03	0.0008	10.03%	1.11 ± 0.089
50%	185.7	100	0.52	6.37E-04	0.08	7.12E-04	0.0011	10.58%	1.12 ± 0.089
75%	185.7	100	0.35	4.30E-04	0.08	4.82E-04	0.0013	10.72%	1.12 ± 0.090
95%	185.7	100	0.27	3.42E-04	0.08	3.83E-04	0.0023	10.87%	1.12 ± 0.090
25%	143.8	100	1.00	2.17E-04	0.08	2.76E-04	0.0017	21.29%	1.27 ± 0.102
50%	143.8	100	0.52	1.16E-04	0.08	1.49E-04	0.0024	22.29%	1.29 ± 0.103
75%	143.8	100	0.35	7.91E-05	0.08	1.02E-04	0.0029	22.53%	1.29 ± 0.103
95%	143.8	100	0.27	6.31E-05	0.08	8.15E-05	0.0049	22.53%	1.29 ± 0.103

MCNP consistently produced a higher efficiency for each UO_2 photon in the given geometry compared to ISOCS. Since the built-in ISOCS intrinsic efficiencies were based on empirical MCNP-derived relationships, it is expected that the comparison would be close for point sources (see Section IV.A.3). The treatment of material attenuation coefficient is where the result diverges. The higher efficiency resulting from MCNP produces conservative (lower) results in the activity and gram calculation for NCS purposes. It would be ideal to compare these numbers for an experimental configuration, but a physical standard for the configurations listed does not exist.

Limitations of the ISOCS Geometry Composer software include its inability to model any more than one source location. The built-in geometry descriptions are general, but would apply to most encountered scenarios, as long as the materials are properly homogenized prior to building the model. In relation to this work, the subterranean piping models were not achievable in the ISOCS software. In addition, ISOCS software is specific to Canberra Industries, whereas, use of MCNP makes the method applicable to any detector.

The primary limitation lies in the implementation of the methods, which is further discussed in Chapter IX. Table B.I in Appendix B includes a sampling of ten measurements performed with the original characterization method using the HPGe with ISOCS software and the InSpector 1000 LaBr with MCNP. The two results are not directly comparable in order to assess validity because the measurement conditions were not controlled; however, it can be used for informational purposes.

VI.B.2 Spectral Comparison

The InSpector 1000 was capable of utilizing an ISOCS geometry for efficiency calculation coupled to an analysis sequence algorithm specified in GENIE 2000. When MCNP geometry efficiencies were utilized as a calibration basis, the ISOCS option was bypassed; however, GENIE 2000 continued to operate as the analysis algorithm to analyze a spectrum.

A visual depiction of the method of characterization is shown in Figure 18 as a dual plot of the ideal 100 wt.% ^{235}U/U loading into a 25% filled FC and an actual FC of waste considered to be HEU, taken from the InSpector 1000 60 second assay. The MCNP spectrum is representative of 75 g ^{235}U homogeneously dispersed in soil. This ^{235}U gram value is large enough to obtain a spectrum with distinct photopeaks for display purposes.

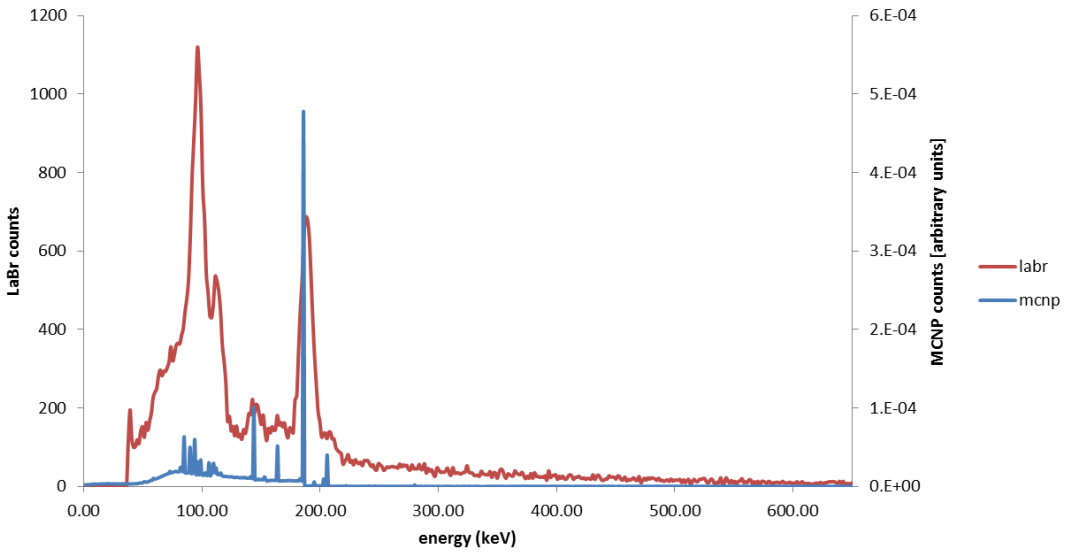

Figure 18. Spectral Overlay of Actual HEU Waste and MCNP Model of 25% Filled FC.

The LaBr spectrum displays a realistic Compton continuum, to be expected, in addition to ^{235}U broadened photopeaks and associated x-rays. The MCNP spectrum is not broadened and peaks represent uncollided photon tallies thus occupy a single energy bin. The count rates resulting from the MCNP tally were applied to the net peak area (area above the Compton continuum) of each photopeak.

VI.C. ACTIVITIES BENCHMARK

A NIST traceable standard was available for a mixed soil gamma source in a 1 liter Marinelli container. Using an ISOCS developed geometry stored on the InSpector 1000, an experimental comparison was made between the standard and the measured activities on the detector. Although these do not include an MCNP comparison, it does bring a software benchmark full circle. Table XXVI displays the results for a three minute count time.

Activities reported on the InSpector1000 were derived using an ISOCS geometry and efficiency, with GENIE 2000 algorithms as described in Section IV.A.4.

This experimental NIST standard measurement, along with that shown in Table XXV, validated the use of the InSpector 1000 with LaBr detector for MCNP characterization for uranium photopeaks. The methodology of this validation is shown in Figure 19.

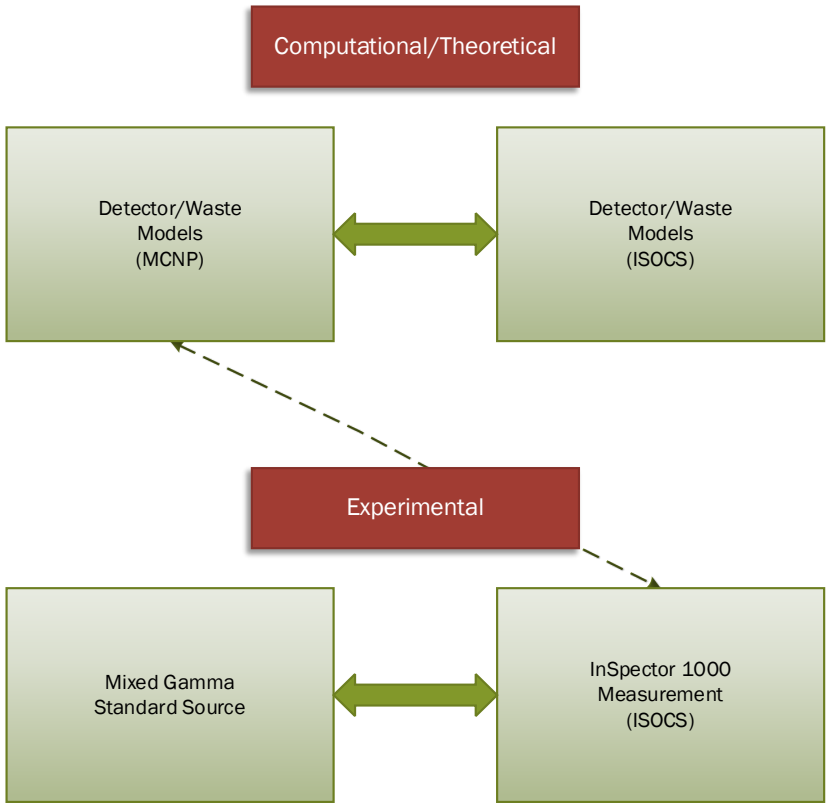

Figure 19. Demonstration Mechanism and Validation Scheme for InSpector 1000 and MCNP.

Table XXVI. Activity Results from InSpector 1000 for Standard Marinelli Mixed Gamma Source

Nuclide	*NIST Traceable Marinelli*			*LaBr - Default InSpector 1000 Report*			Ratio
	Weighted Mean Activity (uCi/unit)	Weighted Mean Activity Uncertainty[5] (%)	Weighted Mean Activity Uncertainty[4] (uCi)	Weighted Mean Activity (uCi/unit)	Weighted Mean Activity Uncertainty[4] (%)	Weighted Mean Activity Uncertainty[4] (uCi)	
Co-57	0.011	7.86	0.001	0.010	15.2	0.002	1.1 ± 0.188
Co-60	0.056	4.33	0.002	0.038	5.8	0.002	1.5 ± 0.106
Cd-109	0.750	10.03	0.075	0.777	11.4	0.089	1.0 ± 0.147
Sn-113	0.008	11.84	0.001	0.005	32.7	0.002	1.6 ± 0.542
Cs-137	0.041	6.52	0.003	0.029	10.1	0.003	1.4 ± 0.169
Ce-139	0.007	22.44	0.002	0.006	20.3	0.001	1.2 ± 0.353
Am-241	0.092	10.00	0.009	0.115	12.3	0.014	0.8 ± 0.127

[5] These results are reported at 2σ

CHAPTER VII

FISSILE MATERIAL CHARACTERIZATION

VII.A. IN-SITU CONCENTRATION LIMITS

Described extensively in Section II.B.1 are the criteria for exemption of waste material from NCS controls. Included in these criteria is waste with an overall concentration of less than 0.1 g ^{235}U/L. Using the results in Section VI, an upper threshold for this concentration in an 18-in radius and 6-in depth was conceived.

With a 185 keV detector response at approximately 5,000 cpm for dry soil/waste and approximately 4,000 cpm for wet soil/waste, the in-situ layer was categorized as less than 0.1 g ^{235}U/L and exempt from NCS controls.

Since these detector limits apply to situations in which the ^{235}U is uniformly distributed (rather than "lumped"), it was necessary to evaluate the potential magnitude of ^{235}U lumps that could potentially go undetected with these specific measurement limits. This issue is addressed in the following section.

VII.B. IN-SITU BOUNDING LUMP SCENARIO

The model for the lump scenario is described extensively in Section V.B.3.a. Table XXVII gives the tabular results for 185.7 keV detector responses for the lump of uranium and soil positioned at the base of various cut depths. The graphical depiction is shown in Figure 20.

Table XXVII. LaBr 185.7 keV Detector Response Results for the MCNP Lump Model

Soil Depth [cm]	Lump Tap Density [g/cc]	Mass ^{235}U [g]	Detector Count Rate [/min]
5.08	3.5	3	6762
	3.5	6	12950
	3.5	10	21087
	3.5	15	31332
	3.5	25	52513
	3.5	50	110370
10.16	3.5	3	1221
	3.5	6	2309
	3.5	10	3723
	3.5	15	5482
	3.5	25	9048
	3.5	50	18566
	3.5	75	28965
	3.5	100	40472
	3.5	125	52773
	3.5	200	96286
	3.5	300	168663
	3.5	350	211480
15.24	3.5	3	257
	3.5	6	483
	3.5	10	771
	3.5	15	1133
	3.5	25	1849
	3.5	50	3740
	3.5	75	5765
	3.5	100	7935
	3.5	125	10305
	3.5	200	18369
	3.5	300	31373
	3.5	350	38759
20.32	3.5	3	59
	3.5	6	112
	3.5	10	179
	3.5	15	260
	3.5	25	420
	3.5	50	830
	3.5	75	1272
	3.5	100	1755
	3.5	125	2245
	3.5	200	3979
	3.5	300	6788
	3.5	350	8310

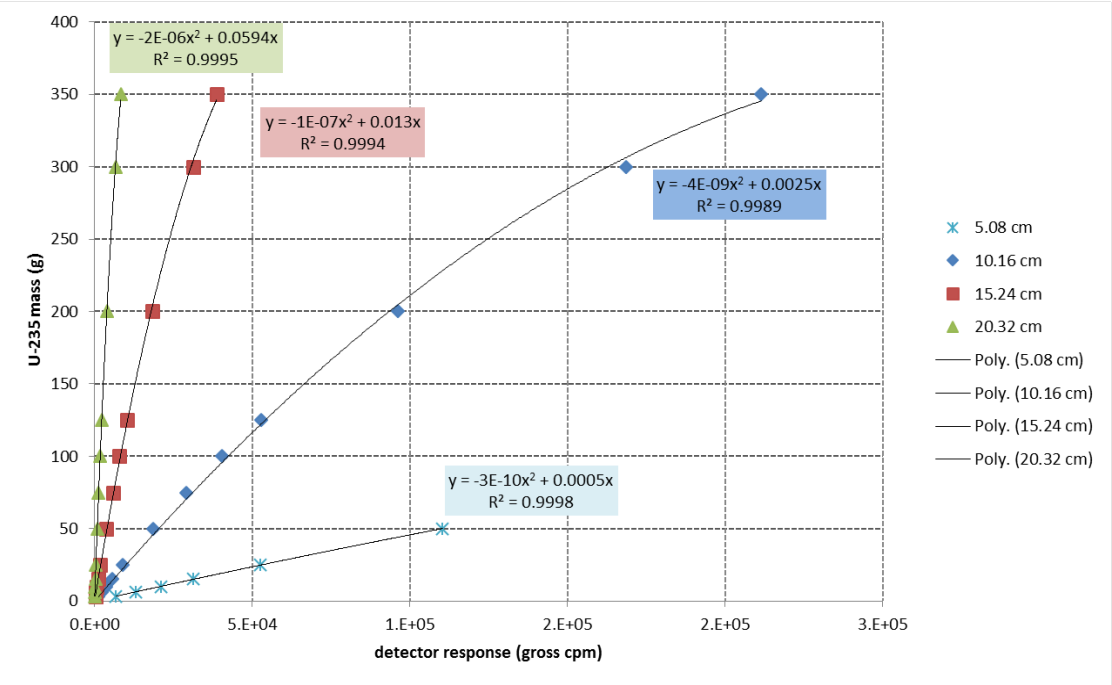

Figure 20. ^{235}U Mass as a Function of 185.7 keV Detector Response with Trend Lines for the MCNP Lump Model.

Although the response variable (detector response) would generally be displayed on the y-axis, the scatter plot was reversed for a reason. Quadratic trend lines were added in Figure 20 to establish a fit to the data. Since the goal was to develop a simple, empirical relationship to estimate grams of ^{235}U, the arrangement of the plot allowed a detector response to be inserted into a best-fit line and obtain a ^{235}U gram estimate.

The results for 20.32 cm of soil (8-inches), shown in green, did not have enough variation per unit mass to be considered for use. These were considered obsolete for actual field use but shown for informational purposes. As ^{235}U loading increases, the size of the lump increases in diameter and becomes closer to the face of the detector, therefore increasing the efficiency. The density of the lump remains constant as the surface area

increases. This does not cause drastic effects to the detected count rate since the increase in surface area and proximity to the detector offsets the increase in self-attenuation.

VII.C. EX-SITU CONCENTRAITON LIMITS

Following excavation of waste material, it was not uncommon to be laid out into a thin layer on a sorting table or sheet of plastic for close proximity radiological survey. For these cases, the detector FOV still applies thus was fixed at a waste radius of 18-in and probe height at 6-in above the waste. Threshold count rates that equate to a concentration of 0.1 g ^{235}U/L were established for a 2-in thick layer of waste. These results are presented in Table XXVIII for both soil types and collimator configurations.

Table XXVIII. LaBr Results for 2-in Waste Depth with 0.1 g ^{235}U/L (100 wt.% ^{235}U/U)

Soil	Collimator	Probe Height (cm)	Waste Radius (in)	Mass (g ^{235}U)	Detector Count Rate [/min] 185.7 keV
wet	Yes	15.24	18	3.336	888
wet	No	15.24	18	3.336	2570
dry	Yes	15.24	18	3.336	982
dry	No	15.24	18	3.336	2855

The threshold count rates established in the previous section for in-situ measurements on 6-in depth of soil do not apply to a 2-in waste depth because the total volume of soil is much less. Since a measurement was assumed to be taken at the point of the highest radiological reading, that point must be mixed with surrounding clean material to achieve a concentration of no more than 0.1 g ^{235}U/L.

By agitating the waste prior to excavation and the LaBr measurement, the likelihood of encountering a lump condition was further reduced. It is likely that a large lump would either be visualized or mixed in the surrounding waste following agitation and/or excavation. In addition, better replication of the uniform modeling conditions was likely, following any amount of mixing. Densities used for soil and waste were conservatively selected for in-situ material. This means that the density used in this analysis was higher than the measured density of samples in order to account for additional packing, uncertainties, and natural variation. Following removal, the density of the material naturally decreased as void space increased. For ex-situ measurements, the real waste density will repeatedly be less than that utilized in the model and produce further conservatism in the application.

In practice, ex-situ measurement methods were preferred for multiple reasons including: additional mixing and visual inspection to correctly apply the calibration basis; reduced waste density; isolation from surrounding material possibly contributing to detector response; increased material control (when waste under interrogation was isolated). These attributes further enhanced the applicability of the calibration basis to actual conditions.

VII.D. CONTAINER MASS ASSIGNMENTS

VII.D.1 Effect of Enrichment

As enrichment increases for a fixed mass of uranium, the detected gross gamma count rate in the 50 keV to 2,000 keV window increases. An illustration of the photon

spectra observed by the LaBr detector for 75 g ^{235}U present as UO_2 within the fissile material mixture at 5% and 100% enrichments are provided in Figure 21.

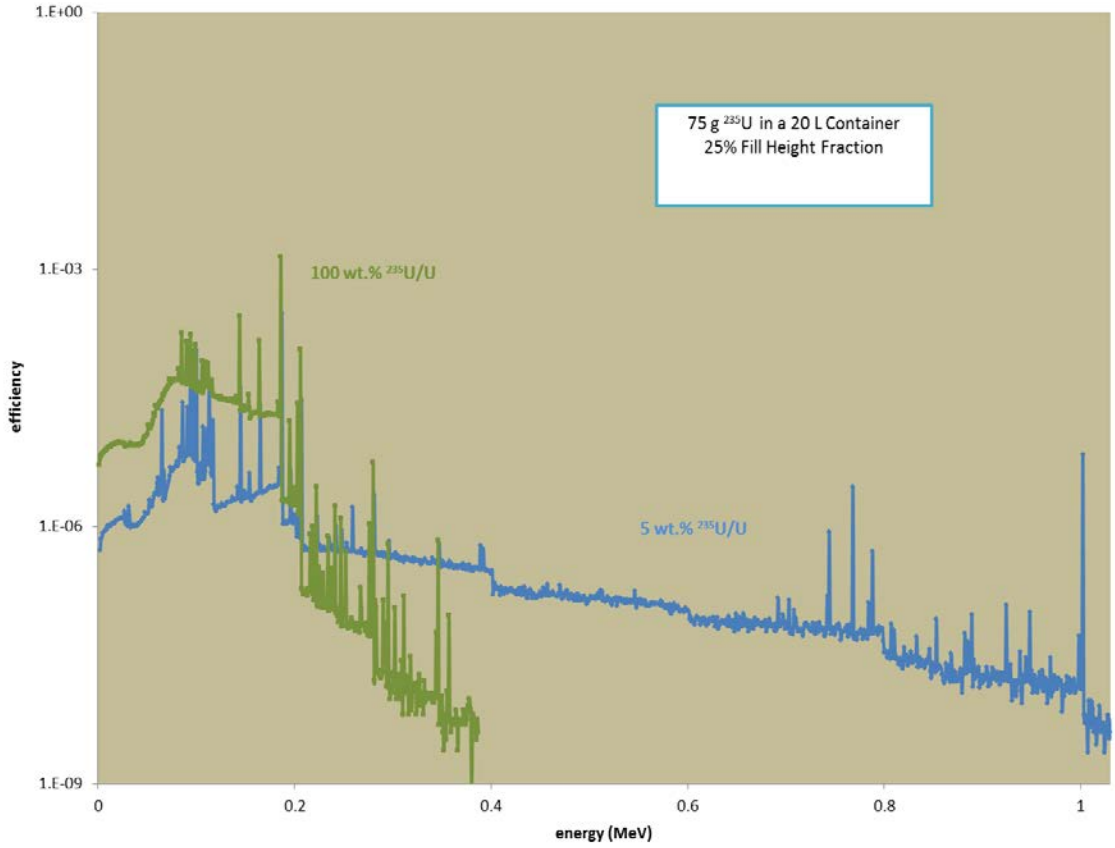

Figure 21. MCNP Simulated LaBr γ Spectra from 75 g ^{235}U at Enrichments of 5% and 100%.

Figure 21 indicates that at higher enrichments, the rate of detection of photons with energies above approximately 200 keV diminishes, because the higher energy photons are produced by the decay of ^{238}U and its daughters. Although the production of photons from uranium decay decreases, the overwhelming effect is a decrease in the uranium self-

shielding. Therefore, more photons are able to escape the fissile material mixture at higher enrichments.

The results also indicate that as the amount of uranium in the container increases, the rate of increase in the count rates (as a function of increasing enrichment) also increases. This is because the attenuation in the fissile region is driven more by the attenuation of uranium rather than the soil material at higher uranium loading.

Because the purpose of the calibration analysis was to provide a robust but conservative method of estimating the amount of ^{235}U in the container, modeling the uranium at low enrichments was appropriate. Specifically, since the 185.7 keV region was isolated for this purpose, and the conservative count rate in that region was at 5 wt.%, enrichment could not be ignored for conservative ^{235}U loading results. In this discussion, conservative is solely meant to represent any value below the real value, in other words, to produce an underestimation of ^{235}U.

VII.D.2 FC Calibration Analysis

Results obtained from the models described in Section V.B.3.b are shown in the following sub-sections. A calibration basis for both 5% and 100% enrichment were retained for field use. Although the more conservative approach would have been to select 5 wt.% $^{235}U/U$ for all applications, this method was intended to provide a conservative, yet accurate characterization through simple calculations. Utilizing both enrichment values remained within the scope.

VII.D.2.a 100 wt.% ^{235}U/U

Table XXIX provides the observed detector response from measurements performed with the LaBr detector placed on contact with the bottom of the assayed container as a function of increasing ^{235}U loadings in wet soil for each fill height.

Criticality safety controls limit the ^{235}U loading of any container to 350 g. For this reason, the maximum analyzed loading was 350 g ^{235}U.

Table XXIX. LaBr Detector Calibration Results for the Loaded FC MCNP Model at 100 wt.% ^{235}U/U

FC Fill Fraction	Mass ^{235}U [g]	Detector Count Rate [/min] 185.7 keV
0.25	3	25260
	6	50376
	10	83652
	15	124898
	25	206198
	50	402985
	75	591463
	100	771449
	125	943909
	200	1420180
	300	1973294
	350	2220411
0.50	3	12687
	6	25340
	10	42154
	15	63082
	25	104645
	50	206899
	75	306716
	100	404237
	125	499652
	200	772856
	300	1109954
	350	1268214

Table XXIX. Continued.

FC Fill Fraction	Mass ^{235}U [g]	Detector Count Rate [/min] 185.7 keV
0.75	3	8449
	6	16882
	10	28099
	15	42081
	25	69918
	50	138693
	75	206510
	100	273166
	125	338861
	200	529944
	300	771861
	350	887632
0.95	3	6667
	6	13324
	10	22184
	15	33229
	25	55243
	50	109803
	75	163650
	100	216890
	125	269519
	200	423295
	300	620012
	350	715005

A dispersed geometry in a low-Z material such as soil does not produce large self-shielding effects. As a result, and as shown in Figure 22, the trend is relatively linear. For better fitting purposes, a quadratic regression was applied in this case. Since the brevity of the fitting equation will have no bearing on the implementation difficulty, a better fit was appropriate.

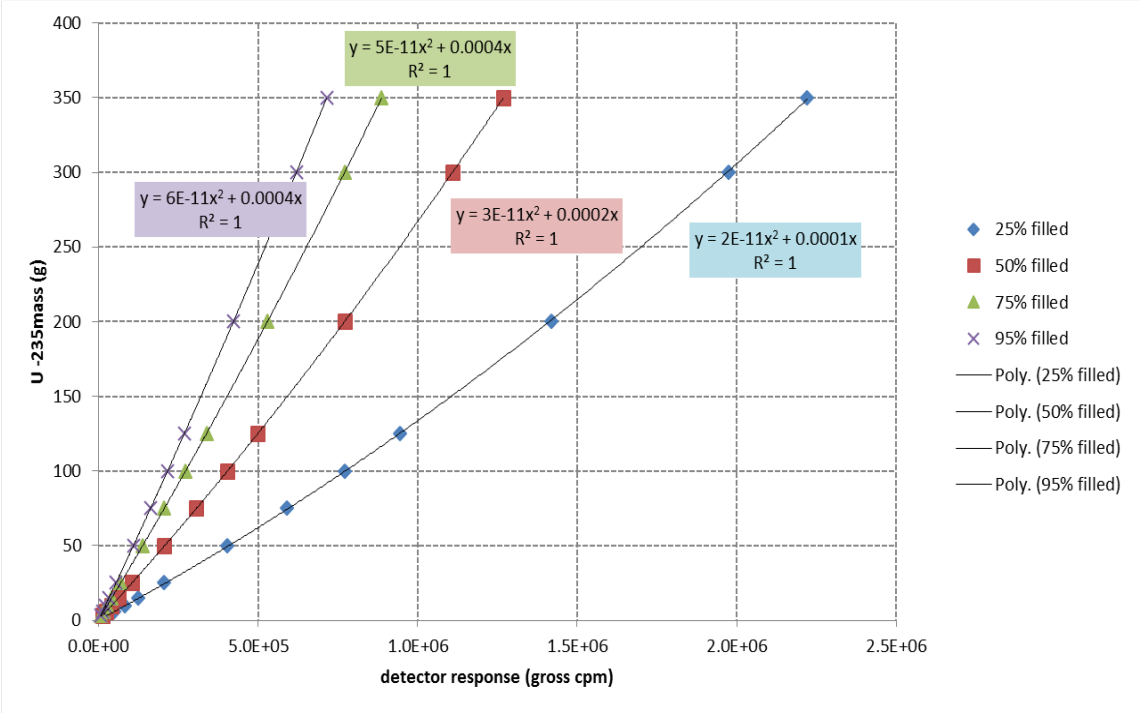

Figure 22. ^{235}U Mass as a Function of 185.7 keV Detector Response for the Loaded FC MCNP Model at 100 wt.% ^{235}U/U.

VII.D.2.b 5 wt.% ^{235}U/U

Table XXX provides the observed detector response from measurements performed with the LaBr detector placed on contact with the bottom of the assayed container as a function of increasing ^{235}U loadings in wet soil for each fill height.

Table XXX. LaBr Detector Calibration Results for the Loaded FC MCNP Model at 5 wt.% $^{235}U/U$

FC Fill Fraction	Mass ^{235}U [g]	Detector Count Rate [/min] 185.7 keV
0.25	0.15	820
	0.3	1635
	0.5	2714
	0.75	4050
	1.25	6684
	2.5	13022
	3.75	19037
	5	24766
	6.25	30233
	10	45117
	15	62063
	17.5	69519
	35	108633
	50	130682
	75	155194
0.5	0.15	412
	0.3	823
	0.5	1369
	0.75	2047
	1.25	3396
	2.5	6698
	3.75	9916
	5	13045
	6.25	16093
	10	24778
	15	35410
	17.5	40354
	35	69375
	50	88511
	75	112434
0.75	0.15	275
	0.3	548
	0.5	913
	0.75	1366
	1.25	2270
	2.5	4499
	3.75	6689
	5	8839

Table XXX. Continued.

FC Fill Fraction	Mass ^{235}U [g]	Detector Count Rate [/min] 185.7 keV
0.75	6.25	10949
	10	17079
	15	24754
	17.5	28411
	35	50920
	50	66875
	75	88176
0.95	0.15	217
	0.3	433
	0.5	721
	0.75	1079
	1.25	1794
	2.5	3564
	3.75	5308
	5	7031
	6.25	8723
	10	13654
	15	19936
	17.5	22971
	35	42029
	50	55950
	75	75163

A graphical representation of the above results is shown in Figure 23. The trends are less linear than those for 100 wt. % ^{235}U/U because of the larger contribution from uranium self-attenuation. As the fill height increases, the capability of detection of photons also decreases because of the increasing effect of self-attenuation. This is shown with the increasing space between response profiles.

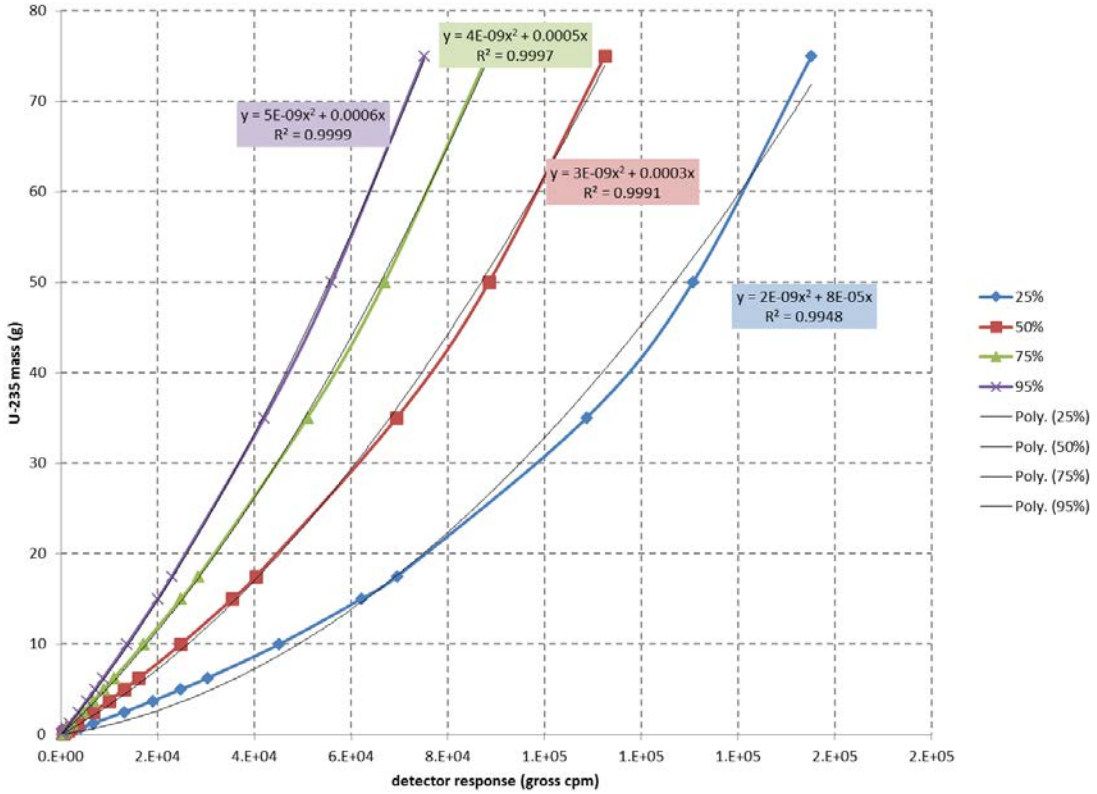

Figure 23. ^{235}U Mass as a Function of 185.7 keV Detector Response for the Loaded FC MCNP Model at 5 wt.% ^{235}U/U.

The typical fill height for an FC in field operation was about 75%. Figure 24 compares the response variation between the two enrichment values for this typical fill height. It is clear that as the mass increases, the range of the detector response at 185.7 keV widens. An increased total mass of uranium in the 5% enrichment case causes significantly more self-attenuation than the 100% enrichment case. This effect becomes more prominent as ^{235}U uranium increases.

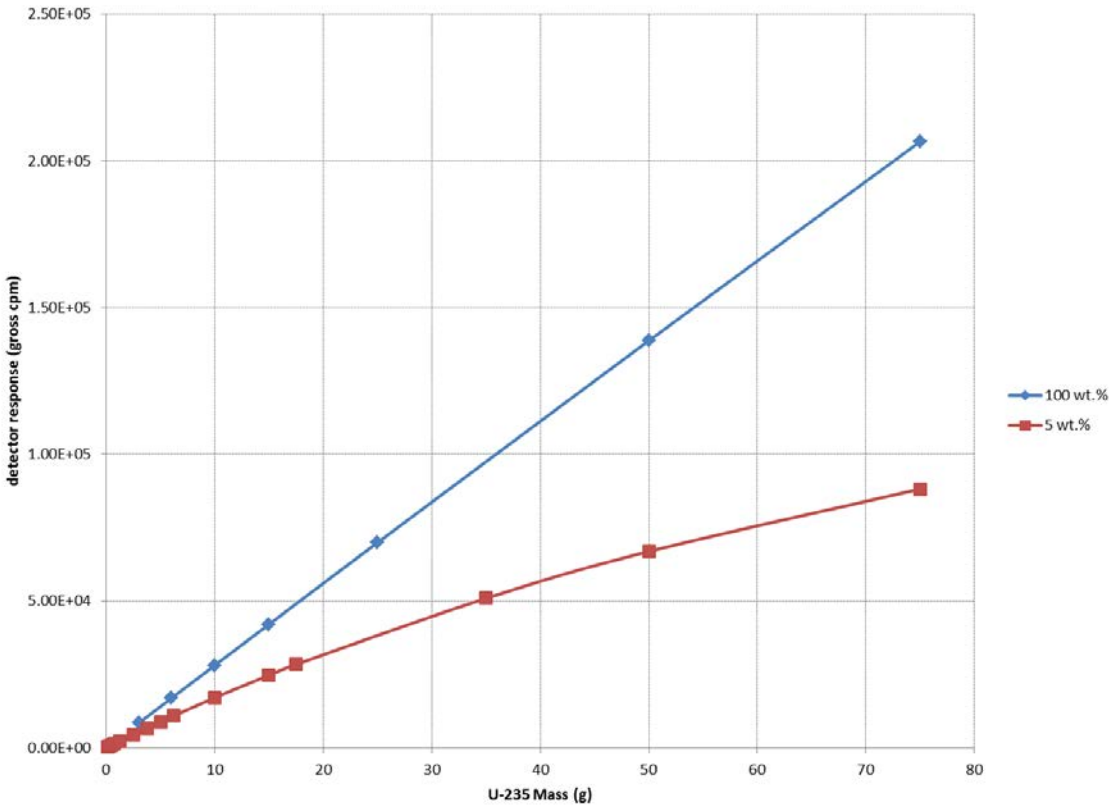

Figure 24. LaBr 185.7 keV Detector Response for 5 wt.% and 100 wt.% ^{235}U/U in a 75% Loaded FC Based on MCNP Calculation.

A summary of the fit equations for each scenario is given in Table XXXI.

Table XXXI. Summary of Quadratic Fit Equations for Estimating ^{235}U in FCs

Enr.	Geometry	Variation	Best Fit Equation
100%	Lump	5.08 cm	g ^{235}U = -3E-10 * cpm^2 + 0.0005 * cpm
		10.16 cm	g ^{235}U = -4E-09 * cpm^2 + 0.0025 * cpm
		15.24 cm	g ^{235}U = -1E-07 * cpm^2 + 0.013* cpm
		20.32 cm	g ^{235}U = -2E-06 * cpm^2 + 0.0594 * cpm
	Field Container	25%	g ^{235}U = 2E-11 * cpm^2 + 0.0001 * cpm
		50%	g ^{235}U = 3E-11 * cpm^2 + 0.0002 * cpm
		75%	g ^{235}U = 5E-11 * cpm^2 + 0.0004 * cpm
		95%	g ^{235}U = 6E-11 * cpm^2 + 0.0004 * cpm
5%	Field Container	25%	g ^{235}U = 2E-9 * cpm^2 + 8E-5 * cpm
		50%	g ^{235}U = 3E-9 * cpm^2 + 0.0003 * cpm
		75%	g ^{235}U = 4E-9 * cpm^2 + 0.0005 * cpm
		95%	g ^{235}U = 5E-9 * cpm^2 + 0.0006 * cpm

VII.E. ENRICHMENT ESTIMATION APPLICATION

Enrichment variation between 5 wt.% $^{235}U/U$ and 100 wt. % $^{235}U/U$ can affect final fissile material loading estimation relatively drastically, depending on the degree to which the total uranium (and other high-Z material) makes up the sample. As shown in Figure 24, small amounts of uranium dispersed in soil do not produce a significant self-shielding effect. As the ^{235}U increases, at 5 wt.% $^{235}U/U$, the total uranium begins to build up and substantially affect the self-attenuation. For these reasons, selecting the appropriate best fit calibration equation from Table XXXI was imperative.

As described in Section III.E, the enrichment estimation process utilized energy lines of ^{235}U and ^{238}U photons at 185.7 keV and 1001 keV, respectively. An activity ratio

associated with the three classifications of uranium was calculated. The classifications were as follows:

- DU ($\leq$ 0.96 wt. % ^{235}U/U)
- LEU (0.96 wt. % ^{235}U/U – 10.0 wt. % ^{235}U/U);
- HEU (> 10.0 wt.% ^{235}U/U)

The associated activity ratio for each key enrichment value is shown in Table XXXII.

Table XXXII. Activity Ratio for Various Enrichment Values

Enrichment (wt. % ^{235}U/U)	Mass Ratio per 100g U (^{235}U/^{238}U)	Activity Ratio (^{235}U/^{238}U)
0.96	0.96 / 99.04	0.0623
5	5 / 95	0.3384
10	10 / 90	0.7144

The general equation used to calculate activity in Bq is given by the following [42]:

$$A = \frac{M}{A} \times N_A \times \frac{ln2}{T_{1/2}} \qquad (12)$$

Where: M: is the total weight of ^{238}U or ^{235}U;

A: is the atomic weight of ^{238}U or ^{235}U;

N_A: is Avogadro's number = 6.022E23 atoms per mole; and

$T_{1/2}$: is the half-life of ^{238}U or ^{235}U.

Using the half-life of ^{235}U (7.038 x 10^8 yr) and ^{238}U (4.468 x 10^9 yr), and a mass ratio specified by enrichment, the activity ratios $^{235}U/^{238}U$ were calculated as listed in Table XXXII.

In order to estimate ^{235}U enrichment from a gamma spectrum, the photopeak count rate ratio was compared to the activity ratios in Table XXXII. In order to use the count rate in each full energy peak, the branching ratios and efficiencies were incorporated as follows:

$$A = \frac{CR}{f \times \eta} \quad (13)$$

Where: *CR*: is the count rate in the energy peak

f: is the branching ratio

η: is the full energy peak efficiency for the sample condition

Since efficiencies and branching ratios were effectively treated for these purposes in the pre-loaded detector characterization and analysis sequence, its dependence was not necessary in field calculations for enrichment estimation. The final ratio was calculated using the following results pulled directly from the gamma spectrum:

$$Ratio = \frac{CR_{185\ keV}}{CR_{1001\ keV}} \quad (14)$$

From this ratio, an enrichment category was selected and the appropriate calibration equation was utilized. This method allowed more appropriate treatment of material with large amounts of total uranium while keeping the calculations and number matching simple [24].

CHAPTER VIII

SUBSURFACE PIPE MEASUREMENTS

VIII.A. SCOPING STUDIES

Scoping calculations were performed in order to determine a bounding analytical approach so that the derived pipe-dependent calibration functions were able to provide accurate, yet conservative mass estimates of residual ^{235}U that may be contained within exposed and/or exhumed subterranean pipes. The mass estimates produced were qualified as accurate by being within approximately 50% of the real result. Often, measurements for NCS are orders of magnitude off from the real result. These scoping studies examined the effects of the following on the observed 185.7 keV detector count rates for the fissile material contained within the inside of a selected NPS or range of NPS.

- collimator presence on detector probe;
- type of piping material;
- distribution of the fissile material within the pipe (segmented versus annular distribution);
- ^{235}U enrichment, which was examined at 5% and 100%. Note that uranium enrichment below 5% was not considered because of the inherent relatively low risk for a criticality with ^{235}U at enrichments below 5%.

Model specifications employed in the scoping studies were outlined in Section V.C. Due to the number of input cases utilized in these studies, all results are presented graphically for analysis. Variables not considered to have an effect on the studied

parameter were held at a constant value. When applicable, the ^{235}U mass was fixed at 20-25 g and the NPS was fixed at 6.625-in. The fissile mass value represents a large, yet realistic loading for HDP subterranean piping. In-pipe probe measurements documented in Reference 59 concluded that the highest observed ^{235}U mass loading is 15.9 g ^{235}U/ft. However, 350 g and 700 g ^{235}U were still considered because these values equate to on-site NCS subcritical limits for material handling and Criticality Accident Alarm System exemption [27].

Because the majority of pipes in the remediation process are small (typically around 4 to 5-in NPS), the fixed value for pipe size should be close to these sizes ; however, some fissile mass loading values are too large (i.e., 350 g, 700 g ^{235}U) to physically fit into the segment of pipe with those diameters. A NPS of 6.625-in is the smallest pipe size that can physically accommodate all uranium loading cases.

VIII.A.1 Collimation

The use of a collimator around a detector probe was advantageous for focusing in on a particular region of interest and inhibiting photon contribution from outside source regions. In order to show that the application of a tungsten silicone collimator has a negligible impact on 185.7 keV computational results, an overlay of the two scenarios for both enrichment values is shown in Figure 25. The results are shown for only a segmented distribution for the nominal ^{235}U mass of 20 g. The debris profile and mass should not have an effect on collimation results.

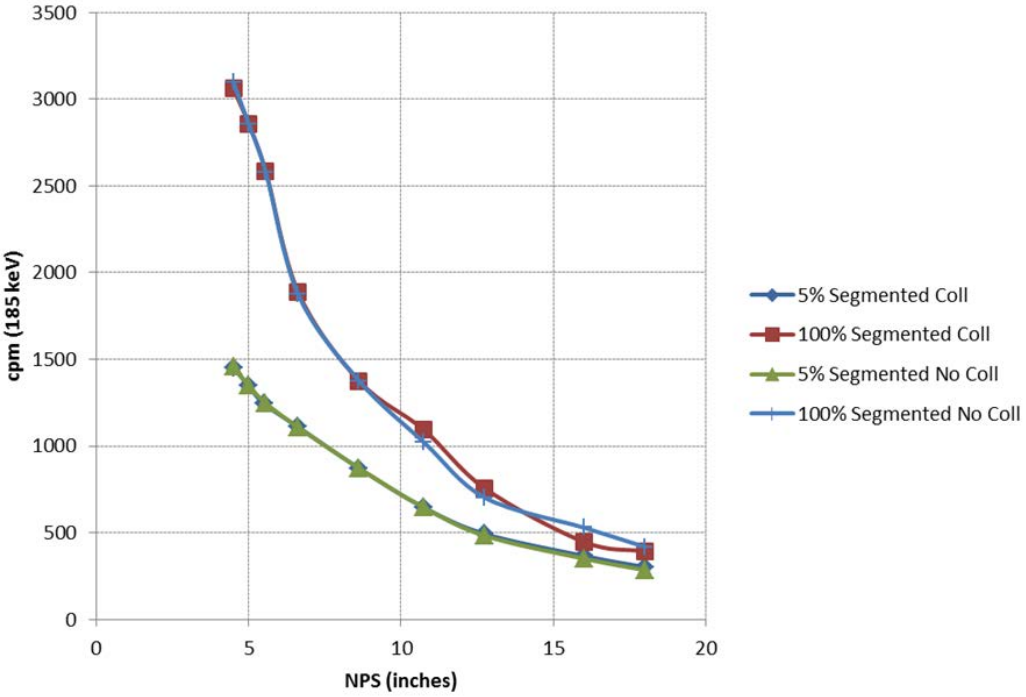

Figure 25. 185.7 keV Detector Response as a Function of NPS for a 20 g ^{235}U Segmented Distribution in Carbon Steel Based on MCNP Calculation.

There was a slightly greater effect at larger NPS and lower enrichment, but not enough to declare the two arrangements different. The tungsten silicone wrap collimator may be used interchangeably with negligible effect on the final 185.7 keV tally. Because the self-attenuation was not significant for 20 g ^{235}U at 100 % enrichment, the trend is relatively smooth and count rate decreases steadily. In the 5% enrichment cases, self-attenuation effects cause the plot to behave less linearly and smooth.

VIII.A.2 Pipe Material

In order to determine the overall conservative pipe material (that providing the most photon attenuation) for modeling of the detection of 185.7 keV photons, two variations were examined: the effect of NPS on detected count rate for each pipe material, and the effect of ^{235}U loading on detected count rate for each pipe material.

Because the collimator was shown to have a negligible effect on the calibration results, the remainder of the scoping studies utilized the results with a collimator included. In addition, the distribution of the fissile material within the 1-ft section of pipe will not affect the scoping study results on pipe material, and therefore, the segmented distribution was utilized. The fissile material mass was fixed at 25 g ^{235}U because this value represents a large, yet realistic mass loading for a 1-ft section of HDP piping. In examining the relationship of ^{235}U mass and detector response, the pipe size was fixed at 6.625-in.

Figure 26 displays the effect of NPS on the detected 185.7 keV photons for a segmented distribution of 25 g ^{235}U at both 5 and 100 wt. % ^{235}U/U. The lower enrichment produced a lower efficiency in both pipe types that did not change as drastically with increased pipe size as the higher enrichment. As pipe size increased, the fixed uranium mass was spread in a thinner layer which decreased self-attenuation, thereby increasing efficiency; however, the fissile material was also further from the detector as pipe size increased, thereby decreasing efficiency slightly. As the results come together at the largest pipe size, it is apparent that the self-shielding and field of view effects eventually cancel each other out. These effects are consistent in both pipe types and therefore produce relatively parallel lines.

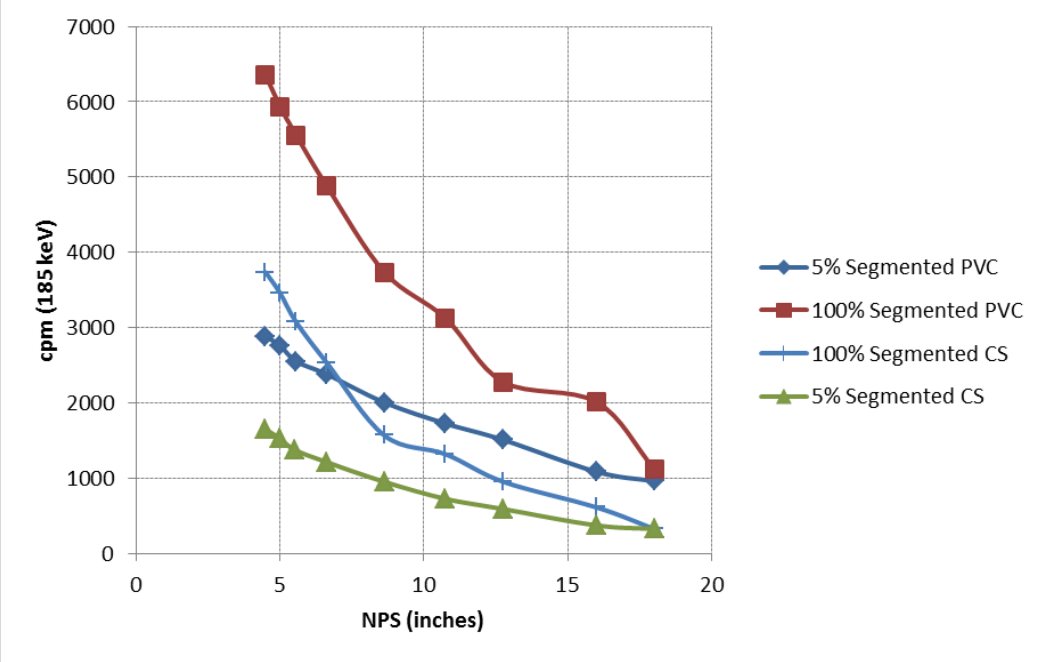

Figure 26. 185.7 keV Detector Response as a Function of NPS for 25 g ^{235}U in Segmented Distribution Based on MCNP Calculation.

Figure 27 displays the effect of ^{235}U mass loading on the detected 185.7 keV photons for a segmented distribution in a 6.625-in NPS at both 5 and 100 wt. % ^{235}U/U. In both pipe types, the pipe size was fixed such that when ^{235}U was added, the depth of debris in the pipe grows thicker. As the material thickens, the self-attenuation increases, but the top plane of the material becomes closer to the detector surface. The red plot represents the lowest amount of material in the pipe and the most transparent pipe material, thereby presenting the lowest amount of attenuation prior to reaching the detector. This explanation follows for each scenario. The interesting point is the crossover of the two blue plots between 20 and 25 g ^{235}U. There is a jump in efficiency in both 100%

enrichment cases. This is likely caused by the increase in height of the material and its proximity to the detector face.

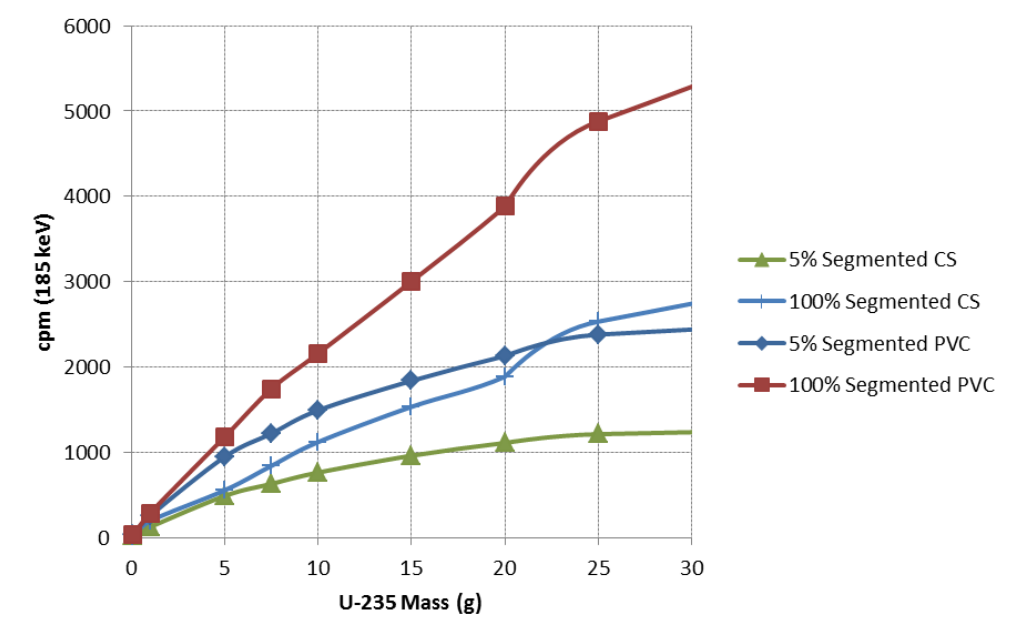

Figure 27. 185.7 keV Detector Response as a Function of ^{235}U Mass (up to 30 g) for a 6.625" NPS Pipe Based on MCNP Calculation.

Because the majority of held up fissile material in a 1-ft section of HDP pipe falls below 50 g, the relationship for the lower ^{235}U quantities was of primary interest.

The information in the above plots revealed the following results:

- In Figure 26, carbon steel was shown to be the conservative pipe material for all pipe sizes above 6.625". PVC was conservative for smaller pipe sizes, but only at 5% enrichment. For enrichment values between 5 and 100 wt. %

^{235}U/U, the carbon steel limiting conservative pipe size would slowly be pushed downward.

- In Figure 27, carbon steel was shown to be the conservative pipe material for all ^{235}U mass values below approximately 22 g. For any enrichment between 5 and 100 wt.% ^{235}U/U, the 22 g value would slowly increase.

The majority of the effects seen in the above figures were due to uranium self-attenuation. As the material continues to pile up on the bottom of the pipe, self-attenuation begins to prevail.

Based on the above observations, the remainder of the relationships examined utilized carbon steel pipe material. This material was the most conservative, meaning that it provided the most photon attenuation in order to produce a potential overestimation in the ^{235}U gram content.

VIII.A.3 Fissile Material Distribution

The actual distribution of the fissile material within the pipe was unknown. Although in some cases, the inside of the pipe may be visually inspected to confirm the material distribution, a limiting profile was still examined. A description of segmented and annular profiles was described in Section V.C.4.

Figure 28 and Figure 29 show the effect of ^{235}U loading on detected count rate for each debris profile and each enrichment value. The pipe size was again fixed at 6.625-in because 350 and 700 g ^{235}U do not physically fit into the smaller NPS. The trends run smoothly until 20 g ^{235}U when attenuation effects start to offset efficiency losses. Generally, a segmented distribution is most conservative, producing the lowest

efficiencies because the material is piled on top of itself at the bottom of a pipe. The 5% annular distribution and 100% segmented distribution produce very similar efficiencies (count rates) until 20 g ^{235}U when the attenuation from material pile up in the segmented distribution jumps in efficiency. The annular distributions have a much more predictable and smooth trend since the material was being added in similar fashion with each data point (filling of a pipe from outside in). The segmented distribution began to show more unpredictable behavior because of self-attenuation effects and their non-linearity responses.

The two annular cases follow closely at large ^{235}U values because the material is becoming no closer to the face of the detector, which has a measurable increase on efficiency.

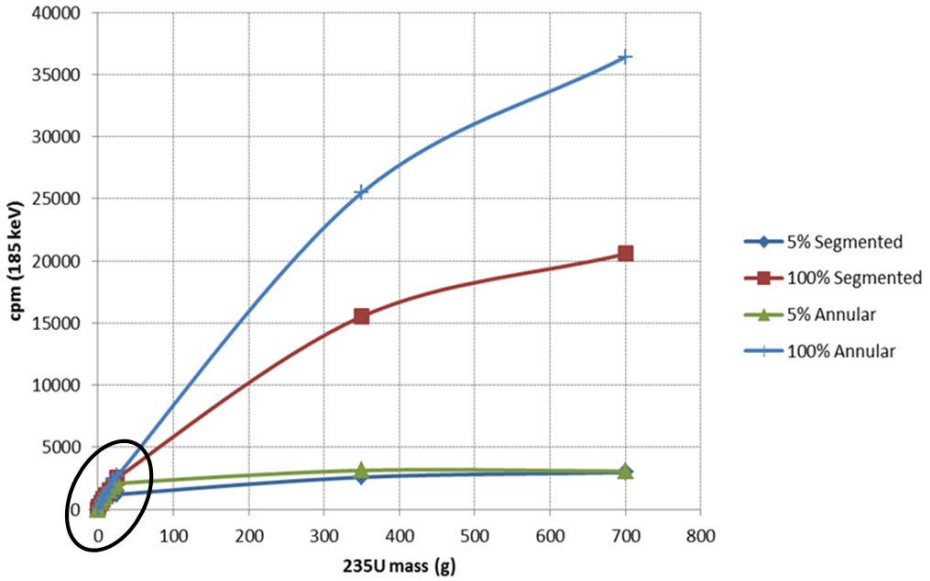

Figure 28. 185.7 keV Detector Response as a Function of ^{235}U Mass (up to 700 g) for a 6.625" NPS Carbon Steel Pipe Based on MCNP Calculation.

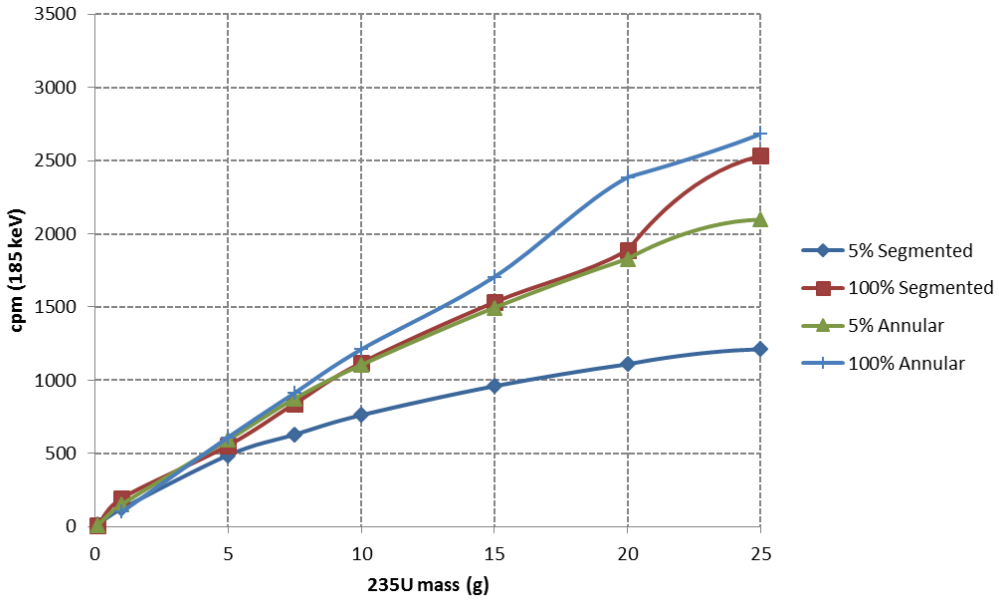

Figure 29. 185.7 keV Detector Response as a Function of ^{235}U Mass (up to 25 g) for a 6.625" NPS Carbon Steel Pipe Based on MCNP Calculation.

Figure 30 displays the same effect as a function of NPS for both enrichment values. The ^{235}U content was fixed at 20 g. As the pipe size increases, there exists a point at which the detector is no longer "seeing" photons as efficiently as for smaller NPS. This causes the efficiency to decrease. With a pipe size of 16 inches in the annular cases, the uranium was spread thin enough along the walls that self-attenuation was significantly reduced, and the efficiency jumped. This effect is most prominent in the case with the least amount of material (100% enrichment).

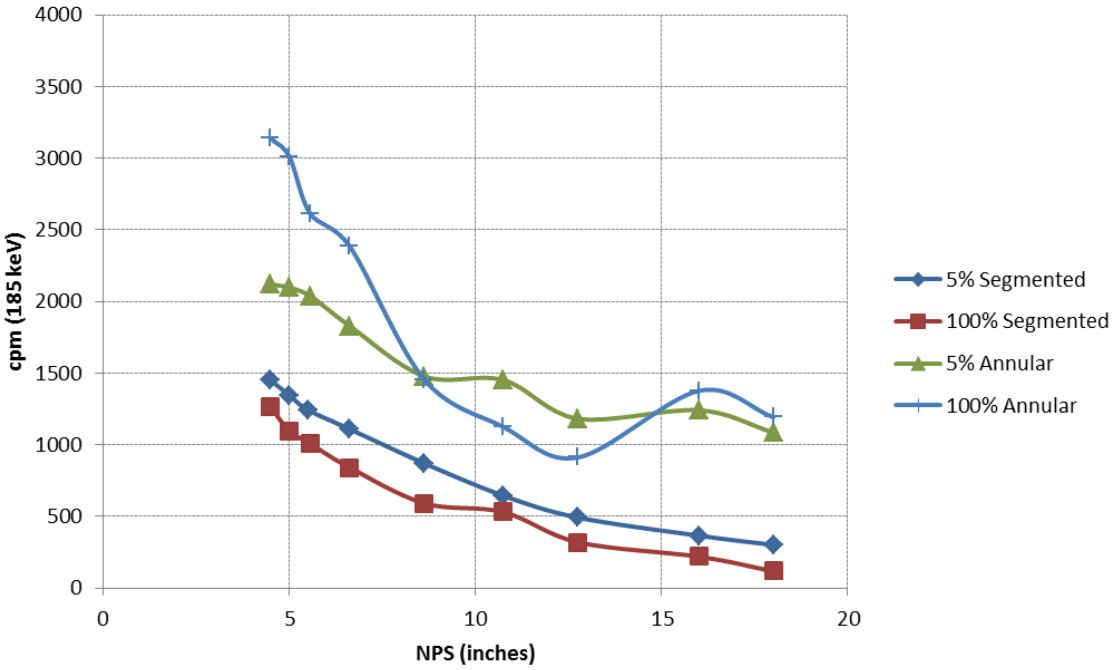

Figure 30. 185.7 keV Detector Response as a Function of NPS for 20 g ^{235}U in a Carbon Steel Pipe Based on MCNP Calculation.

The lines drawn in the above plots merely connects data points for easy visualization and was not intended to show a trend. Because the size of the pipe, the

detector FOV, and way the material was distributed in the annular distribution, the plot can appear odd if viewed as a trend.

The information shown in the above plots yields the following results:

- In Figure 28 and Figure 29, the segmented distribution was shown to be conservative for all gram values at both enrichments up to approximately 20 g ^{235}U. Above 20 g ^{235}U, the 5 wt. % ^{235}U/U annular distribution became conservative until a loading of approximately 650 g ^{235}U.
- In Figure 30, the segmented distribution was shown to be largely conservative for all NPS with the 20 g ^{235}U loading. The annular debris profile displayed odd trends because, with the ^{235}U fixed, the larger interior void space in the pipe offsets the self-attenuation within the fissile material.

The annular debris profile was more difficult to develop an overall conservative application for. In general, the segmented distribution was almost always conservative for these low level fissile material applications. This was likely because the segmented distribution stacked the most material within the pipe and therefore caused the most photon attenuation prior to reaching the detector. Unless the interior of the pipe was visually confirmed to contain the annular distribution of material, the calibration utilized the segmented debris profile.

VIII.A.4 Enrichment

Although the scoping calculations presented in the previous sections displayed trends for both enrichment levels, this section is intended to define a limiting enrichment

value for the final calibration basis. Detected count rate dependence on the uranium enrichment was driven by the linear activity of uranium along the pipe's length

Figure 31 and Figure 32 are identical to the data shown in Figure 27; however, the first is an expanded view for all fissile mass loadings.

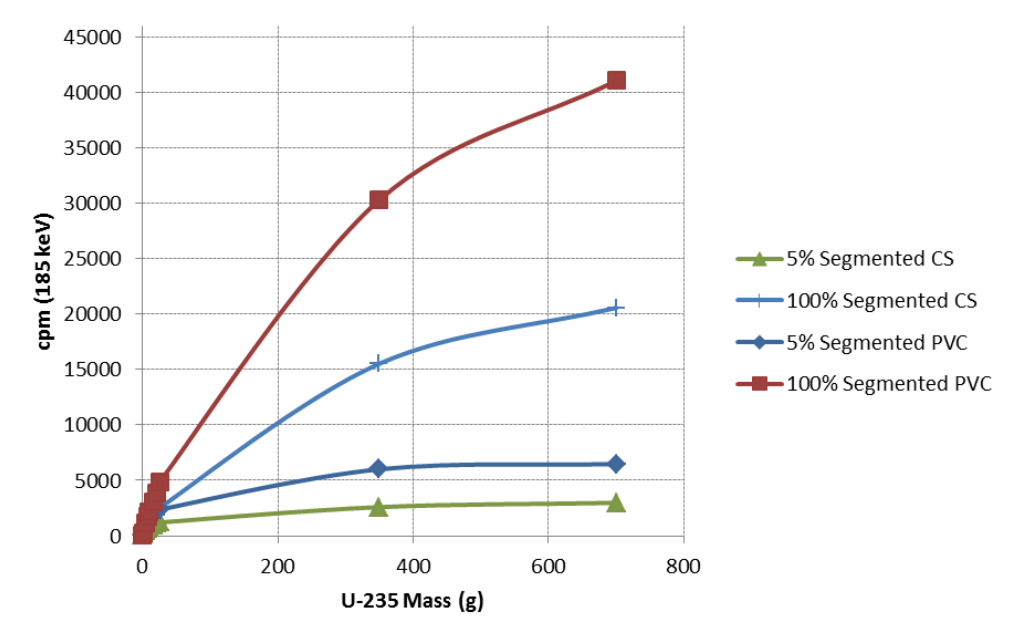

Figure 31. 185.7 keV Detector Response as a Function of ^{235}U Mass (up to 700 g) for a 6.625" NPS Pipe Based on MCNP Calculation.

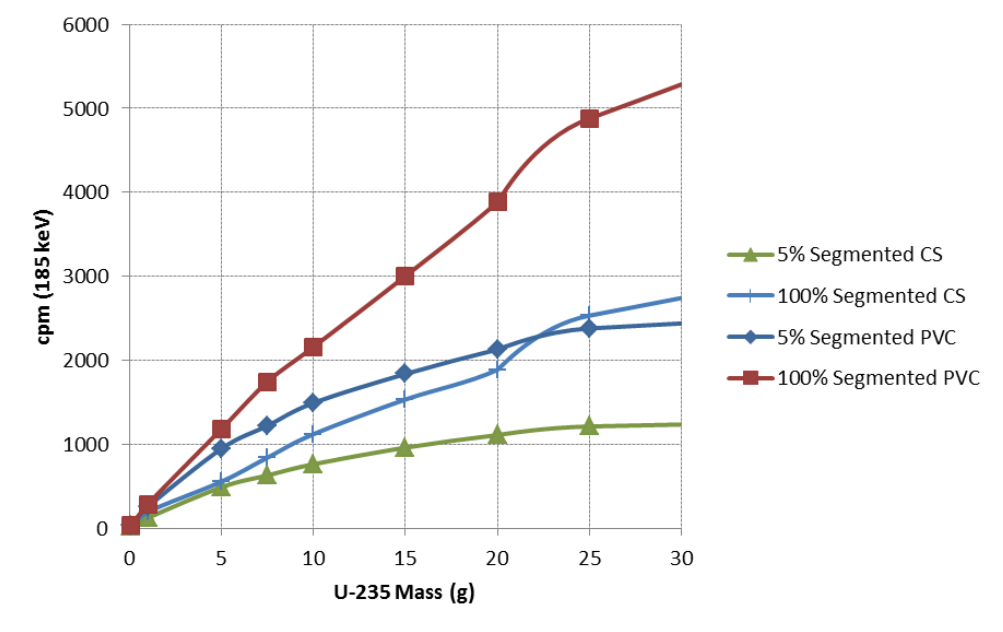

Figure 32. 185.7 keV Detector Response as a Function of ^{235}U Mass (up to 30 g) for a 6.625" NPS Pipe Based on MCNP Calculation.

Since carbon steel was already determined to be the conservative pipe material utilized in the calibration basis, the above plots emphasize the conservative behavior (lowest count rates) of 5 wt.% ^{235}U/U compared to 100 wt. % for all fissile mass loadings in the 6.625-in NPS. The differences in the detected count rates where the 100 wt. % ^{235}U/U no longer produces the lowest count rates were relatively small. This implies that minimum count rates could be represented at the 5% or 100% ^{235}U enrichment level without introducing significant error in the residual ^{235}U mass that may be present in the pipe.

Looking again at Figure 26, it is clear that 5 wt. % ^{235}U/U was also conservative for all NPS with a typical fissile mass loading of 20-25 g ^{235}U. This enrichment value

produced the lowest count rates, and therefore ensures underestimation in the real scenario.

VIII.A.5 Summary of Scoping Studies

Results of comprehensive calculations and graphical depictions in Section VIII.A.1 through Section VIII.A.4 allow several conclusions to be drawn. Unless otherwise noted, the following conclusions are based on results obtain from the scoping studies documented in Section VIII.A.1 through Section VIII.A.4.

Collimation: Use of the tungsten silicone wrap collimator can assist in reducing uncertainties associated with quantifying the amount of ^{235}U that may be present within the subterranean pipes. Since mass values were assigned in 1-ft increments, but the pipes are much longer, collimation reduced the field of view of the detector to almost exactly a 1-ft section, so as to not over quantify the ^{235}U hold up. When compared to uncollimated detectors, collimated detectors are less sensitive to the following:

- Background radiation
- Presence of ^{235}U deposits that are greater than 6-in away along the length of the pipe from the detector's measurement position
- Debris distribution profile

This type of collimator was advantageous for subterranean piping assay. Since the presence of a collimator had very little effect on the detector count rate for each 1-

ft section, the final calibration basis does consider the use of the collimator since it is anticipated in future measurements, as well.

Pipe Material: Among the two types of material considered, as expected, the carbon steel material produced lower count rates in most scenarios since its material attenuation coefficients are large for a 185.7 keV photon. In the few scenarios where PVC resulted in lower detected count rates, the difference between the two count rates for each pipe material is small. A resultant under prediction of ^{235}U mass from utilizing carbon steel pipe material, with all other conservatisms built into this calculation, was highly unlikely.

Fissile Material Distribution: Fissile material in segmented profiles produced lower photon count rates than fissile material in annular distributed profiles. It is conservative to model all uranium hold up in the segmented distribution to establish a ^{235}U mass estimate safely above the real value.

^{235}U Enrichment: Results of the scoping studies indicated that the lowest 185.7 keV photon count rates were generally associated with a lower enrichment level (i.e., 5 wt. % $^{235}U/U$). With other bounding assumptions employed, a 5 wt. % $^{235}U/U$ was considered bounding. Therefore, the calibration basis considered a sole enrichment of 5%.

^{235}U Mass: Scoping calculations concluded that the detector photon count rate had a limited range in which it possess a linear response per mass of ^{235}U, and the applicability of the linear range was highly dependent on the ^{235}U enrichment levels, as follows:

- An enrichment of 100 wt. % ^{235}U/U produced a linear detector response for the segmented profile below approximately 10 g ^{235}U/ft.
- For ^{235}U at 5 wt.%, a linear response could be conservatively assumed for ^{235}U mass loadings below approximately 5 g ^{235}U/ft.

As the size of the pipe increased, the range in the linear response was expected to exceed the upper thresholds stated above. This is because as the pipe size increased, the uranium depth decreased, thereby reducing the effects of uranium self-shielding. For these reasons, the final calibration basis used a polynomial fit to the data.

A summary plot, taking into account the above bounding scenarios, for each pipe size is presented in Figure 33 for the full range of ^{235}U masses examined (on logarithmic scale). A more detailed plot of the lower mass values is shown in Figure 34. Detection capabilities (efficiencies) are greater with smaller pipe sizes since the photons from the material are more likely to interact in the detector. This is the reason that the smaller pipe sizes show a steeper slope in the following figures.

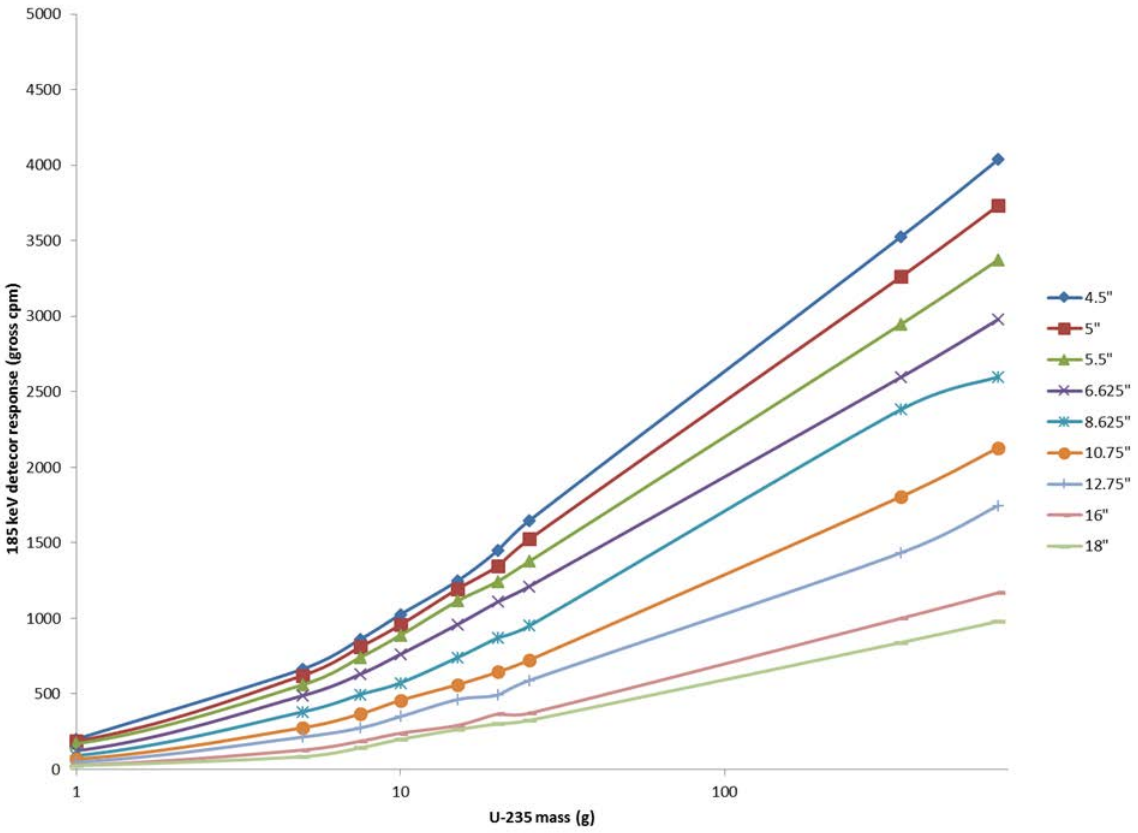

Figure 33. 185.7 keV Collimated Detector Response as a Function of ^{235}U Mass (up to 700 g) for Each NPS in a Carbon Steel Pipe Based on MNCP Calculation.

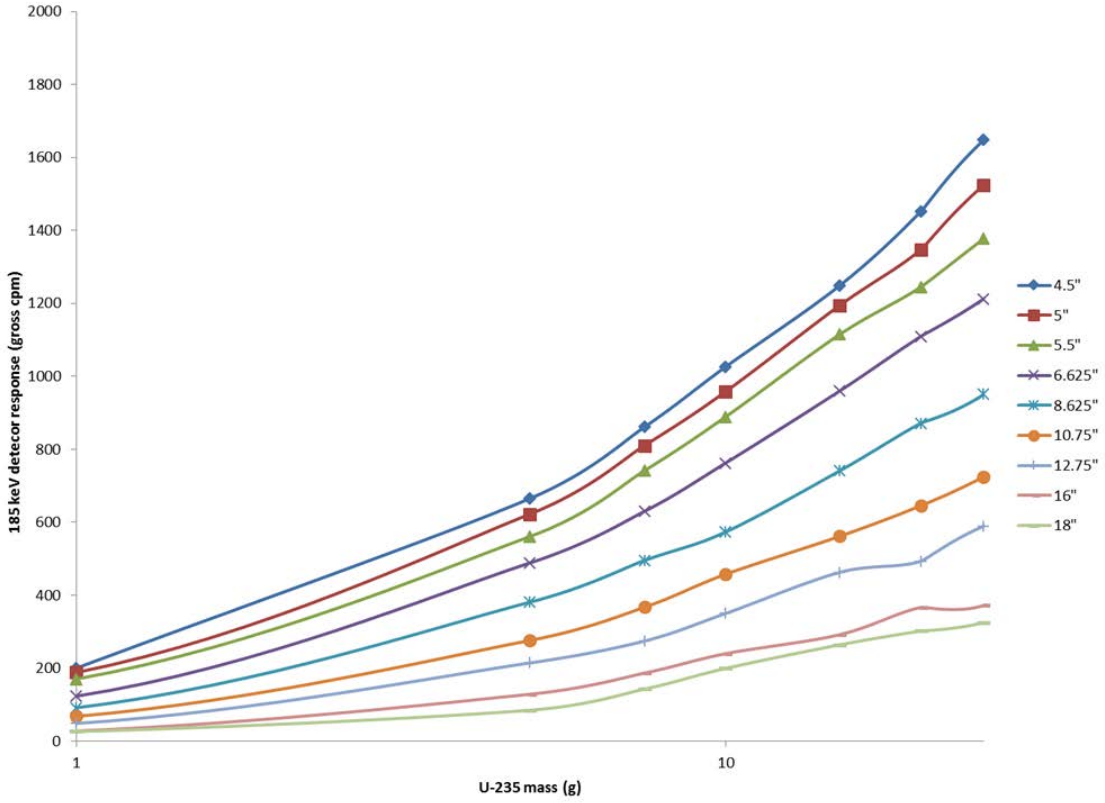

Figure 34. 185.7 keV Collimated Detector Response as a Function of ^{235}U Mass (up to 25 g) for Each NPS in a Carbon Steel Pipe Based on MNCP Calculation.

Table XXXIII. Final Results for MCNP Model Selected from Scoping Studies

Pipe OD (in)	Collimator	Distribution	Material	Enrichment (wt. %)	g ^{235}U	185.7 keV response
4.5	col	Seg	CS	5	0.1	25
	col	Seg	CS	5	1	200
	col	Seg	CS	5	5	665
	col	Seg	CS	5	7.5	861
	col	Seg	CS	5	10	1026
	col	Seg	CS	5	15	1249
	col	Seg	CS	5	20	1451
	col	Seg	CS	5	25	1648
	col	Seg	CS	5	350	3526
	col	Seg	CS	5	700	4038

Table XXXIII. Continued.

Pipe OD (in)	Collimator	Distribution	Material	Enrichment (wt. %)	g ^{235}U	185.7 keV response
5	col	Seg	CS	5	0.1	20
	col	Seg	CS	5	1	188
	col	Seg	CS	5	5	623
	col	Seg	CS	5	7.5	810
	col	Seg	CS	5	10	958
	col	Seg	CS	5	15	1194
	col	Seg	CS	5	20	1347
	col	Seg	CS	5	25	1524
	col	Seg	CS	5	350	3261
	col	Seg	CS	5	700	3734
5.5	col	Seg	CS	5	0.1	20
	col	Seg	CS	5	1	170
	col	Seg	CS	5	5	561
	col	Seg	CS	5	7.5	741
	col	Seg	CS	5	10	889
	col	Seg	CS	5	15	1115
	col	Seg	CS	5	20	1245
	col	Seg	CS	5	25	1377
	col	Seg	CS	5	350	2947
	col	Seg	CS	5	700	3374
6.625	col	Seg	CS	5	0.1	17
	col	Seg	CS	5	1	123
	col	Seg	CS	5	5	489
	col	Seg	CS	5	7.5	630
	col	Seg	CS	5	10	762
	col	Seg	CS	5	15	960
	col	Seg	CS	5	20	1110
	col	Seg	CS	5	25	1212
	col	Seg	CS	5	350	2596
	col	Seg	CS	5	700	2980
8.625	col	Seg	CS	5	0.1	16
	col	Seg	CS	5	1	92
	col	Seg	CS	5	5	381
	col	Seg	CS	5	7.5	495
	col	Seg	CS	5	10	573
	col	Seg	CS	5	15	741
	col	Seg	CS	5	20	872
	col	Seg	CS	5	25	951
	col	Seg	CS	5	350	2382
	col	Seg	CS	5	700	2600

Table XXXIII. Continued.

Pipe OD (in)	Collimator	Distribution	Material	Enrichment (wt. %)	g ^{235}U	185.7 keV response
10.75	col	Seg	CS	5	0.1	14
	col	Seg	CS	5	1	68
	col	Seg	CS	5	5	276
	col	Seg	CS	5	7.5	367
	col	Seg	CS	5	10	457
	col	Seg	CS	5	15	562
	col	Seg	CS	5	20	646
	col	Seg	CS	5	25	725
	col	Seg	CS	5	350	1806
	col	Seg	CS	5	700	2130
12.75	col	Seg	CS	5	0.1	8
	col	Seg	CS	5	1	49
	col	Seg	CS	5	5	214
	col	Seg	CS	5	7.5	274
	col	Seg	CS	5	10	350
	col	Seg	CS	5	15	463
	col	Seg	CS	5	20	493
	col	Seg	CS	5	25	590
	col	Seg	CS	5	350	1434
	col	Seg	CS	5	700	1747
16	col	Seg	CS	5	0.1	0
	col	Seg	CS	5	1	28
	col	Seg	CS	5	5	129
	col	Seg	CS	5	7.5	187
	col	Seg	CS	5	10	240
	col	Seg	CS	5	15	292
	col	Seg	CS	5	20	367
	col	Seg	CS	5	25	372
	col	Seg	CS	5	350	1000
	col	Seg	CS	5	700	1170
18	col	Seg	CS	5	0.1	0
	col	Seg	CS	5	1	26
	col	Seg	CS	5	5	85
	col	Seg	CS	5	7.5	143
	col	Seg	CS	5	10	199
	col	Seg	CS	5	15	264
	col	Seg	CS	5	20	302
	col	Seg	CS	5	25	325
	col	Seg	CS	5	350	840
	col	Seg	CS	5	700	981

VIII.B. ^{235}U CHARACTERIZATION FOR NCS

Results obtained from the scoping calculations documented in the previous section were incorporated into the final model used to derive ^{235}U mass-to-detected 185.7 keV photon conversion functions. The final model must be conservative, in that, it must not under predict the gram value of ^{235}U in the pipe. The assumptions and final model chosen were intended to ensure this. The following conservative simplifications were incorporated into the final calibration basis:

- Ground material was modeled as dry compacted soil;
- Only carbon steel pipe material was considered (which represents all iron alloy pipes and bounds anything less dense);
- The detector was collimated with the tungsten silicone collimator;
- The LaBr probe was positioned 6-in from the pipe's outer surface;
- The debris was modeled to consist only of UO_2 and has a volume fraction consistent with UO_2 at a density of 3 g/cm^3.
- The fissile material region was modeled with a segmented distribution profile, which provided an upper bound estimate of ^{235}U contained within the pipe;
- Only 5 wt.% ^{235}U/U enrichment was considered; and
- The highest ^{235}U mass loading that was considered for the calibration basis was 25 g ^{235}U/ft, which bounds the highest expected ^{235}U linear mass loading of 15.9 g ^{235}U/ft as determined by Reference 59. However, larger mass deposit results are available, as displayed in Table XXXIII, should they be needed.

Because the detector count rate was displayed as the response variable on the instrument, calibration equations were established to allow input of the detector response and output of the ^{235}U mass loading, similar to Section VII.D.2. Figure 35 shows the ^{235}U mass as a function of 185.7 keV detector response up to 25 g ^{235}U. The associated best fit polynomial line with a degree of 3 is also displayed.

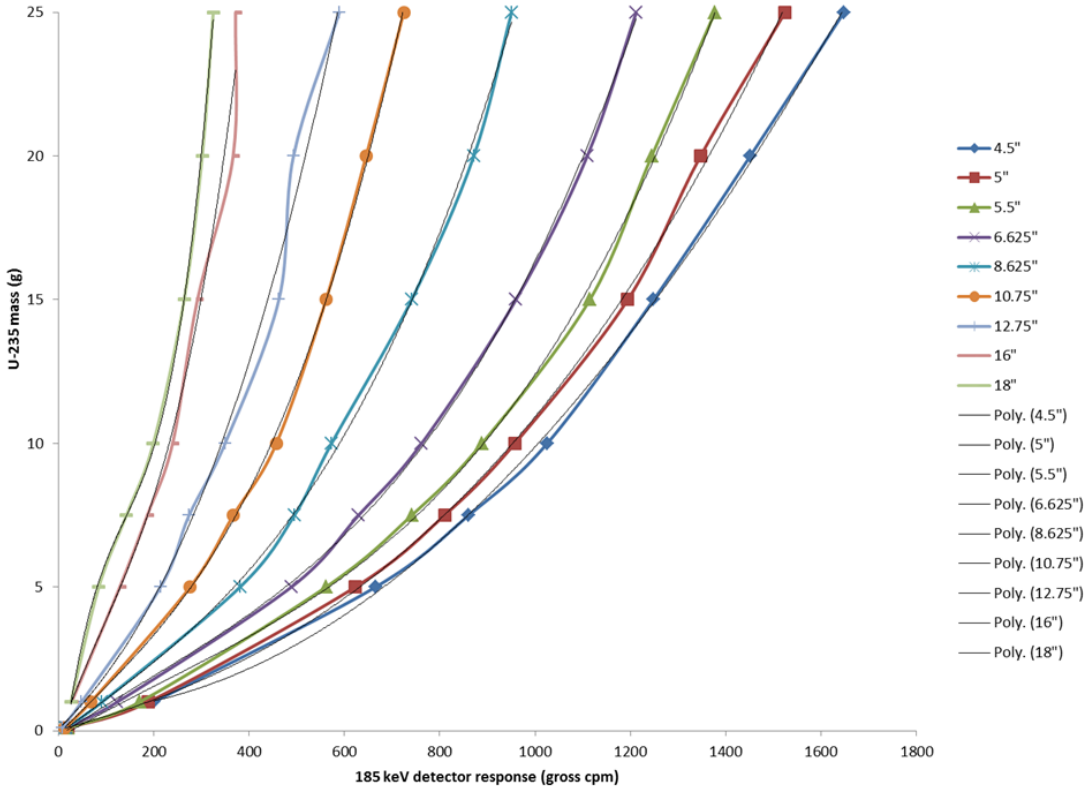

Figure 35. ^{235}U Mass (up to 25 g) as a Function of 185.7 keV Collimated Detector Response for 5 wt.% ^{235}U/U in a Carbon Steel Pipe Based on MCNP Calculation.

A summary of the obtained polynomial best fit equations and their respective goodness of fit parameter values are shown in Table XXXIV.

Table XXXIV. Summary of the Polynomial Best Fit Equations for Each NPS

NPS	Best Fit Equation	R^2
4.5	$g\ ^{235}U = -3E\text{-}10 * cpm^3 + 1E\text{-}5 * cpm^2 + 3E\text{-}5 * cpm$	0.9994
5	$g\ ^{235}U = 3E\text{-}9 * cpm^3 + 4E\text{-}6 * cpm^2 + 0.0044 * cpm$	0.9992
5.5	$g\ ^{235}U = 9E\text{-}9 * cpm^3 - 6E\text{-}6 * cpm^2 + 0.0099x * cpm$	0.9992
6.625	$g\ ^{235}U = 1E\text{-}8 * cpm^3 - 6E\text{-}6 * cpm^2 + 0.0112 * cpm$	0.9995
8.625	$g\ ^{235}U = 2E\text{-}8 * cpm^3 - 2E\text{-}6 * cpm^2 + 0.0112 * cpm$	0.9987
10.75	$g\ ^{235}U = 4E\text{-}8 * cpm^3 - 6E\text{-}6 * cpm^2 + 0.0167 * cpm$	0.9995
12.75	$g\ ^{235}U = 3E\text{-}8 * cpm^3 + 3E\text{-}5 * cpm^2 + 0.0158 * cpm$	0.9909
16	$g\ ^{235}U = 4E\text{-}7 * cpm^3 - 0.0001 * cpm^2 + 0.0477 * cpm$	0.9770
18	$g\ ^{235}U = 2E\text{-}6 * cpm^3 - 0.0007 * cpm^2 + 0.1347 * cpm$	0.9994

CHAPTER IX

FIELD IMPLEMENTATION

The InSpector 1000 is rugged and portable with a wide range of feasible conditions for operation in the field. 60-sec measurements were performed in accordance with the calibration basis described herein and produce a detector response for the 185.7 keV and 1001 keV photopeak. Using these two numbers and the appropriate model, an enrichment estimation and ^{235}U mass estimation were calculated. These estimates were then used to make a decision on the radiological and nuclear safety of the material for handling, transport, and storage purposes.

The calibration basis results established conservative 185.7 keV photopeak count rates (from the 186 keV bin in MCNP) for the LaBr gamma detector which corresponded to the remediation modeling scenarios encountered at the Hematite Decommissioning Project and other similar type projects. The best fit regression lines generated for each scenario were utilized to assign a mass value for ^{235}U present on the material. In addition, the LaBr field of view study revealed that the LaBr detector can reliably detect photons for waste materials containing a uniform 0.1 g $^{235}U/L$ concentration when the detector window is positioned at least 6-in above the surface of the waste and the waste radius does not exceed 18-in.

Using the tungsten silicone collimator ribbon wrapped around the LaBr probe, a conservative ^{235}U gram estimate for each 1-ft section of pipe is assigned and a total mass for the pipe section is established. The quick, in-field fissile material mass assignments

aid in applying proper control of the material and the proper disposition through an early understanding of its radiological nature.

Using MCNP for this calibration eliminates the creation of a new model for each measurement. This decreases the potential for administrative error (an error that weighs heavily in NCS). The implementation of these techniques involve use of thresholds and greatly decreases modeling error and modeling technical review. There is potential for administrative error in addressing the scenario pre-measurement, although this error is also present for ISCOS measurements. Further, ISOCS software displays results as nuclide activity, which must further be calculated into mass for the intended NCS and MC&A purposes. Finally, the final ISOCS result is dependent on the nuclide library loaded and selected on the InSpector 1000, which presents another possible administrative error. The instrument is not intended to perform such measurements [1541] and doing so either requires delivery of the measured spectrum to a computer for analysis (not an in-field result), or performing some “tricks” on the detector in order to analyze the spectrum appropriately.

CHAPTER X

CONCLUSIONS

A new approach to- and method for characterization of fissile nuclide contaminated soils and process piping has been developed and implemented for low and intermediate level wastes, using new calibration bases for photon counting. The method has been demonstrated for feasibility and validated under the guidance of the NRC Software Quality Assurance Program. In addition, the developed methods consider nuclear safety as the priority while retaining appropriate estimation techniques.

Using the developed high-fidelity models, a fast uranium loading and enrichment estimation process was developed by taking advantage of the resolution and discrimination capabilities of the LaBr equipped InSpector 1000 instrument. The analysis takes into account multiple possible scenarios that may be encountered during decommissioning and remediation of a fuel fabrication and/or buried nuclear waste facility, while keeping nuclear safety controls in mind.

The scenarios analyzed in the new calibration basis were selected based on historical knowledge and in-field experience at the Hematite Decommissioning Project. The primary geometric scenarios include a loaded 20 L bucket, an in-situ lump source, a 36-in diameter in-situ contaminated soil/debris area, an ex-situ layer of soil/debris, and subterranean process piping with hold up material. The diversity of the selected geometric models and inherent limitations and bounding conditions of each, allow a wide range of applicability for in-field use.

The source term and material composition for the models were characterized as typical for a facility operating to produce reactor fuel in the middle to end of the 20th century. Unknown material data were defined using bounding conditions in order to err on the side of safety. Scoping studies were performed on most models to ensure use of a bounding condition. In lieu of scoping studies, a qualitative assessment or existing technical assumption was used.

A detailed detector-waste model was developed for analysis of each scenario, using the LaBr crystal description supplied by the manufacturer. As an inherent part of the process, the models were validated by performing a series of code-to-software and software-to-standard benchmarking procedures, which provided substantiation for use of the detector for the derived purposes, in addition to ensuring that the Monte Carlo approach was conservative, as compared to other methods.

Once the method for development of a calibration bases was assembled, the calibration bases themselves were derived. Using MCNP as a conservative derivation approach, a calibration basis for each geometric description with various input parameters was assembled.

Extensive scoping studies were performed for the subterranean piping assay method in order to derive a conservative yet realistic calibration basis. It is ideal to have one go-to calibration standard for quick implementation in the field. The final calibration analysis utilizes 5 wt. % ^{235}U/U in a segmented distribution within a carbon steel pipe. A single equation is derived for each NPS for mass loading estimation up to 700 g ^{235}U in a 1-ft section.

The developed methods provide a quick, simple, and innovative approach to passive non-destructive assay on typical scenarios encountered at remediation or decommissioning sites. Traditional, cheap methods often vastly over-generalize fissile material, while more robust methods are capital intensive, time consuming, and limiting.

The completion of this dissertation has provided techniques to estimate fissile material quantity and enrichment with a portable, passive non-destructive gamma assay system. In addition, it provides early detection of large quantities of fissile material prior to exhumation or disturbance to enhance nuclear safety processes. This places the first priority on nuclear and radiological safety while preserving the time and money saving aspects of production-based projects.

REFERENCES

1. F. BRONSON, Personal Interview, February 2013.

2. J. CHAPMAN, Email Interview, September 2013.

3. D. RIELLY, N. ENSSLIN, S. KREINER, H. SMITH, "Passive Nondestructive Assay of Nuclear Materials", NUREG/CR-5550 (LA-UR-90-732), March 1991, Prepared for Office of Nuclear Regulatory Research, U.S. Nuclear Regulatory Commission.

4. J. CHAPMAN, Personal Interview, November 2013.

5. A. SIMPSON, S. JONES, M. CLAPHAM, R. LUCERO, "Portable Non-Destructive Assay Methods for Screening and Segregation of Radioactive Waste," Proceedings of the 13th International Conference on Environmental Remediation and Radioactive Waste Management, October 3-7, 2010, Tsukuba, Japan.

6. "ISOCS Calibration Software for GENIE 2000", User's Manual, Model S573, Canberra Industries (1998).

7. J. PERRIN, F. CARRIER, L. GUILLOT, "Determination of the Vertical Distribution of Radioelements (K, U, Th, Cs) in Soils from Portable HPGe Spectrometer Measurements: A Tool for Soil Erosion Studies," *Applied Radiation and Isotopes,* **Vol. 64 No. 7**, p. 830-843; (2006).

8. J. FERNANDES, C. APPOLONI, A. ANDRELLO, "Applicability of an X-Ray and Gamma-Ray Portable Spectrometer for Activity Measurement of Environmental Soil Samples," *Radiation Measurements,* **Vol. 45 No. 7**, p. 801-805; (2010).

9. J. GUTIÉRREZ-VILLANUEVA, A. MARTÍN-MARTÍN, V. PEÑA, M. INIGUEZ, B. DE CELIS, "Calibration of a Portable HPGe Detector Using MCNP Code for the Determination of ^{137}Cs in Soils," *Journal of Environmental Radioactivity,* **Vol. 99 No. 10**, p. 1520-1524; (2008).

10. US Environmental Protection Agency, Oil and Gas Production Wastes, http://www.epa.gov/rdpweb00/tenorm/oilandgas.html, accessed 09/15/2013.

11. M. GAZINEU, A. DE ARAUJO, Y. BRANDAO, C. HAZIN, "Radium-226 and Radium-228 in Scale and Sludge Generated in the Petroleum Industry," Proceedings of the 11th International Congress of the International Radiation Protection Association, 2004, Madrid, Spain.

12. M. COOPER, “Naturally Occurring Radioactive Materials (NORM) in Australian Industries—Review of Current Inventories and Future Generation,” ERS-006, 2005, Prepared for the Radiation Health and Safety Advisory Council.

13. A. HABIB, D. BRADLEY, P. REGAN, A. SHUTT, “The Use of MCNP and Gamma Spectrometry in Supporting the Evaluation of NORM in Libyan Oil Pipeline Scale,” *Instruments and Methods in Physics Research*, **Vol. A619**, p. 245-251; (2010).

14. Y. WU, B. TANG, “Monte-Carlo Simulation of Response Functions for Natural Gamma-Rays in $LaBr_3$ Detector System with Complex Borehole Configurations,” *Plasma Science and Technology*, **Vol. 14 No. 6**; June 2012.

15. P. BURRETTO, “Recent Developments in Uranium Exploration,” IAEA Bulletin, **Vol. 23 No. 2**, p. 15-20; (1981).

16. R. CARCHON, M. MOESLINGER, L. BOURVA, C. BASS, M. ZENDEL, “Gamma Radiation Detectors for Safeguards Applications,” *Nuclear Instruments and Methods in Physics Research*, **Vol. A579**, p. 380-383; (2007).

17. S. EL-MONGY, A. HUMAID, “Depleted, Natural and Low Enriched Uranium Verification by Recent Portable Passive Non-Destructive Assay Tools”, *Journal of Nuclear and Radiation Physics*, **Vol. 2 No. 2**, p. 79-87; (2007).

18. F. DIAS, M. GRUND, G. RENHA, E. GALDOZ, O. CRISTALLINI, M. FACCHINETTI, “The Use of Lanthanum Bromide Detectors for Nuclear Safeguards Applications,” Proceedings of the 2009 International Nuclear Atlantic Conference, 2009, September 27-October 2, 2009, Rio de Janerio, Brazil.

19. E. MACE, L. SMITH, “Automated Nondestructive Assay of UF_6 Cylinders: Detector Characterization and Initial Measurements,” *Nuclear Instruments and Methods in Physics Research*, **Vol. A652**, p. 62-65; (2011).

20. K. VEINOT, B. GOSE, T. DAVIS, “Use of Portable Gamma Spectrometers for Identifying Persons Exposed in a Nuclear Criticality Event,” *Nuclear Technology*, **Vol. 168**, p. 17-20; (2009).

21. K. ALZIMAMI, E. ABUELHIA, Z. PODOLYAK, A. IOANNOU, N. SPYROU, “Characterization of $LaBr_3$:Ce and $LaCl_3$:Ce Scintillators for Gamma-Ray Spectroscopy,” *Journal of Radioanalytical and Nuclear Chemistry*, **Vol. 278 No. 3**, p. 755-759; (2008).

22. A. KUHN, S. SURTI, J. KARP, P. RABY, K. SHAH, A. PERKINS, G. MUEHLLEHNER, "Design of Lanthanum Bromide Detector for Time-of-Flight PET," *IEEE Transactions of Nuclear Science*, **Vol. 51 No. 5**, p. 2550-2557; (2004).

23. K. SHAH, J. GLODO, M. KLUGERMAN, W. MOSES, S. DERENZO, M. WEBER, "$LaBr_3$:Ce Scintillators for Gamma-Ray Spectroscopy," *IEEE Transactions of Nuclear Science*, **Vol. 50 No. 6**, p. 2410-2413; (2003).

24. P. MORTREAU, R. BERRNDT, "Measurement of ^{235}U Enrichment with a $LaBr_3$ Scintillation Detector," *Nuclear Instruments and Methods in Physics Research*, **Vol. A620**, p. 324-331; (2010).

25. InSpector 1000 User Manual, ICN 9236111F, Version 1.4, Canberra Industries, 2007.

26. Westinghouse Hematite Decommissioning Plan, NRC License SNM-33, Docket No. 70-36, DO-04-004 Rev. 2, Hematite, Missouri, August 2005.

27. B. MATTHEWS, Nuclear Criticality Safety Assessment of Buried Waste Exhumation and Contaminated Soil Remediation at the Hematite Site, NSA-TR-HDP-09-15, Rev. 3, September 2012.

28. MCNP – A General Monte Carlo N-Particle Transport Code, Version 5, Los Alamos National Laboratory, April 24, 2003 (Revised 10/3/2005).

29. Westinghouse Electric Co., Historical Site Assessment, DO-02-001, May 20, 2003.

30. Code of Federal Regulations, Title 10, Part 20.304, "Disposal by Burial in Soil", 1964.

31. Hematite Burial Pit Log Books, Volumes 1 and 2, July 16, 1965, through November 6, 1970.

32. Westinghouse Electric Co., Employee Interview Records, 2000 to 2008.

33. K.D. IANAKIEV, B.S. ALEXANDROV, P.B. LITTLEWOOD, M.C. BROWNE, Temperature Behavior of NaI(Tl) Scintillation Detectors, Presented at the IEEE NSS-MIC Conference, Puerto Rico, October 2005, *IEEE Transactions on Nuclear Science*.

34. M. MOSZYNSKI, A. NASSALSKI, A. SYNTFELD-KAZUCH, T. SZCZESNIAK, W. CZARNACKI, D. WOLSKI, G. PAUSCH, J. STEIN, Temperature Dependencies of $LaBr_3$(Ce), $LaCl_3$(Ce) and NaI(Tl) Scintillators, *Nuclear Instruments and Methods in Physics Research*, **Vol. A568**, p. 739-751; (2006).

35. Saint-Gobain Data Sheet, BriLance 380, http://www.crystals.saint-gobain.com/uploadedFiles/SG-Crystals/Documents/BrilLanCe%20380%20Data%20Sheet.pdf, accessed 4/25/2014.

36. Saint-Gobain Data Sheet, BriLance 350. http://www.crystals.saint-gobain.com/uploadedFiles/SG-Crystals/Documents/BrillanCe%20350%20data%20sheet.pdf, accessed 4/25/2014.

37. Technical Advantages of ISOCS/LabSOCS, Application Note C39530, Canberra Industries, April 2012.

38. K. KARFOPOULOS, M. ANAGNOSTAKIS, "Parameters Affecting Full Energy Peak Efficiency Determination During Monte Carlo Simulation", *Applied Radiation and Isotopes*, **Vol. 68**, p. 1435-1437; (2010).

39. F. BRONSON, L. WANG, "Validation of the MCNP Monte Carlo Code for Germanium Detector Gamma Efficiency Calibrations", Presented at Waste Management Symposia, February 26, 1996, Tucson, AZ.

40. "Model ISXCLLA1 1.5x1.5 $LaBr_3$ Detectors Characterization Report", 9241263A, Canberra Industries, characterized September 2012, (2007).

41. M.H. NASSEF, W. EL MOWAFI, M.S. EL TAHAWY, "Non Destructive Assay for ^{235}U Determination in Reference Materials of Uranium Oxide", *Journal of Nuclear and Radiation Physics*, **Vol. 4 No. 2**, pp. 65-73; (2009).

42. Y.Y. EBAID, "Use of Gamma-Ray Spectrometry for Uranium Isotopic Analysis in Environmental Samples", *Rom. Journ. Phys.*, **Vol. 55 Nos. 1-2**, p. 69-74; (2010).

43. P. FINCK, N. EDELSTEIN, Y. ALLEN, C. BURNS, et. al., "The Path to Sustainable Nuclear Energy: Basic and Applied Research Opportunities for Advanced Fuel Cycles," Technical Report, Office of Science, U.S. Department of Energy (2005).

44. American National Standard for Nuclear Criticality Safety Operations with Fissionable Materials Outside Reactors, ANS 8.1, American Nuclear Society.

45. Software Quality Assurance Implementation for MCNP Version 5 Nuclear Criticality Safety Software for the NSA Computer System, NSA-CS-06, Rev. 1, Nuclear Safety Associates (2007).

46. “Software Quality Assurance Program and Guidelines”, NUREG/BR-0167, February 1993, Prepared for the Office of Information Resources Management, U.S. Nuclear Regulatory Commission.

47. N. GHAL-EH, G.R. ETAATI, M. MOTTAGHIAN, Monte Carlo Simulation of Inorganic Scintillators Response to Gamma Rays: A Comparative Study, *World Applied Sciences Journal*, **Vol. 8 No. 6**, p. 784-788; (2010).

48. E. PADOVANI, S.A. POZZI, S.D. CLARKE, E.C. MILLER, MCNPX-PoliMi User’s Manual, C00791 MNYCP, Radiation Safety Information Computational Center, Oak Ridge National Laboratory, 2012.

49. M. TAJIK, N. GHAL-EH, G. ETAATI, H. AFARIDEH, Modeling NE213 Scintillator Response to Neutrons Using an MCNPX-PHOTOTRACK Hybrid Code, *Nuclear Instruments and Methods in Nuclear Research*, **Vol. A704,** p. 104-110; (2013).

50. Z.S. HARTWIG, P. GUMPLINGER, Simulating Response Functions and Pulse Shape Discrimination for Organic Scintillation Detectors with GEANT4, *Nuclear Instruments And Methods in Nuclear Research*, **Vol. A737**, p. 155-162; (2014).

51. “SCALE: A Modular Code System for Providing Standardized Computer Analyses for Licensing Evaluation, Version 6”, ORNL/TM-2005/39, 3 Volumes (2009).

52. ORNL/TM-2005/39 Version 6, Vol. II, Sect. F7, ORIGEN-S: SCALE System Module to Calculate Fuel Depletion, Actinide Transmutation, Fission Product Buildup and Decay, and Associated Radiation Source Terms (2009).

53. “GENIE 2000 Tutorials Manual”, Version 3.1, 9235912D, Canberra Industries (2009).

54. J. HANDLEY, Email Interview, February 2014.

55. D.R. MCALISTER, Gamma Ray Attenuation Properties of Common Shielding Materials, Rev. 4.0, PG Research Foundation (2013).

56. R.D. CARTER, G.R. KIEL, AND K.R. RIDGWAY, Criticality Handbook, Atlantic Richfield Hanford Co. Report ARH-600 (1968).

57. L.M. PETRIE, P.B. FOX, K. LUCIUS, Standard Composition Library, ORNL/TM-2005/39 Version 6, Vol. III, Sect M8, January 2009.

58. S. KAHOOK, Calculations to Establish an Estimate of the Mass of ^{235}U Associated with Subsurface Piping in the Hematite Facility, NSA-TR-HDP-11-02, April 2011.

59. Remote Visual Inspection Report, Look Technologies, LLC, DO-10-004-LT, West Lafayette, Indiana, January 2011.

60. Drawing, D-5020-5053, Rev. 0, Process Building Underground Piping and Site Sewer Lines, Westinghouse Electric, LLC, March 2010.

APPENDIX A

SAMPLE MCNP5 AND ORIGEN INPUT FILES

A1: Sample MCNP5 input file for a filled Field Container.

```
LaBr 185 Peak Analysis
c    Field Container with  75.00 grams U,  0.25 fraction filled
c    LaBr detector model
c
_____________________________________________________________________________
c    Cells
c      Source Material inside FC
1    7 -2.0481 -31 -41   imp:p=1
c      Region above source material
2    1 -1.2929E-03 -41 31  imp:p=1
c      IC Wall structure
3    8 -7.92 41 -42   imp:p=1
c      LaBr Detector at bottom
11   6 -5.3000 -16   imp:p=1 $  Detector LaBr crystal
12   1 -1.2929E-03 16 -15  imp:p=1 $  Inside LaBr detector outside
crystal
13   2 -2.6900 15 -14  imp:p=1 $  LaBr Detector housing
14   1 -1.2929E-03 -18   imp:p=1 $  Inside LaBr PM Tube housing
15   2 -2.6900 18 -17  imp:p=1 $  LaBr PM Tube housing
c      Universe
21   1 -1.2929E-03 14 17 -21 42 imp:p=1
22   0 21     imp:p=0 $  External void

c    Surfaces
c      Field Container
31    pz  12.5333  $ Fill height of material inside FC
41   rcc 0.0000 0.0000 0.1230 0.0000 0.0000 50.2330 10.9550 $ Inner
surface
42   rcc 0.0000 0.0000 0.1000 0.0000 0.0000 50.2790 11.0000 $ Outer
surface
c     LaBr Detector
14   rcc 0.0000 0.0000 -6.344 0.0000 0.0000 6.4430 3.1315 $Det Out|
15   rcc 0.0000 0.0000 -6.294 0.0000 0.0000 6.3430 3.0815 $Det Inn|
16   rcc 0.0000 0.0000 -5.341 0.0000 0.0000 3.8100 1.9050 $Det LaB|
17   rcc 0.0000 0.0000 -24.671 0.0000 0.0000 18.3270 2.30 $PMT Out|
18   rcc 0.0000 0.0000 -24.621 0.0000 0.0000 18.2270 2.2500 $PMT Inn|
c      Model Boundary
21   so 400.0000

mode p
c
c    Photon Source Distribution
c
c    Energy cutoff  [keV] 50.0
```

```
c    Intensity cutoff  [%] 0%
c
sdef  rad=d1 axs=0 0 1 ext=d2  pos=0 0  6.2666
      cel=001  erg=d99
si1   0.0000 10.954
si2    -6.2666  6.2666
sp1   -21 1
sp2   0 1
si99  s 6 9
sp99  8.8706E-01  1.1294E-01
c
c    Discrete Gamma Source for u-235
c
si6    l  5.1220E-02 5.4250E-02 6.4370E-02 7.2700E-02
     7.3720E-02 7.4800E-02 8.9958E-02 9.3351E-02 9.6090E-02
     1.0521E-01 1.0832E-01 1.0916E-01 1.1545E-01 1.2035E-01
     1.3655E-01 1.4076E-01 1.4240E-01 1.4377E-01 1.5093E-01
     1.6336E-01 1.7330E-01 1.8261E-01 1.8572E-01 1.9494E-01
     1.9890E-01 2.0211E-01 2.0532E-01 2.1528E-01 2.2138E-01
     2.2878E-01 2.3350E-01 2.4085E-01 2.4684E-01 2.5150E-01
     2.6645E-01 2.7545E-01 2.7950E-01 2.8142E-01 2.8292E-01
     2.8956E-01 2.9165E-01 2.9430E-01 3.0170E-01 3.1069E-01
     3.1710E-01 3.2580E-01 3.4350E-01 3.4590E-01 3.5603E-01
     3.8782E-01 3.9030E-01 4.1029E-01 4.3300E-01 4.4840E-01
     4.5510E-01 5.1720E-01 7.4250E-01 7.9470E-01
sp6   2.0931E-04 1.5699E-04 1.8838E-04 1.1512E-03
     1.0466E-04 6.2794E-04 3.7258E-02 6.0806E-02 9.0005E-04
     2.1036E-02 7.1481E-03 1.6117E-02 7.3260E-04 2.7211E-04
     1.2559E-04 2.3025E-03 5.2329E-05 1.1470E-01 8.3726E-04
     5.3166E-02 1.0466E-04 3.5584E-03 5.9864E-01 6.5934E-03
     4.3956E-04 1.1303E-02 5.2433E-02 2.8258E-04 1.2559E-03
     8.3726E-05 3.0351E-04 7.8493E-04 5.5468E-04 2.0931E-04
     6.2794E-05 5.1282E-04 2.8258E-03 6.2794E-05 5.2329E-05
     7.3260E-05 3.1397E-05 3.4537E-04 5.2329E-05 4.1863E-05
     1.0466E-05 4.1863E-06 3.1397E-05 3.9770E-04 5.2329E-05
     3.9770E-04 4.1863E-04 3.1397E-05 4.1863E-05 1.0466E-05
     8.3726E-05 4.1863E-06 4.1863E-06 6.2794E-06
c
c    Discrete Gamma Source for th-231
c
si9    l     5.8570E-02
     6.3860E-02 6.8500E-02 7.2751E-02 8.1228E-02 8.2087E-02
     8.4214E-02 8.5800E-02 8.9950E-02 9.2288E-02 9.3020E-02
     9.5868E-02 9.7550E-02 9.9278E-02 1.0227E-01 1.0581E-01
     1.0661E-01 1.0801E-01 1.1121E-01 1.1563E-01 1.1682E-01
     1.2491E-01 1.3403E-01 1.3566E-01 1.3675E-01 1.4054E-01
     1.4506E-01 1.4594E-01 1.6310E-01 1.6500E-01 1.6966E-01
     1.7415E-01 1.8350E-01 1.8876E-01 2.1794E-01 2.2410E-01
     2.3601E-01 2.4027E-01 2.4250E-01 2.4960E-01 2.5045E-01
     2.6762E-01  3.0878E-01 3.1100E-01 3.1787E-01
     3.2015E-01 3.5180E-01
sp9      4.1099E-02
     1.8905E-03 4.6853E-04 2.1371E-02 6.9868E-02 3.0413E-02
```

```
     5.5155E-01 4.7675E-04 7.7266E-02 3.3701E-02 3.6989E-03
     5.4250E-02 1.8905E-03 9.8637E-03 3.2879E-02 5.8360E-04
     1.3974E-03 1.8905E-02 6.4936E-03 8.2198E-05 1.7015E-03
     4.9319E-03 2.0549E-03 6.9046E-03 3.4523E-04 5.7538E-05
     4.7675E-04 2.6303E-03 1.2741E-02 3.2057E-04 9.8637E-05
     1.4878E-03 2.7043E-03 2.6303E-04 3.0413E-03 7.3156E-04
     7.5622E-04 2.4659E-05 6.5758E-05 6.5758E-05 5.7538E-05
     9.8637E-05  3.2879E-05 2.3837E-04 8.2198E-06
     8.2198E-06 8.2198E-06
c
c    Tallies
c    Pulse height distribution
f8:p 11
e8   0.0000 1.0000E-05 0.0010 1998i 2.0000E+00
c
c    Energy and Thermal Cards
c    Photon Physics
c    emcpf ides nocoh
phys:p j 0 1
c
c    Case Control Cards
rand gen=2 seed=6042305
print 40 50 102 128 130 140
prdmp 1j -30 0 4
ctme 360
c
c    Material Specification
c      Dry air (density 0.0012929 g/cc)
m1   7014 -0.7550
     8016 -0.2320
     18000 -0.0130
c      Aluminum (density 2.69 g/cc)
m2   13000 -1.0000
c      Sodium Iodide (density 3.70 g/cc)
m3   11000 1
     53000 1
c      dry soil with UO2 lump material
m4   14000 -2.3586E-01
     13000 -2.0001E-02
     20000 -2.3108E-02
     26000 -1.8400E-02
     12000 -7.4855E-03
     11000 -3.7460E-03
     8016 -3.5895E-01
     92235 -3.3245E-01
c      Uncontaminated Wet Soil (density 2.03 g/cc)
m5   8016 -5.6085E-01
     14000 -3.230E-01
     13000 -2.739E-02
     20000 -3.1640E-02
     26000 -2.52E-02
     12000 -1.025E-02
     11000 -5.130E-03
```

```
     1000  -1.654E-02
c      Lanthanum Bromide (density 5.30 g/cc)
m6   1001 -0.18112917
     6012 -0.114265632
     8016 -0.16921527
     57138 -0.000280893
     57139 -0.311822943
     35079 -0.273018919
     35081 -0.265586169
c     Wet soil with UO2 (density  2.0481 g/cc)
m7   14000 -0.32300000
     13000 -0.02739000
     20000 -0.03164000
     26000 -0.02520000
     12000 -0.01025000
     11000 -0.00513000
     8016 -0.55695893
     92235 -0.00774965
c     Stainless Steel
m8   6000 -3.00E-04
     28064 -1.0129E-03
     28062 -3.8301E-03
     28061 -1.1835E-03
     28060 -2.6773E-02
     28058 -6.7201E-02
     26058 -1.9721E-03
     26057 -1.4675E-02
     26056 -6.2394E-01
     26054 -3.8363E-02
     25055 -2.00E-02
     24054 -4.9870E-03
     24053 -1.8345E-02
     24052 -1.5874E-01
     24050 -7.9248E-03
     16000 -3.00E-04
     15031 -4.50E-04
     14030 -3.3084E-04
     14029 -4.8182E-04
     14028 -9.1873E-03

c    Make sure blank line above
```

A2: Sample MCNP5 input file for an in-situ lump.

```
 LaBr 185 Peak Analysis
c    Lump Model with  25.00 grams U, 10.16 cm of soil depth
c    LaBr detector model
c
_____________________________________________________________________________
c    Cells
c      In-Situ Waste Materials and UO2 Source Mixture
1    4 -2.7800 -1   imp:p=1
c      Surrounding and Overlying Uncontaminated Waste Materials
2    5 -1.7300 -2 1  imp:p=1
c      LaBr Detector above Waste Materials
11   6 -5.3000 -16   imp:p=1 $  Detector LaBr crystal
12   1 -1.2929E-03 16 -15  imp:p=1 $  Inside LaBr detector outside
crystal
13   2 -2.6900 15 -14  imp:p=1 $  LaBr Detector housing
14   1 -1.2929E-03 -18   imp:p=1 $  Inside LaBr PM Tube housing
15   2 -2.6900 18 -17  imp:p=1 $  LaBr PM Tube housing
c      Universe
21   1 -1.2929E-03 2 14 17 -21 imp:p=1
22   0 21     imp:p=0 $  External void

c    Surfaces
c      Dry Soil - UO2 Lump Source
1    s 0.0000 0.0000  1.8046  1.8046
c      Surrounding and Overlying Uncontaminated Waste Materials
2    rcc 0.0000 0.0000 0.0000 0.0000 0.0000  10.16 91.4400
c     NaI Detector
11   rcc 0.0000 0.0000 17.7800 0.0000 0.0000 10.0000 3.3338 $  Detector
Outer H|
12   rcc 0.0000 0.0000 17.9375 0.0000 0.0000 9.6850 3.1763 $  Detector
Inner Ho|
13   rcc 0.0000 0.0000 18.5725 0.0000 0.0000 5.0800 2.5400 $  Detector
NaI Crys|
c     LaBr Detector
14   rcc 0.0000 0.0000 17.7800 0.0000 0.0000 6.3930 3.1315 $Det Out|
15   rcc 0.0000 0.0000 17.8300 0.0000 0.0000 6.2930 3.0815 $Det Inn|
16   rcc 0.0000 0.0000 19.3610 0.0000 0.0000 3.8100 1.9050 $Det LaB|
17   rcc 0.0000 0.0000 24.1730 0.0000 0.0000 18.3270 2.30 $PMT Out|
18   rcc 0.0000 0.0000 24.2230 0.0000 0.0000 18.2270 2.2500 $PMT Inn|
c      Model Boundary
21   so 400.0000

mode p
c
c    Photon Source Distribution
c
c    Energy cutoff  [keV] 50.0
c    Intensity cutoff  [%] 0%
c
```

```
sdef erg=d1 pos=0.0  0.0   1.8046
      rad=d2
sc1  50 year decayed UO2 with 100 wt.% u235/u
si1    s  6   9
sp1   8.8706E-01   1.1294E-01
si2  0.0000  1.8046
sp2  -21 2
c
c    Discrete Gamma Source for u-235
c
si6    l  5.1220E-02 5.4250E-02 6.4370E-02 7.2700E-02
     7.3720E-02 7.4800E-02 8.9958E-02 9.3351E-02 9.6090E-02
     1.0521E-01 1.0832E-01 1.0916E-01 1.1545E-01 1.2035E-01
     1.3655E-01 1.4076E-01 1.4240E-01 1.4377E-01 1.5093E-01
     1.6336E-01 1.7330E-01 1.8261E-01 1.8572E-01 1.9494E-01
     1.9890E-01 2.0211E-01 2.0532E-01 2.1528E-01 2.2138E-01
     2.2878E-01 2.3350E-01 2.4085E-01 2.4684E-01 2.5150E-01
     2.6645E-01 2.7545E-01 2.7950E-01 2.8142E-01 2.8292E-01
     2.8956E-01 2.9165E-01 2.9430E-01 3.0170E-01 3.1069E-01
     3.1710E-01 3.2580E-01 3.4350E-01 3.4590E-01 3.5603E-01
     3.8782E-01 3.9030E-01 4.1029E-01 4.3300E-01 4.4840E-01
     4.5510E-01 5.1720E-01 7.4250E-01 7.9470E-01
sp6   2.0931E-04 1.5699E-04 1.8838E-04 1.1512E-03
     1.0466E-04 6.2794E-04 3.7258E-02 6.0806E-02 9.0005E-04
     2.1036E-02 7.1481E-03 1.6117E-02 7.3260E-04 2.7211E-04
     1.2559E-04 2.3025E-03 5.2329E-05 1.1470E-01 8.3726E-04
     5.3166E-02 1.0466E-04 3.5584E-03 5.9864E-01 6.5934E-03
     4.3956E-04 1.1303E-02 5.2433E-02 2.8258E-04 1.2559E-03
     8.3726E-05 3.0351E-04 7.8493E-04 5.5468E-04 2.0931E-04
     6.2794E-05 5.1282E-04 2.8258E-03 6.2794E-05 5.2329E-05
     7.3260E-05 3.1397E-05 3.4537E-04 5.2329E-05 4.1863E-05
     1.0466E-05 4.1863E-06 3.1397E-05 3.9770E-04 5.2329E-05
     3.9770E-04 4.1863E-04 3.1397E-05 4.1863E-05 1.0466E-05
     8.3726E-05 4.1863E-06 4.1863E-06 6.2794E-06
c
c    Discrete Gamma Source for th-231
c
si9    l     5.8570E-02
     6.3860E-02 6.8500E-02 7.2751E-02 8.1228E-02 8.2087E-02
     8.4214E-02 8.5800E-02 8.9950E-02 9.2288E-02 9.3020E-02
     9.5868E-02 9.7550E-02 9.9278E-02 1.0227E-01 1.0581E-01
     1.0661E-01 1.0801E-01 1.1121E-01 1.1563E-01 1.1682E-01
     1.2491E-01 1.3403E-01 1.3566E-01 1.3675E-01 1.4054E-01
     1.4506E-01 1.4594E-01 1.6310E-01 1.6500E-01 1.6966E-01
     1.7415E-01 1.8350E-01 1.8876E-01 2.1794E-01 2.2410E-01
     2.3601E-01 2.4027E-01 2.4250E-01 2.4960E-01 2.5045E-01
     2.6762E-01  3.0878E-01 3.1100E-01 3.1787E-01
     3.2015E-01 3.5180E-01
sp9      4.1099E-02
     1.8905E-03 4.6853E-04 2.1371E-02 6.9868E-02 3.0413E-02
     5.5155E-01 4.7675E-04 7.7266E-02 3.3701E-02 3.6989E-03
     5.4250E-02 1.8905E-03 9.8637E-03 3.2879E-02 5.8360E-04
     1.3974E-03 1.8905E-02 6.4936E-03 8.2198E-05 1.7015E-03
```

```
     4.9319E-03 2.0549E-03 6.9046E-03 3.4523E-04 5.7538E-05
     4.7675E-04 2.6303E-03 1.2741E-02 3.2057E-04 9.8637E-05
     1.4878E-03 2.7043E-03 2.6303E-04 3.0413E-03 7.3156E-04
     7.5622E-04 2.4659E-05 6.5758E-05 6.5758E-05 5.7538E-05
     9.8637E-05  3.2879E-05 2.3837E-04 8.2198E-06
     8.2198E-06 8.2198E-06
c
c    Tallies
c    Track length tally
f4:p 11
fm4  1.0000E+00 6 (-3:-4)
c
c    Pulse height distribution
f8:p 11
e8   0.0000 1.0000E-05 0.0010 1998i 2.0000E+00
c
c    Energy and Thermal Cards
c    Photon Physics
c    emcpf ides nocoh
phys:p j 0 1
c
c    Case Control Cards
rand gen=2 seed=6042305
print 40 50 102 128 130 140
prdmp 1j -30 0 4
ctme 360
c
c    Material Specification
c      Dry air (density 0.0012929 g/cc)
m1   7014 -0.7550
     8016 -0.2320
     18000 -0.0130
c      Aluminum (density 2.69 g/cc)
m2   13000 -1.0000
c      Sodium Iodide (density 3.70 g/cc)
m3   11000 1
     53000 1
c      UO2 lump material
m4   14000 -2.3586E-01
     13000 -2.0001E-02
     20000 -2.3108E-02
     26000 -1.8400E-02
     12000 -7.4855E-03
     11000 -3.7460E-03
     8016 -3.5895E-01
     92235 -3.3245E-01
c      Uncontaminated Waste material
m5   8016 -5.0410E-01
     14000 -3.7901E-01
     13000 -3.2141E-02
     20000 -3.7133E-02
     26000 -2.9567E-02
     12000 -1.2029E-02
```

```
     11000 -6.0196E-03
c      Lanthanum Bromide (density 5.30 g/cc)
m6   1001 -0.18112917
     6012 -0.114265632
     8016 -0.16921527
     57138 -0.000280893
     57139 -0.311822943
     35079 -0.273018919
     35081 -0.265586169

c    Make sure blank line above
```

A3: Sample MCNP5 input file for in-situ homogeneous contamination.

```
In-Situ Surveys Calibration Analysis - Wet
c   Parametric Study on detector viewing area, 0.10 g/L U-235
c   with tungsten silicone collimator
c    18.00 inch waste radius, 10.01 grams U235, 15.24 probe height
c    Cells
c      In-Situ Waste Materials and UO2 Source Mixture
1    4 -2.0301 -1   imp:p=1
c      LaBr Detector above Waste Materials
11   6 -5.3000 -16   imp:p=1 $  Detector LaBr crystal
12   1 -1.2929E-03 16 -15  imp:p=1 $  Inside LaBr detector outside
crystal
13   2 -2.6900 15 -14  imp:p=1 $  LaBr Detector housing
14   1 -1.2929E-03 -18   imp:p=1 $  Inside LaBr PM Tube housing
15   2 -2.6900 18 -17  imp:p=1 $  LaBr PM Tube housing
16   2 -1.29290E-03   014 -019        imp:p=1 $ Outside LaBrDet Inside
Collimator
17   7 -7.00          019 -20       imp:p=1 $ Collimator Shield Region
c      Universe
21   1 -1.2929E-03 1 14 17 -21 20 imp:p=1
22   0  21     imp:p=0 $  External void

c    Surfaces
c      Waste Materials and UO2 Source Mixture
1    rcc 0.0000 0.0000 0.0000 0.0000 0.0000 15.24 45.72
c     NaI Detector
11   rcc 0.0000 0.0000 22.8600 0.0000 0.0000 10.0000 3.3338 $  Detector
Outer H|
12   rcc 0.0000 0.0000 23.0175 0.0000 0.0000 9.6850 3.1763 $  Detector
Inner Ho|
13   rcc 0.0000 0.0000 23.6525 0.0000 0.0000 5.0800 2.5400 $  Detector
NaI Crys|
c     LaBr Detector
14   999  rcc 0.0000 0.0000 22.8600 0.0000 0.0000 6.3930 3.1315 $  LaBr
Detector Out|
15   999  rcc 0.0000 0.0000 22.9100 0.0000 0.0000 6.2930 3.0815 $  LaBr
Detector Inn|
16   999  rcc 0.0000 0.0000 24.4410 0.0000 0.0000 3.8100 1.9050 $  LaBr
Detector LaB|
17   999  rcc 0.0000 0.0000 29.2530 0.0000 0.0000 18.3270 2.3000 $
LaBr PM Tube Out|
18   999  rcc 0.0000 0.0000 29.3030 0.0000 0.0000 18.2270 2.2500 $
LaBr PM Tube Inn|
19   999  RCC 0.0000 0.0000 21.33 0.0000 0.0000 7.62 3.1316 $ Inner
surface of Collim
20   999  RCC 0.0000 0.0000 21.33 0.0000 0.0000 7.62 4.4319 $ Outer
surface of Collim
c      Model Boundary
21   so 400.0000

tr999 0 0  7.62
mode p
```

```
c
c    Photon Source Distribution
c
c    Energy cutoff  [keV] 50.0
c    Intensity cutoff  [%] 0%
c
sdef erg=d1 pos=0.0  0.0  0.0001
     axs=0 0 1 rad=d2 ext=d3
sc1  50 year decayed UO2 with 100 wt.% u235/u
si1    s  6   9
sp1   8.8706E-01   1.1294E-01
si2  0.0000 45.7190
sp2  -21 1
si3  0.0000 15.2390
sp3  0 1
c
c    Discrete Gamma Source for u-235
c
si6    l  5.1220E-02 5.4250E-02 6.4370E-02 7.2700E-02
     7.3720E-02 7.4800E-02 8.9958E-02 9.3351E-02 9.6090E-02
     1.0521E-01 1.0832E-01 1.0916E-01 1.1545E-01 1.2035E-01
     1.3655E-01 1.4076E-01 1.4240E-01 1.4377E-01 1.5093E-01
     1.6336E-01 1.7330E-01 1.8261E-01 1.8572E-01 1.9494E-01
     1.9890E-01 2.0211E-01 2.0532E-01 2.1528E-01 2.2138E-01
     2.2878E-01 2.3350E-01 2.4085E-01 2.4684E-01 2.5150E-01
     2.6645E-01 2.7545E-01 2.7950E-01 2.8142E-01 2.8292E-01
     2.8956E-01 2.9165E-01 2.9430E-01 3.0170E-01 3.1069E-01
     3.1710E-01 3.2580E-01 3.4350E-01 3.4590E-01 3.5603E-01
     3.8782E-01 3.9030E-01 4.1029E-01 4.3300E-01 4.4840E-01
     4.5510E-01 5.1720E-01 7.4250E-01 7.9470E-01
sp6   2.0931E-04 1.5699E-04 1.8838E-04 1.1512E-03
     1.0466E-04 6.2794E-04 3.7258E-02 6.0806E-02 9.0005E-04
     2.1036E-02 7.1481E-03 1.6117E-02 7.3260E-04 2.7211E-04
     1.2559E-04 2.3025E-03 5.2329E-05 1.1470E-01 8.3726E-04
     5.3166E-02 1.0466E-04 3.5584E-03 5.9864E-01 6.5934E-03
     4.3956E-04 1.1303E-02 5.2433E-02 2.8258E-04 1.2559E-03
     8.3726E-05 3.0351E-04 7.8493E-04 5.5468E-04 2.0931E-04
     6.2794E-05 5.1282E-04 2.8258E-03 6.2794E-05 5.2329E-05
     7.3260E-05 3.1397E-05 3.4537E-04 5.2329E-05 4.1863E-05
     1.0466E-05 4.1863E-06 3.1397E-05 3.9770E-04 5.2329E-05
     3.9770E-04 4.1863E-04 3.1397E-05 4.1863E-05 1.0466E-05
     8.3726E-05 4.1863E-06 4.1863E-06 6.2794E-06
c
c    Discrete Gamma Source for th-231
c
si9    l     5.8570E-02
     6.3860E-02 6.8500E-02 7.2751E-02 8.1228E-02 8.2087E-02
     8.4214E-02 8.5800E-02 8.9950E-02 9.2288E-02 9.3020E-02
     9.5868E-02 9.7550E-02 9.9278E-02 1.0227E-01 1.0581E-01
     1.0661E-01 1.0801E-01 1.1121E-01 1.1563E-01 1.1682E-01
     1.2491E-01 1.3403E-01 1.3566E-01 1.3675E-01 1.4054E-01
     1.4506E-01 1.4594E-01 1.6310E-01 1.6500E-01 1.6966E-01
     1.7415E-01 1.8350E-01 1.8876E-01 2.1794E-01 2.2410E-01
```

```
     2.3601E-01 2.4027E-01 2.4250E-01 2.4960E-01 2.5045E-01
     2.6762E-01  3.0878E-01 3.1100E-01 3.1787E-01
     3.2015E-01 3.5180E-01
sp9      4.1099E-02
     1.8905E-03 4.6853E-04 2.1371E-02 6.9868E-02 3.0413E-02
     5.5155E-01 4.7675E-04 7.7266E-02 3.3701E-02 3.6989E-03
     5.4250E-02 1.8905E-03 9.8637E-03 3.2879E-02 5.8360E-04
     1.3974E-03 1.8905E-02 6.4936E-03 8.2198E-05 1.7015E-03
     4.9319E-03 2.0549E-03 6.9046E-03 3.4523E-04 5.7538E-05
     4.7675E-04 2.6303E-03 1.2741E-02 3.2057E-04 9.8637E-05
     1.4878E-03 2.7043E-03 2.6303E-04 3.0413E-03 7.3156E-04
     7.5622E-04 2.4659E-05 6.5758E-05 6.5758E-05 5.7538E-05
     9.8637E-05  3.2879E-05 2.3837E-04 8.2198E-06
     8.2198E-06 8.2198E-06
c
c    Tallies
c    Track length tally
f4:p 11
fm4  1.0000E+00 6 (-3:-4)
c
c    Pulse height distribution
f8:p 11
e8   0.0000 1.0000E-05 0.0010 1998i 2.0000E+00
c
c    Energy and Thermal Cards
c    Photon Physics
c    emcpf ides nocoh
phys:p j 0 1
c
c    Case Control Cards
rand gen=2 seed=6042305
print 40 50 102 128 130 140
prdmp 1j -30 0 4
ctme 120
c
c    Material Specification
c      Dry air (density 0.0012929 g/cc)
m1   7014 -0.7550
     8016 -0.2320
     18000 -0.0130
c      Aluminum (density 2.69 g/cc)
m2   13000 -1.0000
c      Sodium Iodide (density 3.70 g/cc)
m3   11000 1
     53000 1
c      UO2 Contaminated Waste material  (density 2.03011 g/cc)
m4   14000     -3.22978E-01
     13000     -2.73895E-02
     20000     -3.16432E-02
     26000     -2.51961E-02
     12000     -1.02504E-02
     11000     -5.12972E-03
     8016      -5.60823E-01
```

```
     92235     -4.92583E-05
     1000      -1.65404E-02
c      Lanthanum Bromide (density 5.30 g/cc)
m6   35000 3
     57000 1
c     Tungsten Silicone (density 7 g/cc)
m007    74000 -0.89 6000 -0.0356 1001 -0.009
        14028 -0.0417 8016 -0.0237

c    Make Sure blank line above
```

A4: Sample ORIGEN-S input file.

```
=origens
' Data Block 1 - New case
' Max array size lnread(300000)
' -1$$
' Unit numbers kout(6) ndum(13) npun(0) ndsetb(21) ndsetf(0) nvertr(0)
' nvertw(0) ndfb(0) ndff(0) ldset(0) nxtr(71) ndisk(11)
0$$    a4 21
  a8 23     e
' New case or blend noblnd(1)
1$$ 1      1t
5 wt% u-235 - balance u-238
' Data Block 2
' Blend fractions fact[noblnd]
' 2**
' Lib consts ndset(28,30) nolib(4) ntype(0) ngrp(-82) kout(6) mpctab(0)
' inpt(0) ir(0) lpu(0) nn1(0) nn2(0) nn3(0)
' nn4(0) nn5(0) nn6(0) nn7(0) nn8(-1) itmax(1706)
' ilmax(692) iamax(132) ifmax(882) izmax(7500) nreact(7) nfiso(5)
' nelem(99) nmo nday nyr nenac(18) nenle(12)
' nenfp(12) nvert(0) ng(0)
3$$ 21  a3 1 27
    a16 4 -1
   a33 18    e
' Lib consts (ntype=0) therm(1.0) res(1.0) fast(1.0) err(1e-25)
' 4**
' Lib pos (ntype=0) nlibe(2)
' 5$$
' Sep lib (ndset=-20) 6 entries
' 10$$
' Special opts jopt(8)
54$$ a8 0      e
       2t
' Data Block 3 - Actinide nuclide cards (lpu>0)
' newcx[lpu]
' 6$$       3t
' Data Block 4 - Photon energy group structures
35$$ 0      4t
' Data Block 5 - New subcase with same library
' Subcase ints mmn(0) mout(10) index(0) ntable(0) mstar(1) ngo(1)
' mpros(0) npros(0) mfeed(0) msub(0) nterm(21) nshrt(100)
' nxcmp(0) nunit(4) nti(0) npun(0) jto(2) nuc(0)
' nel(0) kblend(0)
56$$ 0 6 0   a6 1
 a13 2 5 3    e
' Subcase floats tmo(0.0) rho(0.0) cut(0.0) fracpw(1.0) tconst
57** 0.0000E+00      e
' Flag sig digit l95(0)
' 95$$ 1
       5t
5 wt% u-235 - balance u-238
per gram U
```

```
' Data Block 6 - Subcase arrays and titles
' Power power[mmn]
' 58** 0.0000E+00
' Flux flux[mmn]
' 59**
' Print times time[mout] warning: do not use results for initial
interval if = 0
60** 1.00 5.00 10.00 15.00 50.00 100.00
' Cutoffs cutoff[7]
61** f1E-20
' Removal consts prate[mpros]
' 62**
' Num elem nopros[mpros]
' 63$$
' Atomic numbers nzpros[mpros*npros]
' 64$$
' Decay print triggers nto[63] see table f7.6.2
65$$ a1 1 a4 1 a7 1
 a22 1 a25 1 a28 1
 a43 1 a46 1 a49 1 e
' Irrad print triggers kw[12] see table f7.6.3
' 66$$
' ID of nuclides inuc1[nxcmp]
73$$  922350  922380
' Concentrations xcom1[nxcmp]
74**  1.0807E-07  3.1931E-07
' Lib kinds nex1[nxcmp]
75$$  2  2
' ID of nuclides inuc2[mfeed]
' 76$$
' Feed rates xcom2[mfeed]
' 77**
' Lib kinds nex2[mfeed]
' 78$$
' Element fractions frepro(0.0)
' 79**
' Gamma lib consts
' lngam(0) ldset(51) ndf(26) mndf(2) n1max(3000) n2max(1000)
81$$ 2  a3 23 1   e
' Time step triggers m[mout]
82$$ f2
' Gamma group structure [ng+1]
83** 1.0000E+07 8.0000E+06 6.5000E+06 5.0000E+06 4.0000E+06 3.0000E+06
 2.5000E+06 2.0000E+06 1.6600E+06 1.3300E+06 1.0000E+06 8.0000E+05
 6.0000E+05 4.0000E+05 3.0000E+05 2.0000E+05 1.0000E+05 5.0000E+04
 1.0000E+04
' Neutron group structure [ngrp+1]
84** 2.0000E+07 6.4340E+06 3.0000E+06 1.8500E+06 1.4000E+06 9.0000E+05
 4.0000E+05 1.0000E+05 1.7000E+04 3.0000E+03 5.5000E+02 1.0000E+02
 3.0000E+01 1.0000E+01 3.0500E+00 1.7700E+00 1.3000E+00 1.1300E+00
 1.0000E+00 8.0000E-01 4.0000E-01 3.2500E-01 2.2500E-01 1.0000E-01
 5.0000E-02 3.0000E-02 1.0000E-02 1.0000E-05
       6t
```

```
' Job terminator
56$$ f0      5t
End
```

A5: Sample MCNP5 input file for an annular pipe model.

```
LaBr pipe
c   Carbon Steel Pipe
C  Calibration for 28.8925 cm Above Ground Assay of Subsurface Piping
c  OD=27.30 cm; wall thickness= 0.927 cm
c   25.0 g U-235; enr=  5.0%
c  Tungsten Silicone collimator, annular model
c
c
001    001  -3.0009  002 -003       imp:p=1 $ Debris Inside Pipe
c 002    002 -1.29290E-03   002 -003       imp:p=1 $ Region above
Debris material
003    002 -1.29290E-03   -002        imp:p=1 $ Region inside Debris
material
004    002 -1.29290E-03   003 -004        imp:p=1 $ Region Outside
Debris Region
005    003 -7.82000E+00   004 -005        imp:p=1 $ Pipe Wall Structure
c  LaBr Detector
006    004 -5.3000       -008        imp:p=1 $ Detector LaBr crystal
007    002 -1.29290E-03   008 -007        imp:p=1 $ Inside LaBr
detector outside crystal
008    005 -2.69000E+00   -006 007        imp:p=1 $ LaBr Detector
housing
009    002 -1.29290E-03  -010             imp:p=1 $ Inside LaBr PM Tube
housing
010    005 -2.69000E+00   010 -009        imp:p=1 $ LaBr PM Tube
housing
011    002 -1.29290E-03   006 -011        imp:p=1 $ Outside LaBrDet
Inside Collimator
012    007 -7.00          011 -013       imp:p=1 $ Collimator Shield
Region
c             My Bubble
014    006 -2.47367E+00   -015        imp:p=1 $ Floor Region, if any
015    002 -1.29290E-03 005 015 -016 006 009 013     imp:p=1 $ My
BUBBLE
999    000              016                          imp:p=0 $ Outside
My World

c      Surfaces
c        Debris
c 001     pz      -20.9099       $ Debris when Segmented
002    RCC      -15.2400 0.0000 0.0000  30.4800 0.0000 0.0000  12.6476
$ Debris when Annulus
003    RCC      -15.2400 0.0000 0.0000  30.4800 0.0000 0.0000  12.7254
$ Inner Surface of Pipe with Debris
c        Pipe
004    RCC      -198.1210 0.0000 0.0000 396.2420 0.0000 0.0000  12.7254
$ Inner Surface of Pipe
005    RCC      -198.1210 0.0000 0.0000 396.2420 0.0000 0.0000  13.6525
$ Outer Surface of Pipe
c        Detector
```

```
006      999     RCC      0.0000 0.0000 0.0  0.0000 0.0000 6.3930
3.1315   $ LaBr Detector Out
007      999     RCC      0.0000 0.0000 0.05  0.0000 0.0000 6.2930
3.0815   $ LaBr Detector Inn
008      999     RCC      0.0000 0.0000 0.1575  0.0000 0.0000 3.8100
1.9050  $ LaBr crystal
009      999     RCC      0.0000 0.0000 6.433  0.0000 0.0000 18.3270
2.3000 $ LaBr PM Tube Out
010      999     RCC      0.0000 0.0000 6.483  0.0000 0.0000 18.2270
2.2500 $ LaBr PM Tube Inn
c         Collimator
011      999     RCC      0.0000 0.0000 -1.531  0.0000 0.0000 7.62
3.1316 $ Inner surface of Collimator
013      999     RCC      0.0000 0.0000 -1.531  0.0000 0.0000 7.62
4.4319 $ Outer surface of Collimator
c         Extra
015    RPP      -297.1815 396.2420 -297.1815 297.1815 -52.8601 -13.6526
$ Floor/Ground Region
016    RPP      -297.1815 396.2420 -297.1815 297.1815 -52.8601 168.2685
$ My Bubble

TR999    0 0 28.8925
mode  p
print 40 50 102 128 130 140
prdmp 1j -15 0 4
phys:p j 0 0
rand gen=2 seed=8335877
ctme             120
c
c       Material Specification
c       Aluminum (density 2.69 g/cc)
m005    13027 1.000
c       Fissile material (density  3.0009 g/cc)
m001    92238 -0.8371 92235 -0.0441 8016 -0.1187
        7014 -0.0001
c       Carbon steel (density 7.82 g/cc)
m003    6000 -1.0000E-02 26054 -5.6022E-02 26056 -9.0967E-01
          26057 -2.1429E-02 26058 -2.8799E-03
c       Air (density 0.001293 g/cc)
m002    7014 -7.5500E-01 8016 -2.3200E-01 18000 -1.3000E-02
c       Lanthanum Bromide (density 5.30 g/cc)
m004    35000 3.0 57000 1.0
c       Tungsten Silicone (density 7 g/cc)
m007    74000 -0.89 6000 -0.0356 1001 -0.009
         14028 -0.0417 8016 -0.0237
c       Soil (density 2.4737 g/cc)
m006    14028 -0.34816 14029 -0.018259 14030 -0.012537 12000 -0.012027
        13027 -0.032136 20000  -0.037127 11023  -0.0060188
        8016  -0.50396 8017 -0.00021476 26054 -0.0016704
        26056 -0.027167 26057  -0.00063895
c mt006    lwtr.60t
c    Tallies - Base Case Model
c    Pulse height distribution
```

```
f08:p    006
e0   0.0000 1E-05 0.0010 1998i 2.0000E+00
fq0       e f
sdef    rad=d1    axs=1 0 0 ext=d2   pos=0 0 0      eff=0.000001
       cel=001 erg=d99 wgt=2.0746E+08
si1    0.0000000  12.72530
si2    -15.23900 15.23900
sp1        -21 1
sp2         0   1
si99   s  006   008   009   010   011   234
sp99    4.4199E-01 1.7084E-04 5.6275E-02 1.3709E-01 1.6451E-02 3.4803E-
01
c          gammas from 235U = 1.528E+06 g's/sec, Dist#006
si6    l     5.1220E-02 5.4250E-02 6.4370E-02 7.2700E-02
        7.3720E-02 7.4800E-02 8.9958E-02 9.3351E-02 9.6090E-02
        1.0521E-01 1.0832E-01 1.0916E-01 1.1545E-01 1.2035E-01
        1.3655E-01 1.4076E-01 1.4240E-01 1.4377E-01 1.5093E-01
        1.6336E-01 1.7330E-01 1.8261E-01 1.8572E-01 1.9494E-01
        1.9890E-01 2.0211E-01 2.0532E-01 2.1528E-01 2.2138E-01
        2.2878E-01 2.3350E-01 2.4085E-01 2.4684E-01 2.5150E-01
        2.6645E-01 2.7545E-01 2.7950E-01 2.8142E-01 2.8292E-01
        2.8956E-01 2.9165E-01 2.9430E-01 3.0170E-01 3.1069E-01
        3.1710E-01 3.2580E-01 3.4350E-01 3.4590E-01 3.5603E-01
        3.8782E-01 3.9030E-01 4.1029E-01 4.3300E-01 4.4840E-01
        4.5510E-01 5.1720E-01 7.4250E-01 7.9470E-01
sp6     2.0931E-04 1.5699E-04 1.8838E-04 1.1512E-03
        1.0466E-04 6.2794E-04 3.7258E-02 6.0806E-02 9.0005E-04
        2.1036E-02 7.1481E-03 1.6117E-02 7.3260E-04 2.7211E-04
        1.2559E-04 2.3025E-03 5.2329E-05 1.1470E-01 8.3726E-04
        5.3166E-02 1.0466E-04 3.5584E-03 5.9864E-01 6.5934E-03
        4.3956E-04 1.1303E-02 5.2433E-02 2.8258E-04 1.2559E-03
        8.3726E-05 3.0351E-04 7.8493E-04 5.5468E-04 2.0931E-04
        6.2794E-05 5.1282E-04 2.8258E-03 6.2794E-05 5.2329E-05
        7.3260E-05 3.1397E-05 3.4537E-04 5.2329E-05 4.1863E-05
        1.0466E-05 4.1863E-06 3.1397E-05 3.9770E-04 5.2329E-05
        3.9770E-04 4.1863E-04 3.1397E-05 4.1863E-05 1.0466E-05
        8.3726E-05 4.1863E-06 4.1863E-06 6.2794E-06
c          gammas from 238U = 5.907E+02 g's/sec, Dist#008
si8    l      8.9958E-02 9.3351E-02 1.0521E-01
        1.0832E-01 1.1350E-01
sp8      5.6000E-02 8.8000E-02 3.2000E-02
        8.0000E-03 8.1600E-01
c          gammas from 235U ->231Th = 1.946E+05 g's/sec, Dist#009
si9    l        5.8570E-02
        6.3860E-02 6.8500E-02 7.2751E-02 8.1228E-02 8.2087E-02
        8.4214E-02 8.5800E-02 8.9950E-02 9.2288E-02 9.3020E-02
        9.5868E-02 9.7550E-02 9.9278E-02 1.0227E-01 1.0581E-01
        1.0661E-01 1.0801E-01 1.1121E-01 1.1563E-01 1.1682E-01
        1.2491E-01 1.3403E-01 1.3566E-01 1.3675E-01 1.4054E-01
        1.4506E-01 1.4594E-01 1.6310E-01 1.6500E-01 1.6966E-01
        1.7415E-01 1.8350E-01 1.8876E-01 2.1794E-01 2.2410E-01
        2.3601E-01 2.4027E-01 2.4250E-01 2.4960E-01 2.5045E-01
        2.6762E-01  3.0878E-01 3.1100E-01 3.1787E-01
```

```
        3.2015E-01 3.5180E-01
sp9        4.1099E-02
        1.8905E-03 4.6853E-04 2.1371E-02 6.9868E-02 3.0413E-02
        5.5155E-01 4.7675E-04 7.7266E-02 3.3701E-02 3.6989E-03
        5.4250E-02 1.8905E-03 9.8637E-03 3.2879E-02 5.8360E-04
        1.3974E-03 1.8905E-02 6.4936E-03 8.2198E-05 1.7015E-03
        4.9319E-03 2.0549E-03 6.9046E-03 3.4523E-04 5.7538E-05
        4.7675E-04 2.6303E-03 1.2741E-02 3.2057E-04 9.8637E-05
        1.4878E-03 2.7043E-03 2.6303E-04 3.0413E-03 7.3156E-04
        7.5622E-04 2.4659E-05 6.5758E-05 6.5758E-05 5.7538E-05
        9.8637E-05  3.2879E-05 2.3837E-04 8.2198E-06
        8.2198E-06 8.2198E-06
c         gammas from 238U ->234Th = 4.740E+05 g's/sec, Dist#010
si10    l       5.7750E-02 6.2860E-02
        6.3290E-02 8.3300E-02 8.7020E-02  9.2380E-02
        9.2800E-02 1.0335E-01  1.0800E-01 1.1281E-01
         1.8480E-01
sp10       6.0816E-04 1.9461E-03
        4.4578E-01 7.2979E-03 1.7637E-03  2.5908E-01
        2.5543E-01 3.6490E-04  9.7306E-04 2.5543E-02
         1.2163E-03
c         gammas from 238U ->234mPa = 5.688E+04 g's/sec, Dist#011
si11    l       6.3000E-02 7.3920E-02
        9.4658E-02 9.8440E-02 9.9853E-02 1.1086E-01 1.1417E-01
        1.4010E-01 1.8470E-01 1.9340E-01 1.9340E-01 1.9990E-01
        2.0330E-01 2.0990E-01  2.3590E-01 2.4350E-01
        2.4770E-01 2.5790E-01 2.7550E-01 2.9900E-01 3.1100E-01
        3.1630E-01 3.3810E-01 3.5750E-01 3.6280E-01 3.8760E-01
        3.8760E-01 4.5120E-01 4.5360E-01 4.5670E-01 4.6810E-01
        4.7550E-01 5.0750E-01 5.0920E-01 5.1720E-01 5.2590E-01
        5.4410E-01 5.5600E-01 5.5730E-01 5.7200E-01 6.2460E-01
        6.4770E-01 6.4900E-01 6.5530E-01 6.7080E-01 6.7390E-01
        6.8340E-01 6.9100E-01 6.9550E-01 6.9900E-01 7.0160E-01
        7.0630E-01 7.0820E-01 7.2050E-01 7.3250E-01 7.4010E-01
        7.4281E-01 7.5070E-01 7.6030E-01 7.6636E-01 7.8230E-01
        7.8310E-01 7.8627E-01 7.9350E-01 8.0600E-01 8.0820E-01
        8.1820E-01 8.2560E-01 8.3150E-01 8.4410E-01 8.5190E-01
        8.6680E-01 8.8090E-01 8.8320E-01 8.8320E-01 8.8750E-01
        9.2230E-01 9.2680E-01 9.3630E-01 9.4250E-01 9.4630E-01
        9.6000E-01 9.9610E-01 1.0010E+00 1.0423E+00 1.0594E+00
        1.0621E+00 1.0819E+00 1.0857E+00 1.1206E+00 1.1257E+00
        1.1257E+00 1.1742E+00 1.1938E+00 1.2200E+00 1.2374E+00
        1.3530E+00 1.3927E+00 1.4142E+00 1.4343E+00 1.4585E+00
        1.5010E+00 1.5105E+00 1.5272E+00 1.5500E+00 1.5541E+00
        1.5584E+00 1.5708E+00 1.5937E+00 1.6018E+00 1.6676E+00
        1.6941E+00 1.7205E+00 1.7322E+00 1.7382E+00 1.7591E+00
        1.7654E+00 1.7962E+00 1.8090E+00 1.8204E+00 1.8315E+00
        1.8638E+00 1.8682E+00 1.8755E+00 1.8944E+00 1.9118E+00
        1.9265E+00 1.9377E+00 1.9700E+00
sp11       1.5785E-03 8.8896E-03
        5.4833E-03 8.8896E-03 3.0740E-04 3.0740E-03 1.0634E-03
        7.4772E-04 9.9696E-04 3.6555E-04 4.9848E-05 3.3232E-04
        5.9818E-04 7.6434E-04  2.6586E-05 2.9078E-04
```

```
        5.5664E-04 4.7356E-02 1.8278E-04 3.7386E-04 2.9909E-04
        8.3080E-05 6.5633E-04 4.6525E-04 3.9878E-04 2.4924E-04
        5.8156E-04 1.7447E-03 1.4124E-03 4.1540E-04 1.3708E-03
        1.6616E-03 9.1388E-04 1.2462E-03 9.9696E-06 1.8278E-05
        2.1601E-03 1.1631E-05 4.1540E-04 5.0679E-04 8.3080E-04
        9.1388E-04 6.2310E-04 8.0588E-04 2.1601E-04 3.7386E-04
        3.3232E-04 4.5694E-03 9.1388E-04 4.6525E-04 4.4863E-03
        2.3262E-03 4.1540E-04 1.9108E-05 7.5603E-04 5.8987E-03
        4.7023E-02 1.1631E-05 9.1388E-04 1.7198E-01 4.4032E-03
        3.3232E-05 2.8413E-02 4.9848E-05 2.4924E-03 1.7447E-03
        5.8156E-04 8.2249E-04 2.0770E-03 6.3141E-04 3.6555E-03
        6.2310E-04 2.2432E-03 1.0800E-03 9.9696E-04 4.3202E-03
        6.8957E-03 7.2280E-04 1.0800E-03 1.7447E-03 5.8156E-03
        4.9848E-04 2.4093E-03 4.9017E-01 8.3080E-04 6.3972E-04
        1.1631E-03 5.2340E-04 2.8247E-04 9.9696E-04 5.5664E-04
        1.7447E-03 1.1133E-03 7.4772E-03 5.8156E-04 2.9909E-03
        3.6555E-04 9.1388E-04 1.2462E-03 4.8186E-03 1.0800E-03
        7.4772E-04 7.5603E-03 1.2462E-03 1.0800E-03 5.2340E-03
        4.4032E-04 7.1449E-04 2.2432E-03 2.7416E-04 4.8186E-04
        2.6586E-04 1.9108E-04 1.0800E-03 1.1797E-02 1.3293E-03
        5.0679E-03 1.8278E-04 2.4924E-03 6.8957E-04 9.3050E-03
        7.0618E-04 4.4032E-03 4.5694E-03 1.2462E-03 3.0740E-03
        2.5755E-04 1.7447E-03 3.2401E-04
c         gammas from 238U ->234mPa, Bremss = 1.203E+06 g's/sec,
Dist#234
si234  H    1.0000E-02 2.0000E-02 3.0000E-02 6.0000E-02 1.0000E-01
        2.0000E-01 4.0000E-01 6.0000E-01 7.0000E-01 8.0000E-01
        1.0000E+00 1.5000E+00 2.0000E+00 3.0000E+00
sp234     0.0000E+00 2.9451E-01 1.5367E-01 2.1081E-01 1.2426E-01
        1.1667E-01 6.5824E-02 2.0725E-02 5.0496E-03 3.2295E-03
        3.3738E-03 1.7891E-03 9.5880E-05 2.9386E-07

c  Make sure blank line above
```

A6: Sample MCNP5 input file for a segmented pipe model.

```
LaBr pipe
c   Carbon Steel Pipe
C  Calibration for 28.8925 cm Above Ground Assay of Subsurface Piping
c  OD=27.30 cm; wall thickness= 0.927 cm
c   10.0 g U-235; enr=100.0%
c  theta= 0.20816; debris distance= 12.657
c  Tungsten Silicone collimator, segmented model
c
c
001    001  -3.0009  -001 -004       imp:p=1 $ Debris Inside Pipe
002    002 -1.29290E-03   001 -004       imp:p=1 $ Region above Debris
material
c 003    002 -1.29290E-03   -002        imp:p=1 $ Region inside Debris
material
c 004    002 -1.29290E-03   003 -004        imp:p=1 $ Region Outside
Debris Region
005    003 -7.82000E+00   004 -005        imp:p=1 $ Pipe Wall Structure
c  LaBr Detector
006    004 -5.3000       -008        imp:p=1 $ Detector LaBr crystal
007    002 -1.29290E-03   008 -007        imp:p=1 $ Inside LaBr
detector outside crystal
008    005 -2.69000E+00   -006 007        imp:p=1 $ LaBr Detector
housing
009    002 -1.29290E-03  -010             imp:p=1 $ Inside LaBr PM Tube
housing
010    005 -2.69000E+00   010 -009        imp:p=1 $ LaBr PM Tube
housing
011    002 -1.29290E-03   006 -011        imp:p=1 $ Outside LaBrDet
Inside Collimator
012    007 -7.00          011 -013       imp:p=1 $ Collimator Shield
Region
c             My Bubble
014    006 -2.47367E+00   -015        imp:p=1 $ Floor Region, if any
015    002 -1.29290E-03 005 015 -016 006 009 013     imp:p=1 $ My
BUBBLE
999    000              016                          imp:p=0 $ Outside
My World

c      Surfaces
c        Debris
001     pz      -12.6565       $ Debris when Segmented
c 002    RCC      -15.2400 0.0000 0.0000  30.4800 0.0000 0.0000
12.7238 $ Debris when Annulus
c 003    RCC      -15.2400 0.0000 0.0000  30.4800 0.0000 0.0000
12.7254 $ Inner Surface of Pipe with Debris
c        Pipe
004    RCC      -198.1210 0.0000 0.0000 396.2420 0.0000 0.0000  12.7254
$ Inner Surface of Pipe
005    RCC      -198.1210 0.0000 0.0000 396.2420 0.0000 0.0000  13.6525
$ Outer Surface of Pipe
c        Detector
```

```
006      999     RCC      0.0000 0.0000 0.0  0.0000 0.0000 6.3930
3.1315   $ LaBr Detector Out
007      999     RCC      0.0000 0.0000 0.05  0.0000 0.0000 6.2930
3.0815   $ LaBr Detector Inn
008      999     RCC      0.0000 0.0000 0.1575  0.0000 0.0000 3.8100
1.9050  $ LaBr crystal
009      999     RCC      0.0000 0.0000 6.433  0.0000 0.0000 18.3270
2.3000 $ LaBr PM Tube Out
010      999     RCC      0.0000 0.0000 6.483  0.0000 0.0000 18.2270
2.2500 $ LaBr PM Tube Inn
c         Collimator
011      999     RCC      0.0000 0.0000 -1.531  0.0000 0.0000 7.62
3.1316 $ Inner surface of Collimator
013      999     RCC      0.0000 0.0000 -1.531  0.0000 0.0000 7.62
4.4319 $ Outer surface of Collimator
c         Extra
015    RPP      -297.1815 396.2420 -297.1815 297.1815 -52.8601 -13.6526
$ Floor/Ground Region
016    RPP      -297.1815 396.2420 -297.1815 297.1815 -52.8601 168.2685
$ My Bubble

TR999    0 0 28.8925
mode  p
print 40 50 102 128 130 140
prdmp 1j -15 0 4
phys:p j 0 0
rand gen=2 seed=8335877
ctme             120
c
c       Material Specification
c       Aluminum (density 2.69 g/cc)
m005    13027 1.000
c       Fissile material (density  3.0009 g/cc)
m001    92238 -0.0001 92235 -0.8798 8016 -0.1200
        7014 -0.0001
c       Carbon steel (density 7.82 g/cc)
m003    6000 -1.0000E-02 26054 -5.6022E-02 26056 -9.0967E-01
          26057 -2.1429E-02 26058 -2.8799E-03
c       Air (density 0.001293 g/cc)
m002    7014 -7.5500E-01 8016 -2.3200E-01 18000 -1.3000E-02
c       Lanthanum Bromide (density 5.30 g/cc)
m004    35000 3.0 57000 1.0
c       Tungsten Silicone (density 7 g/cc)
m007    74000 -0.89 6000 -0.0356 1001 -0.009
         14028 -0.0417 8016 -0.0237
c       Soil (density 2.4737 g/cc)
m006    14028 -0.34816 14029 -0.018259 14030 -0.012537 12000 -0.012027
        13027 -0.032136 20000  -0.037127 11023  -0.0060188
        8016  -0.50396 8017 -0.00021476 26054 -0.0016704
        26056 -0.027167 26057  -0.00063895
c mt006    lwtr.60t
c    Tallies - Base Case Model
c    Pulse height distribution
```

```
f08:p    006
e0   0.0000 1E-05 0.0010 1998i 2.0000E+00
fq0       e f
sdef    rad=d1    axs=1 0 0 ext=d2   pos=0 0 0      eff=0.000001
       cel=001 erg=d99 wgt=2.0746E+08
si1    0.0000000  12.72530
si2    -15.23900 15.23900
sp1        -21 1
sp2         0   1
si99   s  006   008   009   010   011   234
sp99    4.4199E-01 1.7084E-04 5.6275E-02 1.3709E-01 1.6451E-02 3.4803E-
01
c         gammas from 235U = 1.528E+06 g's/sec, Dist#006
si6    l     5.1220E-02 5.4250E-02 6.4370E-02 7.2700E-02
        7.3720E-02 7.4800E-02 8.9958E-02 9.3351E-02 9.6090E-02
        1.0521E-01 1.0832E-01 1.0916E-01 1.1545E-01 1.2035E-01
        1.3655E-01 1.4076E-01 1.4240E-01 1.4377E-01 1.5093E-01
        1.6336E-01 1.7330E-01 1.8261E-01 1.8572E-01 1.9494E-01
        1.9890E-01 2.0211E-01 2.0532E-01 2.1528E-01 2.2138E-01
        2.2878E-01 2.3350E-01 2.4085E-01 2.4684E-01 2.5150E-01
        2.6645E-01 2.7545E-01 2.7950E-01 2.8142E-01 2.8292E-01
        2.8956E-01 2.9165E-01 2.9430E-01 3.0170E-01 3.1069E-01
        3.1710E-01 3.2580E-01 3.4350E-01 3.4590E-01 3.5603E-01
        3.8782E-01 3.9030E-01 4.1029E-01 4.3300E-01 4.4840E-01
        4.5510E-01 5.1720E-01 7.4250E-01 7.9470E-01
sp6     2.0931E-04 1.5699E-04 1.8838E-04 1.1512E-03
        1.0466E-04 6.2794E-04 3.7258E-02 6.0806E-02 9.0005E-04
        2.1036E-02 7.1481E-03 1.6117E-02 7.3260E-04 2.7211E-04
        1.2559E-04 2.3025E-03 5.2329E-05 1.1470E-01 8.3726E-04
        5.3166E-02 1.0466E-04 3.5584E-03 5.9864E-01 6.5934E-03
        4.3956E-04 1.1303E-02 5.2433E-02 2.8258E-04 1.2559E-03
        8.3726E-05 3.0351E-04 7.8493E-04 5.5468E-04 2.0931E-04
        6.2794E-05 5.1282E-04 2.8258E-03 6.2794E-05 5.2329E-05
        7.3260E-05 3.1397E-05 3.4537E-04 5.2329E-05 4.1863E-05
        1.0466E-05 4.1863E-06 3.1397E-05 3.9770E-04 5.2329E-05
        3.9770E-04 4.1863E-04 3.1397E-05 4.1863E-05 1.0466E-05
        8.3726E-05 4.1863E-06 4.1863E-06 6.2794E-06
c         gammas from 238U = 5.907E+02 g's/sec, Dist#008
si8    l      8.9958E-02 9.3351E-02 1.0521E-01
        1.0832E-01 1.1350E-01
sp8      5.6000E-02 8.8000E-02 3.2000E-02
        8.0000E-03 8.1600E-01
c         gammas from 235U ->231Th = 1.946E+05 g's/sec, Dist#009
si9    l        5.8570E-02
        6.3860E-02 6.8500E-02 7.2751E-02 8.1228E-02 8.2087E-02
        8.4214E-02 8.5800E-02 8.9950E-02 9.2288E-02 9.3020E-02
        9.5868E-02 9.7550E-02 9.9278E-02 1.0227E-01 1.0581E-01
        1.0661E-01 1.0801E-01 1.1121E-01 1.1563E-01 1.1682E-01
        1.2491E-01 1.3403E-01 1.3566E-01 1.3675E-01 1.4054E-01
        1.4506E-01 1.4594E-01 1.6310E-01 1.6500E-01 1.6966E-01
        1.7415E-01 1.8350E-01 1.8876E-01 2.1794E-01 2.2410E-01
        2.3601E-01 2.4027E-01 2.4250E-01 2.4960E-01 2.5045E-01
        2.6762E-01  3.0878E-01 3.1100E-01 3.1787E-01
```

```
        3.2015E-01 3.5180E-01
sp9        4.1099E-02
        1.8905E-03 4.6853E-04 2.1371E-02 6.9868E-02 3.0413E-02
        5.5155E-01 4.7675E-04 7.7266E-02 3.3701E-02 3.6989E-03
        5.4250E-02 1.8905E-03 9.8637E-03 3.2879E-02 5.8360E-04
        1.3974E-03 1.8905E-02 6.4936E-03 8.2198E-05 1.7015E-03
        4.9319E-03 2.0549E-03 6.9046E-03 3.4523E-04 5.7538E-05
        4.7675E-04 2.6303E-03 1.2741E-02 3.2057E-04 9.8637E-05
        1.4878E-03 2.7043E-03 2.6303E-04 3.0413E-03 7.3156E-04
        7.5622E-04 2.4659E-05 6.5758E-05 6.5758E-05 5.7538E-05
        9.8637E-05  3.2879E-05 2.3837E-04 8.2198E-06
        8.2198E-06 8.2198E-06
c         gammas from 238U ->234Th = 4.740E+05 g's/sec, Dist#010
si10    l       5.7750E-02 6.2860E-02
        6.3290E-02 8.3300E-02 8.7020E-02  9.2380E-02
        9.2800E-02 1.0335E-01  1.0800E-01 1.1281E-01
         1.8480E-01
sp10       6.0816E-04 1.9461E-03
        4.4578E-01 7.2979E-03 1.7637E-03  2.5908E-01
        2.5543E-01 3.6490E-04  9.7306E-04 2.5543E-02
         1.2163E-03
c         gammas from 238U ->234mPa = 5.688E+04 g's/sec, Dist#011
si11    l       6.3000E-02 7.3920E-02
        9.4658E-02 9.8440E-02 9.9853E-02 1.1086E-01 1.1417E-01
        1.4010E-01 1.8470E-01 1.9340E-01 1.9340E-01 1.9990E-01
        2.0330E-01 2.0990E-01  2.3590E-01 2.4350E-01
        2.4770E-01 2.5790E-01 2.7550E-01 2.9900E-01 3.1100E-01
        3.1630E-01 3.3810E-01 3.5750E-01 3.6280E-01 3.8760E-01
        3.8760E-01 4.5120E-01 4.5360E-01 4.5670E-01 4.6810E-01
        4.7550E-01 5.0750E-01 5.0920E-01 5.1720E-01 5.2590E-01
        5.4410E-01 5.5600E-01 5.5730E-01 5.7200E-01 6.2460E-01
        6.4770E-01 6.4900E-01 6.5530E-01 6.7080E-01 6.7390E-01
        6.8340E-01 6.9100E-01 6.9550E-01 6.9900E-01 7.0160E-01
        7.0630E-01 7.0820E-01 7.2050E-01 7.3250E-01 7.4010E-01
        7.4281E-01 7.5070E-01 7.6030E-01 7.6636E-01 7.8230E-01
        7.8310E-01 7.8627E-01 7.9350E-01 8.0600E-01 8.0820E-01
        8.1820E-01 8.2560E-01 8.3150E-01 8.4410E-01 8.5190E-01
        8.6680E-01 8.8090E-01 8.8320E-01 8.8320E-01 8.8750E-01
        9.2230E-01 9.2680E-01 9.3630E-01 9.4250E-01 9.4630E-01
        9.6000E-01 9.9610E-01 1.0010E+00 1.0423E+00 1.0594E+00
        1.0621E+00 1.0819E+00 1.0857E+00 1.1206E+00 1.1257E+00
        1.1257E+00 1.1742E+00 1.1938E+00 1.2200E+00 1.2374E+00
        1.3530E+00 1.3927E+00 1.4142E+00 1.4343E+00 1.4585E+00
        1.5010E+00 1.5105E+00 1.5272E+00 1.5500E+00 1.5541E+00
        1.5584E+00 1.5708E+00 1.5937E+00 1.6018E+00 1.6676E+00
        1.6941E+00 1.7205E+00 1.7322E+00 1.7382E+00 1.7591E+00
        1.7654E+00 1.7962E+00 1.8090E+00 1.8204E+00 1.8315E+00
        1.8638E+00 1.8682E+00 1.8755E+00 1.8944E+00 1.9118E+00
        1.9265E+00 1.9377E+00 1.9700E+00
sp11       1.5785E-03 8.8896E-03
        5.4833E-03 8.8896E-03 3.0740E-04 3.0740E-03 1.0634E-03
        7.4772E-04 9.9696E-04 3.6555E-04 4.9848E-05 3.3232E-04
        5.9818E-04 7.6434E-04  2.6586E-05 2.9078E-04
```

```
        5.5664E-04 4.7356E-02 1.8278E-04 3.7386E-04 2.9909E-04
        8.3080E-05 6.5633E-04 4.6525E-04 3.9878E-04 2.4924E-04
        5.8156E-04 1.7447E-03 1.4124E-03 4.1540E-04 1.3708E-03
        1.6616E-03 9.1388E-04 1.2462E-03 9.9696E-06 1.8278E-05
        2.1601E-03 1.1631E-05 4.1540E-04 5.0679E-04 8.3080E-04
        9.1388E-04 6.2310E-04 8.0588E-04 2.1601E-04 3.7386E-04
        3.3232E-04 4.5694E-03 9.1388E-04 4.6525E-04 4.4863E-03
        2.3262E-03 4.1540E-04 1.9108E-05 7.5603E-04 5.8987E-03
        4.7023E-02 1.1631E-05 9.1388E-04 1.7198E-01 4.4032E-03
        3.3232E-05 2.8413E-02 4.9848E-05 2.4924E-03 1.7447E-03
        5.8156E-04 8.2249E-04 2.0770E-03 6.3141E-04 3.6555E-03
        6.2310E-04 2.2432E-03 1.0800E-03 9.9696E-04 4.3202E-03
        6.8957E-03 7.2280E-04 1.0800E-03 1.7447E-03 5.8156E-03
        4.9848E-04 2.4093E-03 4.9017E-01 8.3080E-04 6.3972E-04
        1.1631E-03 5.2340E-04 2.8247E-04 9.9696E-04 5.5664E-04
        1.7447E-03 1.1133E-03 7.4772E-03 5.8156E-04 2.9909E-03
        3.6555E-04 9.1388E-04 1.2462E-03 4.8186E-03 1.0800E-03
        7.4772E-04 7.5603E-03 1.2462E-03 1.0800E-03 5.2340E-03
        4.4032E-04 7.1449E-04 2.2432E-03 2.7416E-04 4.8186E-04
        2.6586E-04 1.9108E-04 1.0800E-03 1.1797E-02 1.3293E-03
        5.0679E-03 1.8278E-04 2.4924E-03 6.8957E-04 9.3050E-03
        7.0618E-04 4.4032E-03 4.5694E-03 1.2462E-03 3.0740E-03
        2.5755E-04 1.7447E-03 3.2401E-04
c         gammas from 238U ->234mPa, Bremss = 1.203E+06 g's/sec,
Dist#234
si234  H    1.0000E-02 2.0000E-02 3.0000E-02 6.0000E-02 1.0000E-01
        2.0000E-01 4.0000E-01 6.0000E-01 7.0000E-01 8.0000E-01
        1.0000E+00 1.5000E+00 2.0000E+00 3.0000E+00
sp234     0.0000E+00 2.9451E-01 1.5367E-01 2.1081E-01 1.2426E-01
        1.1667E-01 6.5824E-02 2.0725E-02 5.0496E-03 3.2295E-03
        3.3738E-03 1.7891E-03 9.5880E-05 2.9386E-07

c  Make sure blank line above
```

APPENDIX B

ADDITIONAL ANALYSIS DATA

Table B.I. Sample Results Comparing MCNP/LaBr Measurement and HPGe/ISOCS Measurement

		HPGe/ISOCS		*InSpector 1000/MCNP*			
Identifier	**Description**	**U-235 Mass**	**Enrichment**	**CPM in 186 keV ROI***	**Model**	**U-235 Mass**	**Notes**
AC-101312-08	60% full, soil/debris	12.06	N/A	47908	FC 50%	9.84	
				47908	FC 75%	19.36	
				47908	FC 60%	13.52	Linear interpolation of 50% and 75%
				47908	Lump 2"	22.33	Taken on contact, model depicts 3" away
AC-101312-10	75% full, 90% soil	14.12	N/A	80031	FC 75%	32.41	
				80031	Lump 2"	36.33	
				80031	FC 50%	16.39	
AC-101312-09	15% full	1.82	2.50%	6081	FC 25% (5% enr)	1.20	peak ratio enrich estimation=179/6081=2.9%
				6081	Lump 2"	2.54	Taken on contact, model depicts 3" away
AC-103512-02	75% full, soil	27.63	24.90%	61807	FC 75%	24.99140526	
				61807	FC 75% (5% enr)	46.183921	
AC-103512-02	15% full, cloths	7.7	N/A	170344	FC 25%	18.21	
				170344	FC 15%	10.93	linear interpolation from 25%
AC-112112-08	95% full, soil/debris	85.44	3.20%	92344	FC 95% (5% enr)	98.04	
				92344	FC 95% (100% enr)	37.45	
AC-113012-01	30% full, small bottles	4.02	N/A	42360	FC 25%	4.87	
				42360	FC 50%	8.71	
				42360	FC 30%	5.04	linear interpolation
AC-120212-04	95% full, soil	42.7	54.30%	120677	FC 95% (5% enr)	145.22	
				120677	FC 95% (100% enr)	49.14	
AC-122012-02	60% full, sludge	24.55	16.70%	95440	FC 75%	38.71	
				94440	FC 60%	30.97	linear interpolation
AC-010513-05	75% full, caustic sludge	114.99	5.54%	130706	FC 75% (5% enr)	133.69	
				130706	FC 75% (100% enr)	53.21	

Table B.II. Raw Computational Results from 100 wt.% ^{235}U/U Field Container Model

g U	percent filled	energy	response	s	normalization	cps	cpm
100	0.25	1.86E-01	1.49E-03	0.0007	8612616.229	12857.49103	771449.4621
100	0.5	1.86E-01	7.84E-04	0.001	8612616.229	6737.290943	404237.4566
100	0.75	1.86E-01	5.30E-04	0.0013	8612616.229	4552.766875	273166.0125
100	0.95	1.86E-01	4.21E-04	0.0014	8612616.229	3614.831322	216889.8793
10	0.25	1.86E-01	1.62E-03	0.0007	861261.6229	1394.193546	83651.61279
10	0.5	1.86E-01	8.17E-04	0.001	861261.6229	702.5657716	42153.9463
10	0.75	1.86E-01	5.45E-04	0.0013	861261.6229	468.3157876	28098.94726
10	0.95	1.86E-01	4.30E-04	0.0014	861261.6229	369.7323874	22183.94324
125	0.25	1.86E-01	1.46E-03	0.0007	10765770.29	15731.81921	943909.1525
125	0.5	1.86E-01	7.75E-04	0.001	10765770.29	8327.526381	499651.5828
125	0.75	1.86E-01	5.26E-04	0.0013	10765770.29	5647.685343	338861.1206
125	0.95	1.86E-01	4.18E-04	0.0014	10765770.29	4491.979214	269518.7528
15	0.25	1.86E-01	1.61E-03	0.0007	1291892.434	2081.627592	124897.6555
15	0.5	1.86E-01	8.15E-04	0.001	1291892.434	1051.373185	63082.39109
15	0.75	1.86E-01	5.44E-04	0.0013	1291892.434	701.342349	42080.54094
15	0.95	1.86E-01	4.30E-04	0.0016	1291892.434	553.8236704	33229.42022
200	0.25	1.86E-01	1.38E-03	0.0008	17225232.46	23669.67202	1420180.321
200	0.5	1.86E-01	7.49E-04	0.001	17225232.46	12880.93261	772855.9567
200	0.75	1.86E-01	5.14E-04	0.0013	17225232.46	8832.399006	529943.9404
200	0.95	1.86E-01	4.11E-04	0.0016	17225232.46	7054.924182	423295.4509
25	0.25	1.86E-01	1.60E-03	0.0008	2153154.057	3436.63231	206197.9386
25	0.5	1.86E-01	8.12E-04	0.001	2153154.057	1744.077894	104644.6736
25	0.75	1.86E-01	5.43E-04	0.0013	2153154.057	1165.304611	69918.27669
25	0.95	1.86E-01	4.29E-04	0.0014	2153154.057	920.7087681	55242.52609
300	0.25	1.86E-01	1.27E-03	0.0008	25837848.69	32888.22618	1973293.571
300	0.5	1.86E-01	7.17E-04	0.001	25837848.69	18499.23258	1109953.955
300	0.75	1.86E-01	4.99E-04	0.0013	25837848.69	12864.35781	771861.4689
300	0.95	1.86E-01	4.01E-04	0.0015	25837848.69	10333.5266	620011.5959
3	0.25	1.86E-01	1.63E-03	0.0007	258378.4869	421.0007821	25260.04692
3	0.5	1.86E-01	8.20E-04	0.001	258378.4869	211.4559015	12687.35409
3	0.75	1.86E-01	5.46E-04	0.0013	258378.4869	140.8217661	8449.305966
3	0.95	1.86E-01	4.31E-04	0.0014	258378.4869	111.1150187	6666.901123
350	0.25	1.86E-01	1.23E-03	0.0008	30144156.8	37006.85367	2220411.22
350	0.5	1.86E-01	7.03E-04	0.0011	30144156.8	21136.90104	1268214.062
350	0.75	1.86E-01	4.92E-04	0.0013	30144156.8	14793.86803	887632.0818
350	0.95	1.86E-01	3.97E-04	0.0015	30144156.8	11916.7525	715005.1502

50	0.25	1.86E-01	1.56E-03	0.0008	4306308.115	6716.421851	402985.311
50	0.5	1.86E-01	8.02E-04	0.001	4306308.115	3448.320449	206899.2269
50	0.75	1.86E-01	5.38E-04	0.0014	4306308.115	2311.552076	138693.1245
50	0.95	1.86E-01	4.26E-04	0.0014	4306308.115	1830.05495	109803.297
6	0.25	1.86E-01	1.63E-03	0.0007	516756.9738	839.6020083	50376.1205
6	0.5	1.86E-01	8.19E-04	0.001	516756.9738	422.3326456	25339.95874
6	0.75	1.86E-01	5.46E-04	0.0013	516756.9738	281.3729402	16882.37641
6	0.95	1.86E-01	4.31E-04	0.0014	516756.9738	222.0594698	13323.56819
75	0.25	1.86E-01	1.53E-03	0.0007	6459462.172	9857.723714	591463.4228
75	0.5	1.86E-01	7.93E-04	0.001	6459462.172	5111.934739	306716.0843
75	0.75	1.86E-01	5.34E-04	0.0013	6459462.172	3441.82764	206509.6584
75	0.95	1.86E-01	4.24E-04	0.0015	6459462.172	2727.504285	163650.2571
0.95	0.5	1.86E-01	8.21E-04	0.001	81819.85	67.03771067	4022.26264
0.47	0.25	1.86E-01	1.64E-03	0.0007	40479.30	66.10918249	3966.550949
1.42	0.75	1.86E-01	5.47E-04	0.0013	122299.15	66.68637521	4001.182512
1.8	0.95	1.86E-01	4.31E-04	0.0014	155027.09	66.68617106	4001.170263

Table B.III. Sample of Raw Computational Results for Pipe Calibration

Case	Detector	Collimator	Geometry	Pipe Material	Pipe OD	235U grams	Enrichment	normalization	Ener	response 185 keV photope	cts/min
LaBr_col_Ann_CS_10.75.i_99.99_20_in.out	LaBr	col	Ann	CS	10.75.	20	100	1722523.246	50	1.0804E+04	5.3767E+03
LaBr_col_Ann_CS_12.75.i_99.99_20_in.out	LaBr	col	Ann	CS	12.75.	20	100	1722523.246	50	8.0258E+03	3.9936E+03
LaBr_col_Ann_CS_16.i_99.99_20_40.64_in.out	LaBr	col	Ann	CS	16	20	100	1722523.246	50	2.7747E+03	1.3775E+03
LaBr_col_Ann_CS_16.i_99.99_20_45.72_in.out	LaBr	col	Ann	CS	18	20	100	1722523.246	50	2.4039E+03	1.1930E+03
LaBr_col_Ann_CS_16.i_99.99_20_in.out	LaBr	col	Ann	CS	16	20	100	1722523.246	50	3.9552E+03	1.9657E+03
LaBr_col_Ann_CS_18.i_99.99_20_in.out	LaBr	col	Ann	CS	18	20	100	1722523.246	50	3.5311E+03	1.7528E+03
LaBr_col_Ann_CS_4.5.i_99.99_20_in.out	LaBr	col	Ann	CS	4.5.	20	100	1722523.246	50	2.7586E+04	1.3739E+04
LaBr_col_Ann_CS_5.563.i_99.99_20_in.out	LaBr	col	Ann	CS	5.563.	20	100	1722523.246	50	2.3469E+04	1.1688E+04
LaBr_col_Ann_CS_5.i_99.99_20_in.out	LaBr	col	Ann	CS	5	20	100	1722523.246	50	2.5617E+04	1.2758E+04
LaBr_col_Ann_CS_6.625.i_99.99_20_in.out	LaBr	col	Ann	CS	6.625.	20	100	1722523.246	50	2.0686E+04	1.0301E+04
LaBr_col_Ann_CS_8.625.i_99.99_20_in.out	LaBr	col	Ann	CS	8.625.	20	100	1722523.246	50	1.5274E+04	7.6029E+03
LaBr_col_Ann_PVC_5.563.i_5_25_in.out	LaBr	col	Seg	CS	10.75	20	100	1722523.246	50	2.7645E+04	1.3771E+04
LaBr_col_Ann_PVC_5.i_5_0.1_in.out	LaBr	col	Seg	CS	12.75	20	100	1722523.246	50	6.6224E+04	3.2968E+04
LaBr_col_Ann_PVC_6.625.i_5_15_in.out	LaBr	col	Seg	CS	18	20	100	1722523.246	50	3.4857E+04	1.7363E+04
LaBr_col_Seg_CS_10.75_20_100.i_in.out	LaBr	col	Seg	CS	10.75	20	100	1722523.246	50	7.1660E+03	3.5668E+03
LaBr_col_Seg_CS_12.75_25_100.i_in.out	LaBr	col	Seg	CS	12.75	20	100	1722523.246	50	5.0031E+03	2.4886E+03
LaBr_col_Seg_CS_16_25_100.i_in.out	LaBr	col	Seg	CS	16	20	100	1722523.246	50	3.1606E+03	1.5710E+03
LaBr_col_Seg_CS_18_20_100.i_in.out	LaBr	col	Seg	CS	18	20	100	1722523.246	50	2.7120E+03	1.3469E+03
LaBr_col_Seg_CS_5.563_20_100.i_in.out	LaBr	col	Seg	CS	5.563	20	100	1722523.246	50	1.8991E+04	9.4582E+03
LaBr_col_Seg_CS_5_20_100.i_in.out	LaBr	col	Seg	CS	5	20	100	1722523.246	50	2.1273E+04	1.0595E+04
LaBr_col_Seg_CS_6.625_20_100.i_in.out	LaBr	col	Seg	CS	6.625	20	100	1722523.246	50	1.5165E+04	7.5517E+03
LaBr_col_Seg_CS_8.625_20_100.i_in.out	LaBr	col	Seg	CS	8.625	20	100	1722523.246	50	1.0544E+04	5.2488E+03

APPENDIX C

DECAY SCHEMES

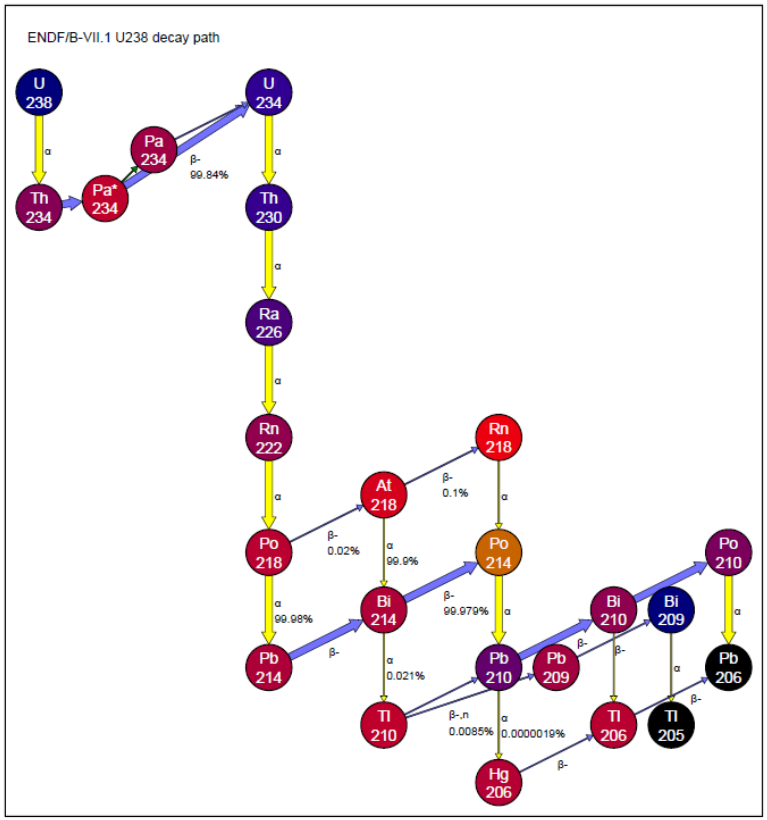

Figure C.1. ^{238}U Decay Scheme

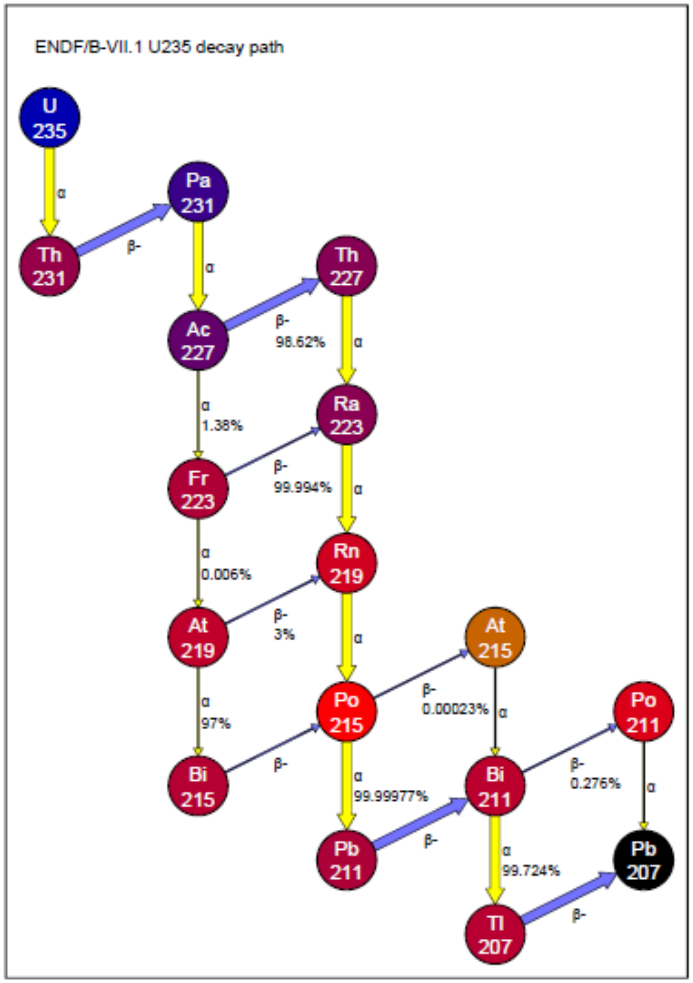

Figure C.2. ^{235}U Decay Scheme